BRL

REPORT NO. 1692

THE FLOW FIELD ABOUT THE MUZZLE OF AN M-16 RIFLE

by

Edward M. Schmidt
Donald D. Shear

January 1974

USA BALLISTIC RESEARCH LABORATORIES
ABERDEEN PROVING GROUND, MARYLAND

Destroy this report when it is no longer needed.
Do not return it to the originator.

Secondary distribution of this report by originating or sponsoring activity is prohibited.

Additional copies of this report may be obtained from the Defense Documentation Center, Cameron Station, Alexandria, Virginia 22314.

The findings in this report are not to be construed as an official Department of the Army position, unless so designated by other authorized documents.

BALLISTIC RESEARCH LABORATORIES

REPORT NO. 1692

JANUARY 1974

THE FLOW FIELD ABOUT THE MUZZLE OF AN M-16 RIFLE

Edward M. Schmidt
Donald D. Shear

Exterior Ballistics Laboratory

RDT&E Project No. 1T061102A33D

ABERDEEN PROVING GROUND, MARYLAND

BALLISTIC RESEARCH LABORATORIES

REPORT NO. 1692

EMSchmidt/DDShear/ner
Aberdeen Proving Ground, Md.
January 1974

THE FLOW FIELD ABOUT THE MUZZLE OF AN M-16 RIFLE

ABSTRACT

An experimental technique is developed which permits the obtaining of detailed time-displacement histories of observable discontinuities in the muzzle gas flow fields that form about weapons during firing. The technique is applied to the flow from the muzzle of an M-16 rifle firing standard ball ammunition. Data is presented both as full discontinuity contours and as discontinuity trajectories along the axis of symmetry. The former indicate the details of muzzle jet-free air blast coupling; while the latter demonstrate the applicability of analytical techniques to the flow field. Additionally, a data reduction scheme is proposed which permits the inference of property values in the flow based on a combination of empirical and analytical techniques.

TABLE OF CONTENTS

LIST OF ILLUSTRATIONS

LIST OF ILLUSTRATIONS

LIST OF SYMBOLS

A	area
a	speed of sound
c_p, c_v	coeficients of specific heat
D	reference dimension (gun caliber)
$\dot{E}$	energy flux
M	mach number
p	pressure
R	gas constant
T	temperature
t	time
u	axial velocity (in-bore)
V	velocity (exterior to muzzle)
V_p	projectile velocity (constant)
X	axial distance from muzzle
Y	lateral distance from axis of symmetry
γ	ratio of specific heats
ς	energy ratio
ρ	density
τ	time from projectile exit to gun emptying

Subscripts

e	muzzle exit conditions
s	stagnation conditions
∞	ambient conditions

Superscripts

$*$	sonic conditions

I. INTRODUCTION

The gases discharged from the muzzle of a gun during firing affect projectile motion, determine the magnitude of blast and flash generated, and provide the medium in which muzzle attachments are immersed Thus, the muzzle gas flow field directly effects accuracy, crew safety and efficiency, firing signature, and weapon functioning. Previous surveys of this flow consist of qualitative optical experiments coupled with theoretical analyses based on existing blast and steady, supersonic jet theories. Recently, considerable effort has been invested in the application of finite difference techniques to the computation of the detailed, time dependent properties of the propellant gas flow field as it expands around the projectile into the surrounding atmosphere. In order to investigate the validity of the predictions of these and other computational techniques, a body of quantitative experimental data is required. This report presents the results of an experimental survey of the phenomena occurring at the muzzle of a 5.56mm M-16 rifle during firing. Since the techniques applied are based on approaches taken by previous researchers, it is useful to briefly review this work.

Cranz[1*] reports using spark schlieren techniques to obtain photographs of the muzzle gas flow field about a rifle in 1911. The sequences of photographs produced show the development of the precursor flow field formed by the air in the tube being forced out ahead of the projectile. This is followed by the projectile separation from the muzzle resulting in the release of the high pressure propellant gases. Subsequent photographs trace the development of the strong air blast and the propellant gas jet, schematically illustrated in Figure 1. At later times, the decay of the propellant gas jet due to the emptying of the gun tube is shown. Cranz recognized the qualitative nature of these photographs and attempted to obtain quantitative data by probing the muzzle jet[2]. His technique consisted of inserting conically tipped probes into the muzzle jet and taking spark schlieren photographs of the shock structure surrounding the probe tips. From the measured shock angle, the flow Mach number may be calculated using inviscid flow theory. However, in a similar effort to probe a steady, supersonic air jet, Ladenburg[3] noted the strong influence of the jet shock structure on the accuracy of this probing technique. Ladenburg concluded that the effect of shock-boundary layer interactions on the probes produced significant deviations from predictions of inviscid flow theory. The data of Cranz and Glatzel[2] reflect this situation. The velocity fields they show demonstrate strong anomalies in the vicinity of shock waves.

Cranz[1] notes that within the strong air blast formed at projectile separation the propellant gases expand from the muzzle exhibiting the flow structure of a supersonic, underexpanded jet. Therefore to obtain a better understanding of the propellant gas flow field, Cranz turned

*References are listed on page 78.

to investigations of steady jet structures. Cranz observes that the linearized theory of Prandtl[4] qualitatively predicts the behavior of the propellant gas jet. In particular, he notes that once the jet shock structure has grown to its maximum size, the subsequent decay of the jet as the gun tube empties results in the Mach disc[5] moving in toward the muzzle. Linearized theory predicts a variation in the characteristic wavelength of a supersonic jet that is proportional to the square root of the exit to surroundings pressure ratio. Thus, as the muzzle pressure decays, the jet structure collapses toward the muzzle.

The work of Cranz is typical of subsequent research into muzzle phenomena. Optical techniques are applied to obtain photographs of the muzzle gas flow field. Examination of the photographs shows that the muzzle exhaust goes through an initial period when the propellant gas jet and free air blast form in a highly unsteady, coupled manner. At later times, the blast moves sufficiently far from the muzzle region and becomes uncoupled from phenomena occurring there. During this "late" time, the propellant gases exhaust into a nearly undisturbed atmosphere. The structure of the propellant gas flow during this period is that of a supersonic, underexpanded jet. With the observation that over a significant portion of the exhaust cycle the muzzle gas flow has a typical jet structure, it becomes convenient to model the flow field using the techniques of steady jet or plume theory. This approach has been successfully used to model the flow over muzzle devices[6-11]. However, the gasdynamic loadings on the projectile in the muzzle gas flow are applied at very early times, and the applicability of the steady jet theory must be established.

Oswatitsch[12] examines this problem and notes that the initial unsteady expansion of the muzzle gases could be modeled as a spherical blast. Using the method of characteristics, he computes the blast field that would be generated about the muzzle of a gun. He observes that in the region between the muzzle and the second or inward-facing shock, temporal variations in flow properties occur at a rate proportional to the change in the muzzle properties. Since the muzzle properties change slowly relative to the time scales of the blast field growth and projectile residence in the muzzle region, Oswatitsch concludes that this region, between the muzzle and the inward facing shock, may be approximately modeled by steady jet theory. He further notes that since the highest pressures exist in the neighborhood of a few calibers of the muzzle, loadings on the projectile may be approximated by computing a projectile motion through a steady jet flow field.

The model proposed by Oswatitsch neglects certain important features of the muzzle gas flow. Among them are the effects of initial propellant gas expansion between the base of the projectile and the muzzle rim and the effects of interactions between the precursor and propellant gas flows. Since these features occur near the muzzle where gas pressures are maximum, a more exact treatment of this portion of the problem would appear justified. Another problem that steady jet theory can not treat

is the details of the development of the air blast. Since the initial growth of the blast is directly coupled to the growth of the propellant gas jet, any attempt to construct a model of the air blast in the immediate vicinity of the weapon would require information on the nature of this coupling.

Recently, a number of attempts[13-17] have been made to apply finite difference techniques to the calculation of the properties of these type flows. The calculations are capable of predicting the development of the muzzle gas flow in great detail; however, the accuracy and validity of these calculations must be compared with experiment. At present, the body of quantitative data relating to the muzzle flow field is extremely limited. This report presents the results of an experimental survey of the muzzle flow about a 5.56mm M-16 rifle firing standard ball ammunition. The technique used is time resolved spark shadowgraphy. Detailed trajectories of observable discontinuities are constructed. An analytical technique is presented which permits the reduction of the data so as to produce property profiles.

II. EXPERIMENTAL APPARATUS AND TEST TECHNIQUES

Data was taken of the phenomena about the muzzle of an M-16 rifle firing ball ammunition. The weapon has a nominal muzzle diameter of 5.56mm, a barrel length of 470mm, and a twist of rifling of 1 turn in 305mm. The ammunition fired was from a single lot, number FA 565. The projectile was ball M-193 weighing 54.1 grains with a length of 19.1mm. The propellant was 27.5 grains of WC 846. The muzzle velocity was measured to be 945 meters per second.

Since data was to be obtained optically, a technique was required which provided penetration of the muzzle gas jet without suffering from overexposure due to muzzle flash. Of the several techniques available[18], a spark shadowgraph approach was selected which uses backlighting in conjunction with a Fresnel lens to reduce exposure, Figure 2. The technique places a spark source and the object of interest on one side of a Fresnel lens. The spark source is beyond the focal point while the object of interest is between the focal point and the lens. In this manner, the light from the source is focused at a point on the opposite side of the lens while the luminosity from the object of interest is diffused away. The camera is positioned with its objective lens at the source image point and is focused on the plane of the Fresnel lens. In this manner, shadowgraphs may be obtained using the spark to provide stop-action without overexposing the film in the open shutter camera. To provide sufficient light for optical penetration of the muzzle gases, a unique circuit design was developed for the operation of an air gap spark source.

The typical ballistic range spark source is designed to minimize inductance through the coaxial mounting of capacitors. This provides a bright source of approximately 0.5 microsecond duration. To increase the

source strength while maintaining the spark duration of such a source requires careful component selection and circuit design. An alternative approach to the construction of a higher energy circuit is the incorporation of a current interrupter. The circuit is illustrated in Figure 3. A 0.5 microfarad capacitor charged to 8.5 kilovolts is fused through an exploding wire in series with an arc light source. The wire is selected[19] to vaporize at the first quarter cycle peak, thereby opening the circuit. The cold resistance of the wire is low. The resistance increases out of phase with the current flow rising sharply near the quarter cycle peak where the wire explodes. This provides for minimal diminishment of the power delivered across the arc during the light output period. A comparison between the typical behavior of the fused and unfused circuits is shown in Figure 4.

To investigate the effectiveness of this source, a qualitative measurement of the light output of the arc was made for the cases with and without the exploding wire. It is recognized that a more valid comparison of sources would be between this source and a typical coaxial capacitor type; however, this will provide an illustration of the principle involved. Figure 5 shows the two output curves taken from an uncalibrated phototube. The advantage of the fuse shut off is readily seen. The source with the exploding wire decreases from the peak luminosity much more rapidly than the other source. This technique allows for the construction of high intensity, short duration arc light sources with locally available materials and relatively simple circuitry. It must be noted that the effects of ionization within the air gap may limit the intensities and duration of light output.

It is advantageous to obtain multiple photographs of one firing; therefore, a set of three spark sources was used in each test. Using the Cranz-Schardin method[18], it is possible to obtain multiple, sequential shadowgraphs of a single event. The basic approach is to place an array of sparks on one side of a lens and to focus them on the objective lenses of a complimentary array of cameras on the opposite side of the lens. Either shadow or schlieren photographs may be obtained from the apparatus which essentially is identical to the schematic shown in Figure 2 with the addition of multiple sparks and cameras. By adjusting the delay between spark firings, a sequential history of the events of interest is obtained. The number of photographs taken in this manner is limited by the geometry and physical dimensions of the spark and photographic equipment and by the dimensions and quality of the main lens.

In the current tests, three sequential photographs are obtained from each firing. The experimental apparatus and pertinent dimensions are shown in Figure 6. A set of three photographs of a single firing are shown in Figure 7. The sequence shows the precursor flow field, the propellant gas flow field at early time (projectile in residence), and the propellant gas flow field at late time. Photographs may be obtained at any time desired through adjustment of the spark gap

triggering apparatus. Triggering is initiated by the interruption of a light beam passed across the muzzle of the weapon. The interruption is sensed at a photoamplifier with its sensitivity adjusted such that the arrival of the precursor tube gas flow provides the initial sensed interruption. The output signal of the photoamplifier is fed into a set of time delay generators which permit the firing of the spark gaps at delays of from 0-10,000 microseconds. The delays are preset such that the spark gaps fire in the desired sequence. The times of spark firings are measured by looking at the gaps with photodiodes and recording the signals on counters. These counters have a least count of ± 0.1 microsecond. Once testing was initiated, it was possible to set the triggering apparatus such that an event could be photographed to within 5 microseconds of the desired time.

To construct a time-displacement history of observable discontinuities, a test technique is used which gives a reliable time base to the sequence of three photographs and permits the correlation of data from various firings. The basic assumptions of the technique are that the projectile velocity is constant during its travel through the muzzle gases and that the projectile velocity is consistent from shot to shot. Once these assumptions are made, it is necessary to insure that at least one photograph in each sequence of three contains an image of the projectile. By measuring the distance between the projectile base and the muzzle of the gun, a reference distance is obtained. Division of this distance by the known muzzle velocity yields a reference time (this approach was used by Smith[10] in a multiple-exposure application). In these tests, time zero is defined as the time when the base of the projectile separates from the muzzle of the gun. Once the reference time for one photograph of the sequence is obtained, it is a simple matter to use the measured intervals between spark firings to obtain the time of each photograph relative to the defined time zero. To illustrate this procedure, consider the photographs shown in Figure 7. The center photograph contains the projectile which is a distance of 156mm (measured to the projectile base) from the muzzle. Division by a reference projectile velocity of 945 m/sec yields a time for this photograph of 165 microseconds. The measured time intervals of the other photographs to the reference photograph are - 185 and + 1035 microseconds. This yields times of -20 and + 1200 microseconds, respectively, relative to time zero. Variation of these delays permits the construction of a complete time history of the gun emptying process.

The accuracy of this technique depends heavily upon the validity of the basic assumptions. While no measurements of projectile acceleration in the muzzle flow are available, estimates[20,21] of the incremental velocity increase through this region have been attempted. Both estimates rely on the assumption that the projectile is subject purely to linear acceleration in the muzzle flow with no change in its spin rate. A comparison of the measured spin rate with that predicted from the known twist of rifling and measured velocity indicates that the projectile

velocity had to increase by approximately one percent through the muzzle flow. It has been shown[12] that the gasdynamic forces on the projectile are maximum near the muzzle decreasing to negligible values within two or three calibers of the muzzle. Therefore, the projectile is accelerated near the muzzle and remains at a nearly constant velocity through the remainder of its flight through the muzzle gases. For this reason, the reference velocity is taken to be that value measured in the first thirty calibers of travel. This velocity was measured using the described triple shadowgraph apparatus in a series of ten firings. Spark triggering delays were set such that the projectile was in each photograph. The consistency of projectile velocity from shot to shot was measured to be plus or minus one percent of the nominal value of 945 meters per second. This value is similar to that measured in other studies[22]. Thus, both of the sources of error are on the order of one percent of the nominal projectile velocity which transforms to a variation between real and measured time of ± 0.1 microseconds per centimeter of projectile travel. This value is of the same order as the counter accuracy and well within the 0.5 microsecond duration of the spark source. Thus, velocity variation is not expected to be a significant source of experimental inaccuracy. Data shown in the subsequent sections will demonstrate the overall validity of the measurement technique.

III. RESULTS

More than sixty rounds were fired in the test program resulting in approximately 200 photographs for analysis. In order to obtain an initial display of the data, the motion of the observable discontinuities along the axis of symmetry was plotted. Figures 8 and 9 show the data taken of the precursor flow, i.e., tube air forced out ahead of the projectile, and propellant gas flow, respectively. The plots show the motion of the normal shock (Mach disc), contact surface and free air blast along the axis of symmetry (bore line) versus time measured from the instant the projectile base clears the muzzle. The data is seen to be consistent and repeatable. It should be noted that only three photographs are taken of a single shot; therefore, these plots are a composite of many firings and indicate the validity of the assumptions of the experimental technique. From these plots, a sequence of 31 photographs was selected as being representative, Figure 10. The photographs clearly show the growth of the precursor flow, the appearance of the projectile at the muzzle, the release and growth of the propellant gas flow, and the decay of the propellant gas jet. In this report, the discussion of these features of the muzzle flow will be divided into three phases: Precursor Flow Development, Propellant Gas Flow Development, and Quasi-Steady Propellant Gas Jet Decay.

A. Precursor Flow Development

The precursor flow forms as tube gases are pushed out of the gun bore by the moving projectile. These gases are composed of air and residual and leaked propellant gases. Since the current tests involved single

firings with relatively long times between shots, the amount of residual propellant gases present in the gun tube is minimal. Additionally, for the weapon considered in these studies, leakage is not significant and will be neglected. Thus, the precursor flow is composed of the air present in the gun tube ahead of the projectile. The calculation of the properties of this air as it is set into motion by the accelerating projectile is a straightforward problem of one-dimensional gasdynamics. Oswatitsch[12] used the method of characteristics coupled with the Rankine-Hugoniot relations to construct the flow in front of projectiles for both subsonic and supersonic launch velocities. A schematic of the flow development for supersonic launch is shown in Figure 11.

As the projectile accelerates, compression waves move ahead of it into the tube air. These waves rapidly coalesce into a shock which gains in strength as more compression waves reach it. Since the shock strength varies as it moves down the gun tube, entropy gradients obviously exist in the slug of accelerated tube air. However, Oswatitsch[12] points out that an adequate approximation of the properties of the gas behind the shock upon arrival at the muzzle can be obtained under the assumption that the gas velocity is equal to the projectile launch velocity. The remaining properties are calculated by applying the Rankine-Hugoniot relations. He bases this upon the fact that for high speed projectiles, the most significant accelerations occur near the breech leaving the projectile velocity relatively constant over most of the latter portion of its in-bore trajectory. Using this approximation, the variation of precursor gas properties at the muzzle are calculated and plotted as a function of projectile launch Mach number, Figure 12.

This figure shows the variation of the pressure and Mach number of the precursor gases and velocity of the precursor shock as the projectile launch Mach number changes. The pressure of the precursor gases increases rapidly with the projectile launch velocity. Thus, for high velocity launch, tube air back pressure on the projectile can be significant. The precursor gas Mach number becomes unity for a projectile launch Mach number of 1.35. Once these gases reach a sonic velocity, signals generated at the muzzle can not propagate back up the tube; thus, the gas properties remain constant until the projectile reaches the muzzle. The launch Mach number of the current tests is 2.75. For this value, the precursor gas pressure is 15 atmospheres, the Mach number is 1.48, and the shock leaves the muzzle at a velocity of 1240 m/s.

As the precursor gas flows from the muzzle, it expands two-dimensionally forming an underexpanded, supersonic jet. The growth of the precursor jet displaces the surrounding air generating a nearly spherical blast, Figure 10. The development of this type flow has been examined in connection with shock propagation from the open end of shock tubes[23-26]. These studies show the initial expansion of the gas to be quite complex. Two-dimensional, unsteady expansions propagate into the flow from the edge of the muzzle, Figure 13. These waves move along the shock front turning the flow behind it away from its purely axial direction. In the

precursor flow, these waves form into the stationary wave structure of a steady jet. While along the precursor boundaries and in the blast field, a highly unsteady flow continues to exist. The blast is seen to propagate into the atmosphere in a nearly spherical manner. In fact, the spark shadowgraphs, Figure 10, indicate that the Mach disc, contact surface, and blast form concentric spherical surfaces during the early growth of the precursor flow field. As the blast expands radially, its strength diminishes due to the deposition of its energy into a geometrically increasing volume of air. The data shows the effect of radial expansion, Figure 8.

The initial discontinuity velocities decrease rapidly until the jet normal shock (Mach disc) becomes stationary, the contact surface slows to a subsonic velocity, and the blast diminishes in strength and propagates at the sonic velocity. It is of interest to compare the location of the precursor jet Mach disc with the location predicted by steady jet[27-28] correlations. For steady jets, the following empirical relation applies for Mach disc location:

$$\frac{X}{D} = 0.70\, M_e \left(\frac{\gamma_e\, p_e}{p_\infty}\right)^{\frac{1}{2}} ;$$

our computations give:

$$M_e = 1.48;$$

$$p_e/p_\infty = 15.0;$$

$$\gamma_e = 1.4;$$

substitution gives a steady Mach disc location

$$X/D = 4.75;$$

Figure 8 shows the Mach disc experimentally reaches a steady state

$$X/D = 5.50.$$

The difference of 0.75 calibers or 4.17mm may be attributed to two effects. First, the muzzle values used are based on an assumption of constant entropy throughout the precursor gases. Obviously, this is not the case. The projectile increases in velocity at a finite rate thereby causing the shock strength to increase from zero to some finite value. This creates an entropy gradient in the flow which corresponds to a flow Mach number decrease from the projectile to the precursor shock. Since the gas flowing through the Mach disc at late times is the gas nearest the projectile, the exit Mach number would be greater than the above value. The second effect is the interaction between the

blast and jet flows. The surroundings seen by the precursor jet is part of a blast field, making the assumption of atmospheric pressure of questionable validity. Since a typical property of a blast flow is overexpansion behind the lead shock wave, the pressure sensed by the jet could be lower than atmospheric. Obviously, this would have the effect moving the normal shock further from the muzzle.

If the time-displacement histories of Figure 8 are plotted logarithmically, an interesting result is obtained, Figure 14. The data is plotted in a time scale which commences when the precursor shock first breaks the muzzle at roughly -100 microseconds. The following power laws are seen to apply:

$$X_{\text{Mach Disc}} \sim t^{0.625}$$

$$X_{\text{Cont. Surf.}} \sim t^{0.727}$$

$$X_{\text{Blast}} \sim t^{0.767}$$

This type of power law variation when combined with the overall spherical nature of the flow is strongly suggestive of the applicability of blast wave theory to this flow.

To obtain a comprehensive view of the overall flow development, discontinuity contours are constructed at selected time intervals, Figures 15A - 15C. Of particular interest is the development of the precursor jet structure, Figures 15A and 15B. The figures show the strong time dependence in the longitudinal direction; however, once established, the lateral structure remains unchanged over the observed jet lifetime. A simple explanation would be to claim that since the flow inside bounding shocks is supersonic, no downstream disturbances are sensed upstream. However, this explanation neglects the fact that the surrounding air can carry signals around the jet periphery. What the data seems to indicate is that such signals are extremely weak and, further, that the pressure in the lateral portion of the blast field rapidly decreases to a nearly constant value soon after the precursor flow commences. This data demonstrates the applicability of steady jet theory to the flow between the muzzle and the Mach disc. To account for the motion of the Mach disc, an analysis of the blast layer is required. The data corroborates an identical conclusion made by Oswatitsch[12], based on a theoretical analysis, showing that the flow upstream of the Mach disc could be treated with a quasi-steady jet theory. The quasi-steady nature of the solution is brought about by the dependence of jet properties upon conditions existing at the muzzle of the gun. In the present case, the muzzle flow properties are nearly constant. Even for the propellant gas efflux, it will be shown that the muzzle properties vary at a rate much slower than the rate of signal propagation through the jet.

The final figure in the sequence, Figure 14C, shows the development of the precursor blast. At early times, the effect of the flow momentum is seen in the blast shock structure. Since the majority of the flow momentum is concentrated along the axis, the energy imparted to the blast is greatest in that vicinity. Thus, the blast velocity is highest near the axis dropping off around its periphery. However, as the blast grows, the effect of the jet structure becomes less obvious. At late times, the blast wave is spherical in shape and propagates at the sonic velocity. The later contours are incomplete due to the arrival of the propellant gas flow. When the propellant gases are released, they rapidly expand effectively destroying the precursor flow structure.

B. Propellant Gas Flow Development

Prior to release, the propellant gas velocity varies from zero at the breech to that of the projectile at the muzzle. While the projectile launch velocity may be supersonic relative to the atmospheric speed of sound, the high temperature of the propellant gas results in a speed of sound which may be three or four times greater than the ambient value[12]. For the M-16 used in these tests, the Mach number of the propellant gas at the base of the projectile is approximately 0.7. Thus, when these gases are released, an expansion propagates back up the gun tube bringing the muzzle velocity to a sonic value. The velocity remains sonic until the gun tube is nearly exhausted. The calculation of the gas properties at the muzzle during the gun tube emptying is not tractable using standard interior ballistic techniques. However, Celmins[29] has performed a method of characteristics computation which produces consistent results, Figure 16.

The plot of velocity at the muzzle versus time shows the effect of the one-dimensional expansion to sonic velocity. The gas arrives at the muzzle with the velocity of the projectile. Immediately upon release, it expands to a sonic velocity. Thereafter, the velocity and temperature decrease while the Mach number at the muzzle remains at unity. The second plot shows the variation in muzzle pressure with time. Since the Mach number is one, the muzzle velocity and pressure plots are sufficient to compute all other gas properties given that $\gamma = 1.24$ and $R = 325\ m^2/s^2\ {}^{o}K$. Using a piezoelectric gage[30] installed at the gun muzzle, Baran and Brosseau[31] obtained measurements of the muzzle gas pressure during the emptying process, Figure 17.

The pressure is non-dimensionalized with respect to atmospheric and plotted against time on a semi-log scale. A sample data trace is included in the plot to show the noise level present in such measurements. Data readings were taken from the midpoint of the trace at a given time; however, there is considerable latitude for the selection of this value, especially at early time. With this in mind, the agreement between the theoretical and experimental values is quite good. Also shown on the figure is the extent of projectile residence in various portions of the propellant gas flow. It is apparent that over the periods shown, the muzzle properties are not strongly varying. Additionally, steady jet

theory[32,33] shows that at these high pressure ratios, the jet structure is only weakly effected by pressure ratio variation. Again, this supports the contention of Oswatitsch[12] that within the muzzle jet the flow is nearly independent of time.

The motion of observable discontinuities along the axis of symmetry has been plotted in Figure 9. The data show the initial rapid propagation of the propellant gas around the projectile. Radial expansion causes the discontinuity velocities to drop off such that after 140 microseconds, the projectile penetrates the blast and passes into free flight. During the first twenty microseconds, the presence of the projectile significantly affects the flow field development. At uncorking, the propellant gas is forced to expand around the projectile and into the precursor flow field. This expansion and the velocity field of the precursor flow seem to prevent the forward portion of the blast from building in strength until the precursor flow has been completely engulfed by the propellant gases, e.g., see Figure 10 shots of -3 through +37 microseconds. The details of the interaction between the propellant and precursor flows are difficult to see in the data. There are apparent changes in the slopes of the propellant gas discontinuity trajectories at 17, 27, and 65 microseconds when intersections with precursor discontinuities occur, Figure 9. However, obscuration of the photographs by dense powder gas prevents a reliable assessment of these interactions. The trajectory of the normal shock is constrained by the projectile base until 50 microseconds when it begins to separate and merge with the Mach disc. Subsequent to this time, the motion of the Mach disc is governed by the variation in the blast field pressure and by the decay of the muzzle pressure. The motion of the contact surface and blast do not appear to be dependent upon the projectile presence at late times; however, the initial expansion of the propellant gases is controlled by both the projectile and the precursor flow. The discontinuity trajectories are plotted logarithmically in Figure 18.

While the motion of the jet normal shock does not appear to follow a power law variation, the motion of the contact surface and blast obey the following:

$$X_{\text{Cont. Surf.}} \sim t^{0.445}$$

$$X_{\text{Blast}} \sim t^{0.608}$$

Erdos and Del Guidice[34] point out that for a constant rate of energy addition, blast wave theory[35,36] predicts a spherical, strong blast motion which obeys:

$$X_{\text{Blast}} \sim t^{0.600}$$

A similar observation was made by Buckmaster[26] for the case of a cylindrical blast with constant energy addition. It is of interest to

examine the actual rate of energy efflux from the muzzle as predicted by Celmins[29]. Since he uses a one-dimensional flow model, the rate at which energy passes the muzzle is:

$$\dot{E} = \rho_e u_e \left(c_v T_e + \frac{u_e^2}{2}\right) A_e.$$

Under the assumption of a perfect gas:

$$p_e = \rho_e R T_e,$$

$$c_p - c_v = R,$$

$$a_e = (\gamma R T_e)^{\frac{1}{2}},$$

the energy efflux may be expressed as:

$$\dot{E} = \frac{p_e u_e}{\gamma - 1} \left(1 + \frac{\gamma(\gamma - 1)}{2} M_e^2\right) A_e$$

For sonic exit velocities this reduces to:

$$\dot{E} = p^* u^* \left(\frac{\gamma (\gamma - 1) + 2}{2 (\gamma - 1)}\right) A_e$$

Define a parameter, ξ, as being the ratio of the energy which has passed the muzzle up to time, t, to the total energy of the propellant gases:

$$\xi = \frac{\int_0^t \dot{E}\, dt}{\int_0^\tau \dot{E}\, dt}$$

Where: τ = time to gun emptying

Substituting for $\dot{E}$ and noting that γ and A_e are constant:

$$\xi = \frac{\int_0^t p^* u^*\, dt}{\int_0^\tau p^* u^*\, dt}$$

The variations of p^* and u^* with time are given in Figure 16. Performance of the integration results in the plot of the variation of ξ with time shown in Figure 19. During the first 100 microseconds, the variation is seen to follow a nearly linear power law:

$$\xi = t^{.956}$$

Since

$$\frac{d\xi}{dt} = \frac{\dot{E}}{E_\tau} \sim \text{constant},$$

it is seen that the propellant gas energy passes the muzzle at a nearly constant rate over the initial portion of the gun tube emptying. Thus, it would appear that the observed data closely follows the predictions of strong blast theory at early time.

The full contour plots of discontinuity location at selected times are shown in Figures 20A - 20C. Figure 20A depicts the growth of the jet shock structure. Like the precursor jet, the propellant gas jet growth shows strong temporal variations in the longitudinal direction. The normal shock moves continuously away from the muzzle for the first 300 microseconds. During this period, the intercepting shock structure remains unaltered once established. After 300 microseconds, the muzzle pressure decay causes the jet structure to begin collapsing toward the muzzle. This process will be treated in the following section. The data indicate that while the projectile locates the position of the normal shock on the axis, the off-axis Mach disc structure forms due to interaction between the jet and blast fields. After 91 microseconds, the projectile no longer affects the internal shock structure of the jet.

Figure 20B plots the growth of the propellant gas contact surfaces. The jet grows rapidly in time again exhibiting relatively constant lateral dimensions once they are established. As long as it was in the field of view of the optics, the forward front of the jet moved downrange. At late times, turbulent mixing caused the lateral dimensions to grow very large; however, by this time, the supersonic jet core had collapsed. Apparently carried by its own momentum, the turbulent "cloud" moves slowly downrange, e.g., Figure 10, times 520 through 6400 microseconds. While the presence of a vortex ring at the boundary of these type flows is a well-documented fact[1,2, 7-12, 23-25], the turbulence along the jet boundary prevents any inference of the details of its growth and subsequent motion.

The history of the air blast formed by the release of the propellant gases is shown in Figure 20C. Due to leakage around the boat tail of the projectile, the blast formation precedes the separation of the projectile base. The growth of the blast is most rapid in the downrange direction. This is due to both the directed nature of the propellant gas flow and the presence of the precursor gas velocity field. The propellant blast continues to maintain its downrange strength for a considerably longer period than did the precursor gas. Only as it passes from the field of view, does the blast begin to exhibit a roughly spherical nature.

Since the muzzle blast is composed of two interacting but distinct type of flows, the propellant gas jet and the free air blast, it is of

interest to use existing treatments of these flows to increase the amount of information which may be acquired from the experimental data. Owen and Thornhill[37] use the method of characteristics to show that for steady, supersonic, highly underexpanded jets, the flow properties within the bounding shock structure are not effected by variations in the ambient pressure. This conclusion is supported by interferometric analysis of air jets conducted by Ladenburg[38]. Using a method of characteristics code developed by NASA[33], N. Gerber of BRL computed the properties of a sonic jet with γ=1.25 exhausting at various pressure ratios, Figure 21. The variation of the flow Mach number along the jet centerline is seen to be unaffected by order of magnitude changes in the pressure ratio. Thus, using the "universal" jet core postulation of Owen and Thornhill, all flow properties of the propellant gas jet may be evaluated in the region bounded by the intercepting and normal shock waves. Further, since the experimental data provides information on shock location, velocity, and inclination, the Rankine-Hugoniot relations may be used to compute shock jump conditions.

Also shown in Figure 21, is the centerline Mach number variation computed by Oswatitsch[12] using the assumption that the propellant jet flow may be treated as a spherical source. Comparison with the method of characteristics solution shows that the source flow model predicts a more rapid expansion from the muzzle properties. However, the two analyses predict similar far field behavior. It is interesting to note that Oswatitsch based this source model on a method of characteristics computation which indicated that the jet streamlines diverge in a source-like manner after initial expansion near the muzzle. Oswatitsch shows that the center of this divergence is located 0.2 calibers ahead of the muzzle; however, he locates the origin of his analytical source model 0.5 calibers behind the muzzle in order to provide a sonic exit flow. It is noted that displacement of the source origin to the former location (+0.2 calibers) would produce a predicted variation nearly identical to that of the method of characteristics results. This is of interest since the source flow solution is analytic whereas the method of characteristics requires a numerical solution.

Having obtained a description of the jet flow properties, it is necessary to obtain a method to treat the blast wave and contact surface. The blast shock velocity may be obtained from the experimental data. The Rankine-Hugoniot relations then permit the computation of the shock jump conditions. The velocity of the contact surface may also be measured; however, there are no techniques available to compute the properties of the gases on either side of this discontinuity. In summary, it is possible to obtain information on the gas properties from the muzzle of the gun up to and on the other side of the jet shock structure. The gas properties behind the blast shock may be calculated, and the velocity of the contact surface may be measured. However, other gas properties in the layer between the jet shock structure and the blast shock may not be obtained. To demonstrate the procedure, a calculation of the gas properties along the axis of symmetry will be performed.

The discontinuity velocities of the propellant gas flow may be obtained by differencing the traces of Figure 9. The resulting variations are shown in Figure 22. This phase plane representation shows the velocity of each observable discontinuity versus axial location. Lines of constant time are also indicated. Velocities are non-dimensionalized with respect to the projectile velocity; thus, the initial blast and contact surface velocities are seen to be significantly higher than the projectile velocity but drop rapidly in the axial direction. At early times, the jet normal shock is seen to be fixed to the projectile base. Property calculations are started at 80 microseconds when projectile interaction effects are minimal.

Using the calculations of Celmins[29], Figure 16, the muzzle properties at a given time are obtained. Gerber's results, Figure 21, give the centerline Mach number distribution from which all other flow properties may be computed using the isentropic flow relations and known muzzle properties. The measured normal shock location and velocity are coupled with the jet calculation and the Rankine-Hugoniot relations to obtain shock jump conditions. The contact surface velocity is measured. From the shock relations and the measured blast shock location and velocity, conditions in the air just behind the blast shock are computed. The velocity profile along the axis calculated in this manner is shown in Figure 23.

The velocity increases rapidly from the muzzle value as the propellant gases expand through the jet. At the moving Mach disc, the velocity drops sharply and remains at a low level through the gas layer between the Mach disc and blast shock. Since the centerline velocity distribution changes slowly (affected only by the muzzle property variation, Figures 16 and 17), the remaining plots of velocity distribution show only the behavior in the region between the Mach disc and the blast shock, Figures 24. Profiles for times from 80 through 240 microseconds are shown. In all cases, the velocity decreases from the Mach disc to the contact surface due to radial expansion of the subsonic flow. Between the contact surface and blast, a reversal in behavior occurs. Initially, the velocity at the contact surface is higher than the gas velocity behind the blast shock. After 120 microseconds, the contact surface velocity drops below the gas velocity at the blast. This could indicate a region of uncoupling where the blast flow is no longer strongly driven by the propellant gases and begins to decay more or less independently.

The centerline pressure distribution was also calculated, Figure 25. The pressure drops from the muzzle value extremely rapidly. At the Mach disc, the flow is recompressed, but to a pressure considerably below that existing in the air at the blast shock. No data point is shown for the contact surface since only its velocity is known. The remaining pressure distributions in the gas layer between the two shock waves are shown in Figures 26. It is interesting to note that at 180 microseconds, the pressure behind the Mach disc begins to drop below

atmospheric, e.e., the ratio p/p_∞ becomes less than unity. This indicates that the overexpansion typical of spherical blast fields is affecting the pressure in the jet. Thus, while the blast shock may not be driven by the jet, it is apparent that the jet senses variation in the blast field. This behavior will be seen in the subsequent discussions on the propellant gas jet decay.

C Quasi-Steady Propellant Gas Jet Decay

During the first 400 microseconds after the propellant gas release, the supersonic jet structure grows to its maximum size. After this period, the structure decays due to the decreasing muzzle pressure, Figure 16. The motion of the propellant gas jet Mach disc along the axis of symmetry illustrates this behavior, Figure 27. As previously indicated, the axial position of the jet normal shock is constrained by the projectile base for the first 40 microseconds; thereafter, it separates from the projectile joining the jet Mach disc. The subsequent motion of the Mach disc is governed by the blast field growth and muzzle pressure decay. The time scales of these two phenomena are quite different. Radial expansion of the blast causes the pressure behind the blast shock to decay from a value of approximately 85 atmospheres at the muzzle (computed by assuming the propellant gases expand one-dimensionally into air from a pressure corresponding to the stagnation pressure behind the projectile just prior to exit) to 2.3 atmospheres in 200 microseconds, Figure 26. Compared to this order of magnitude variation in blast field pressure, the muzzle pressure decreases from 600 atmospheres at time zero to 450 atmospheres in 200 microseconds. To obtain an estimate of how the Mach disc motion is affected, the empirical relation obtained for the Mach disc location in steady jets is useful:

$$\frac{X}{D} = 0.70 \left(\frac{\gamma_e p^*}{p_\infty}\right)^{\frac{1}{2}}$$

In this case, the muzzle pressure is p^*, and the blast field pressure is the effective p_∞. Obviously, the order of magnitude variation in blast field pressure dominates Mach disc location at early times. Subsequent to 200 microseconds, the blast field pressure can no longer decay by orders of magnitude and the decrease of the muzzle pressure from 450 atmospheres, Figure 17, predominates.

The data shown in Figure 27 indicate these trends. Also shown on the figure is the Mach disc location as predicted by the steady state relation. The pressure ratio used corresponds to the values given by Celmins[29], Figure 17. In reaching its maximum separation from the muzzle at 400 microseconds, the Mach disc overshoots the value predicted by steady jet theory. This overshoot reflects the influence of the blast field overexpansion[35,39] on the supersonic jet structure. For spherical blasts in air, the momentum imparted to the gases processed by the blast field causes them to expand radially reaching pressures below atmospheric.

atmospheric, e.c., the ratio p/p_∞ becomes less than unity. This indicates that the overexpansion typical of spherical blast fields is affecting the pressure in the jet. Thus, while the blast shock may not be driven by the jet, it is apparent that the jet senses variation in the blast field. This behavior will be seen in the subsequent discussions on the propellant gas jet decay.

C Quasi-Steady Propellant Gas Jet Decay

During the first 400 microseconds after the propellant gas release, the supersonic jet structure grows to its maximum size. After this period, the structure decays due to the decreasing muzzle pressure, Figure 16. The motion of the propellant gas jet Mach disc along the axis of symmetry illustrates this behavior, Figure 27. As previously indicated, the axial position of the jet normal shock is constrained by the projectile base for the first 40 microseconds; thereafter, it separates from the projectile joining the jet Mach disc. The subsequent motion of the Mach disc is governed by the blast field growth and muzzle pressure decay. The time scales of these two phenomena are quite different. Radial expansion of the blast causes the pressure behind the blast shock to decay from a value of approximately 85 atmospheres at the muzzle (computed by assuming the propellant gases expand one-dimensionally into air from a pressure corresponding to the stagnation pressure behind the projectile just prior to exit) to 2.3 atmospheres in 200 microseconds, Figure 26. Compared to this order of magnitude variation in blast field pressure, the muzzle pressure decreases from 600 atmospheres at time zero to 450 atmospheres in 200 microseconds. To obtain an estimate of how the Mach disc motion is affected, the empirical relation obtained for the Mach disc location in steady jets is useful:

$$\frac{X}{\bar{D}} = 0.70 \left(\frac{\gamma_e p^*}{p_\infty}\right)^{\frac{1}{2}}$$

In this case, the muzzle pressure is p^* and the blast field pressure is the effective p_∞. Obviously, the order of magnitude variation in blast field pressure dominates Mach disc location at early times. Subsequent to 200 microseconds, the blast field pressure can no longer decay by orders of magnitude and the decrease of the muzzle pressure from 450 atmospheres, Figure 17, predominates.

The data shown in Figure 27 indicate these trends. Also shown on the figure is the Mach disc location as predicted by the steady state relation. The pressure ratio used corresponds to the values given by Celmins[29], Figure 17. In reaching its maximum separation from the muzzle at 400 microseconds, the Mach disc overshoots the value predicted by steady jet theory. This overshoot reflects the influence of the blast field overexpansion[35,39] on the supersonic jet structure. For spherical blasts in air, the momentum imparted to the gases processed by the blast field causes them to expand radially reaching pressures below atmospheric.

disc or incandescent particles. Dust generation evolves through the scouring action of the vortex ring and subsonic jet which continue to grow both laterally and longitudinally even after the gun is emptied.

IV. Conclusions

A set of experiments were conducted using an optical technique which permits the construction of accurate time-displacement histories of observable discontinuities about the muzzle of an M-16 rifle during firing. The data give a detailed description of the flow structure and permit development of selected property profiles. While both the precursor and propellant gas flows were observed, this section will consider the salient conclusions which may be drawn from the propellant gas data.

As it develops immediately after projectile launch, the propellant gas flow is composed of two distinct, but interacting, flow fields; a supersonic, propellant gas jet and a free air blast. The development of the propellant gas jet boundaries with time is shown to occur anisotropically. In the longitudinal or downrange direction, the jet boundaries grow continually for the first 400 microseconds. However, during this same period, the lateral jet boundaries remain invariant once established. This behavior is directly related to the blast field. In the longitudinal direction, a strong blast is generated; while in the lateral directions, the blast is weak and decays rapidly. After 400 microseconds, the blast and jet fields are weakly coupled, finally decaying independently after 800 microseconds.

Based on the experimental data, a model is proposed which permits the computation of property values. The basic assumption of the model is that within the bounding shocks, the propellant gas flow may be treated as a steady, supersonic jet. Using established models of the gun tube emptying and supersonic jet, all flow properties within the bounding shocks may be computed. From the experimentally determined shock locations, inclinations, and velocities, the jet properties are combined with shock jump relations to obtain property values in the shock layer. At late times, the experiments indicate that the propellant gas jet may be accurately modeled using steady jet theory.

The work also indicates areas requiring further study. At very early times, the initial unsteady expansion of the propellant gases around the projectile is not tractable with existing jet theory. Additionally, the interaction of the propellant gas and precursor gas flows should be considered. Also, the mixing of propellant gases with air and subsequent chemical kinetics is a problem of interest in the generation of flash. The late time motion of the subsonic jet and vortex ring are important if dust scouring is to be investigated. Finally, it should be emphasized that this data was taken from firing a single weapon under set conditions. The conclusions to be drawn from such a study require checking under different firing conditions. For this reason, future testing is planned on the M-16 and other weapons under a range of launch conditions.

Steady Jet Structure:

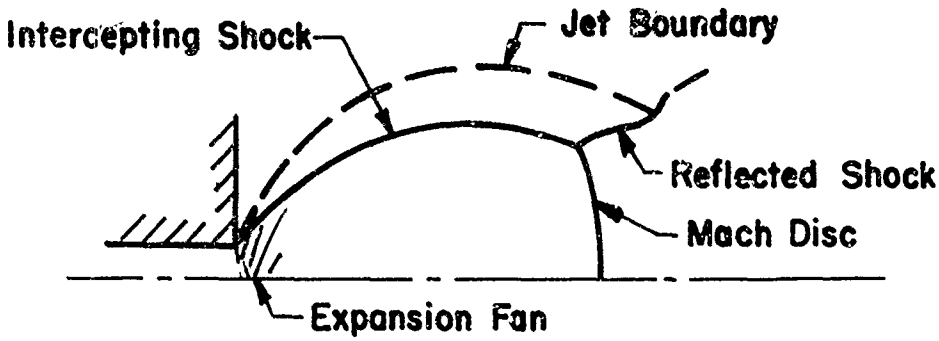

Muzzle Flow Structure:

Precursor Gas:

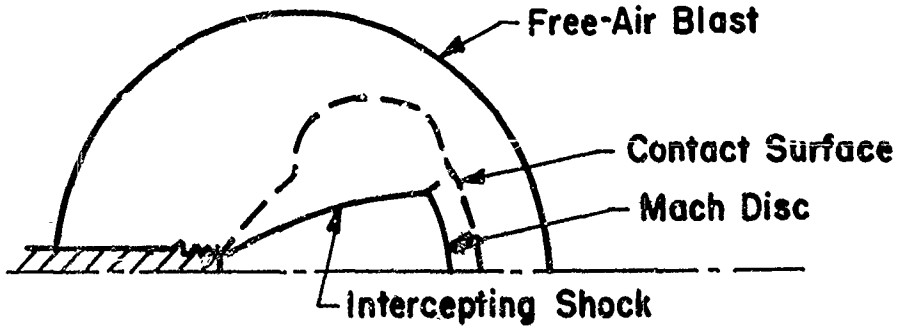

Propellant Gas:

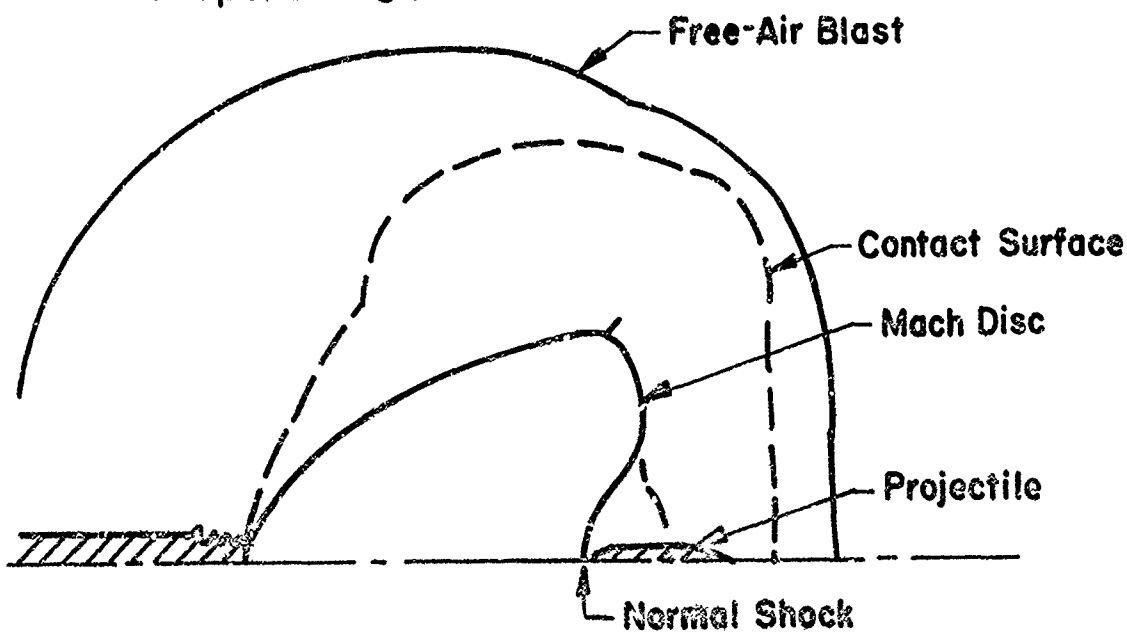

FIGURE 1 FLOW FIELD SCHEMATICS

CAMERA : 4 X 5 SPEED GRAPHIC, 178mm , f 2.5
FILM : KODAK TRI-X ORTHO
SOURCE : 0.020" APERTURE, INTERRUPTED AIR GAP SPARK
LENS : 45.7CM. X 60.9CM. --- 63.5CM. F.L.

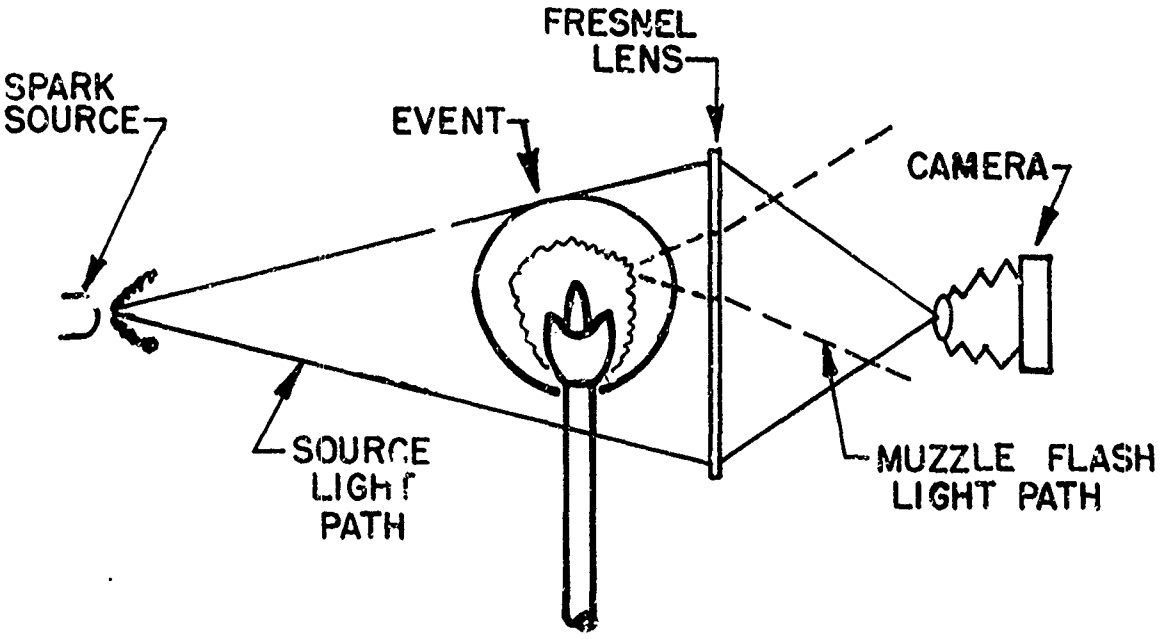

FIGURE 2 OPTICAL ARRANGEMENT

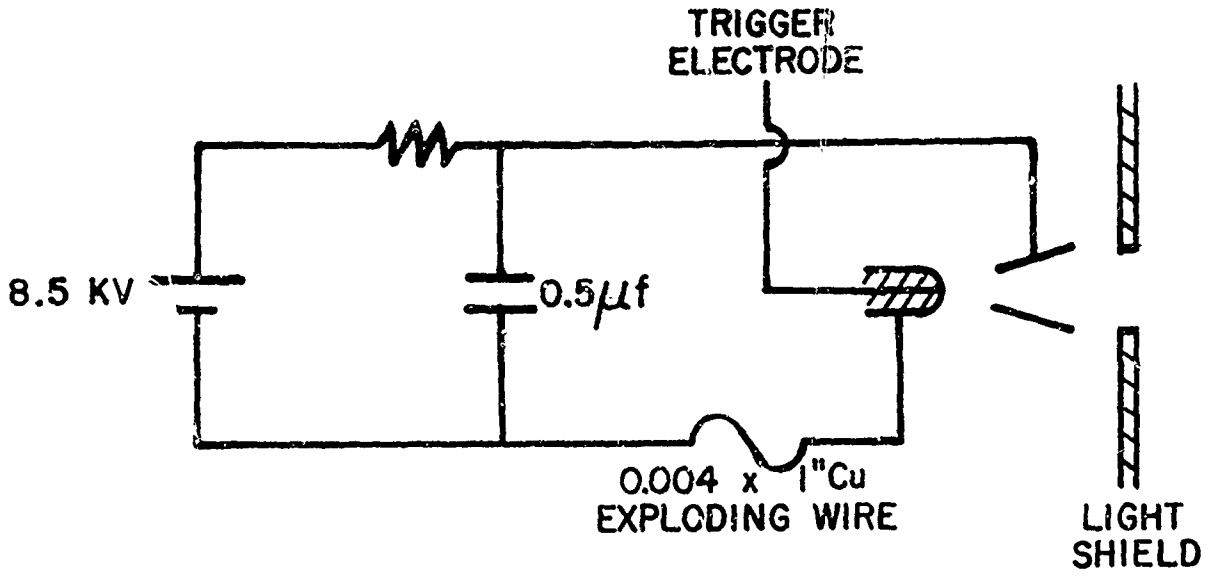

FIGURE 3 SPARK SOURCE CIRCUIT

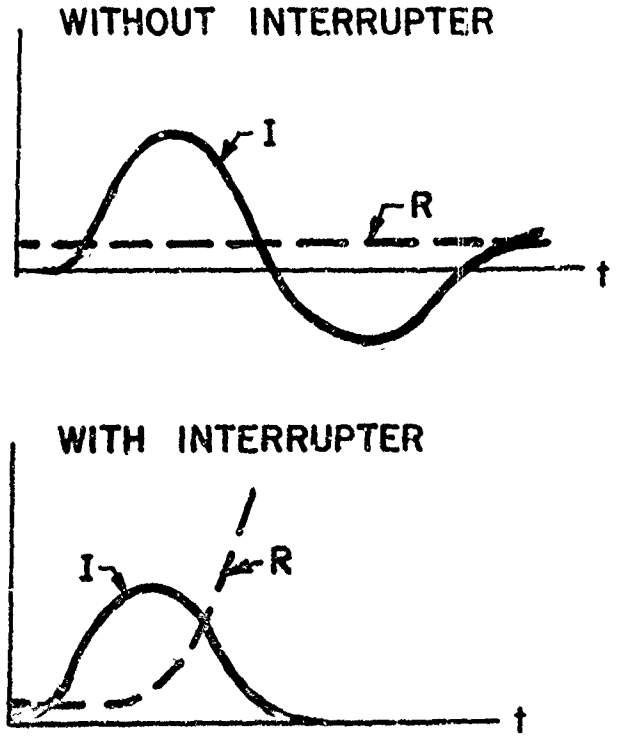

FIGURE 4 CIRCUIT ELECTRICAL PROPERTIES

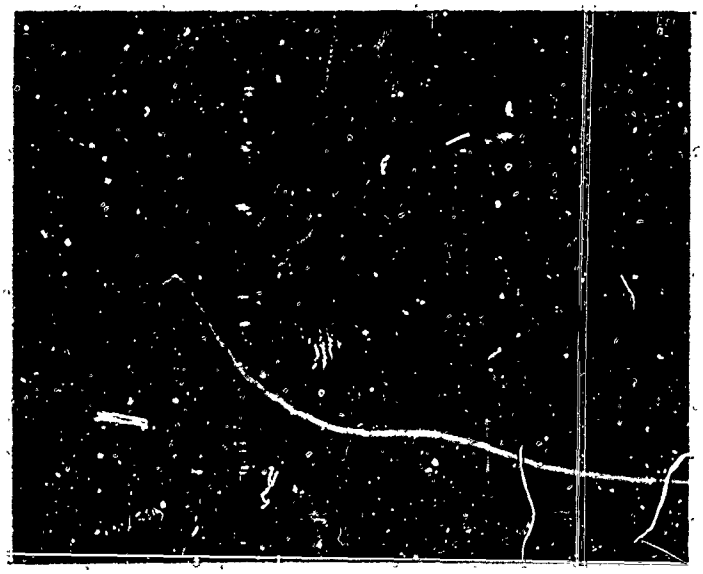

Without Interrupter

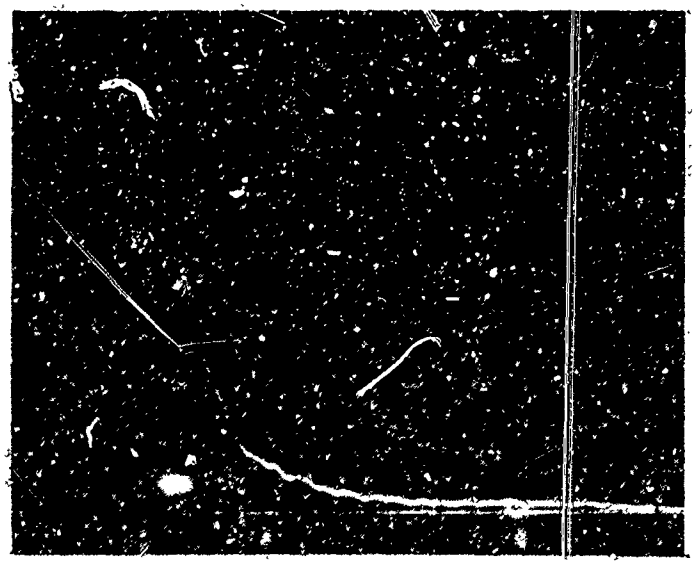

With Interrupter

FIGURE 5 LIGHT OUTPUT OF SPARK GAP
(I vs t ; 0.5 μsec/div.)

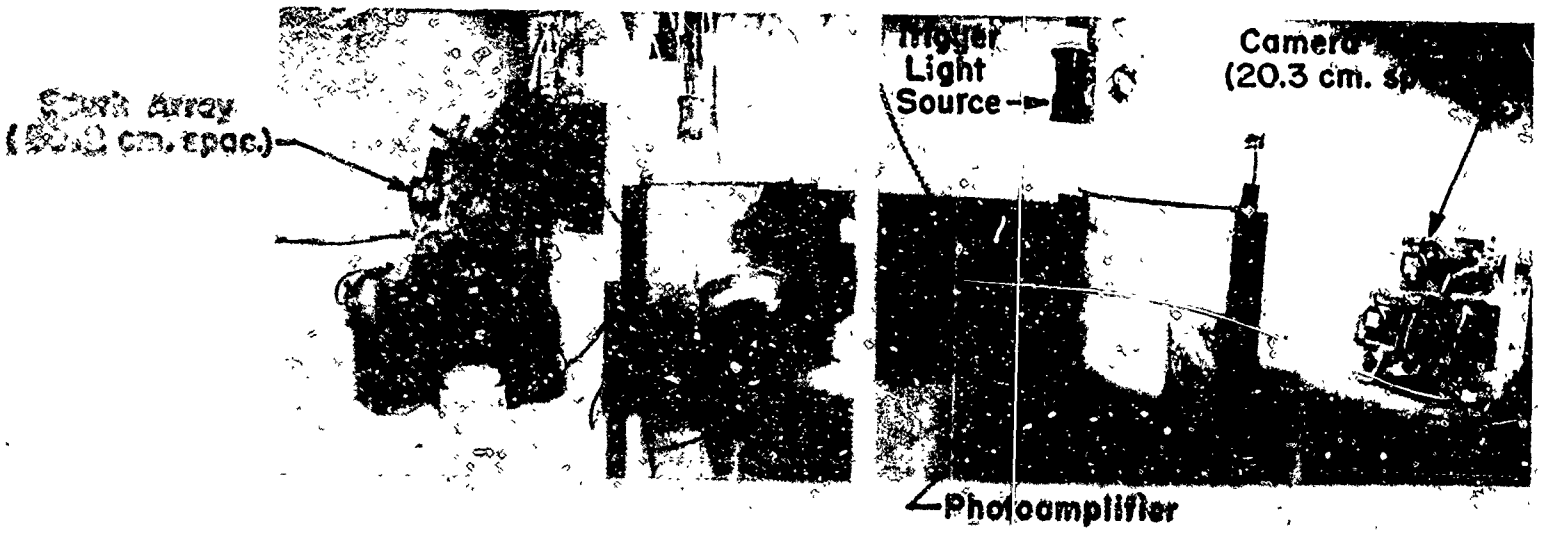

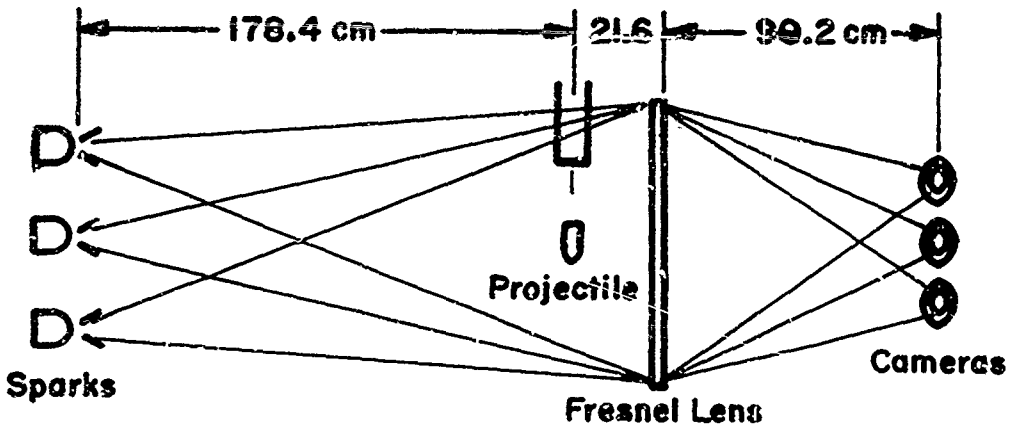

FIGURE 6 EXPERIMENTAL APPARATUS

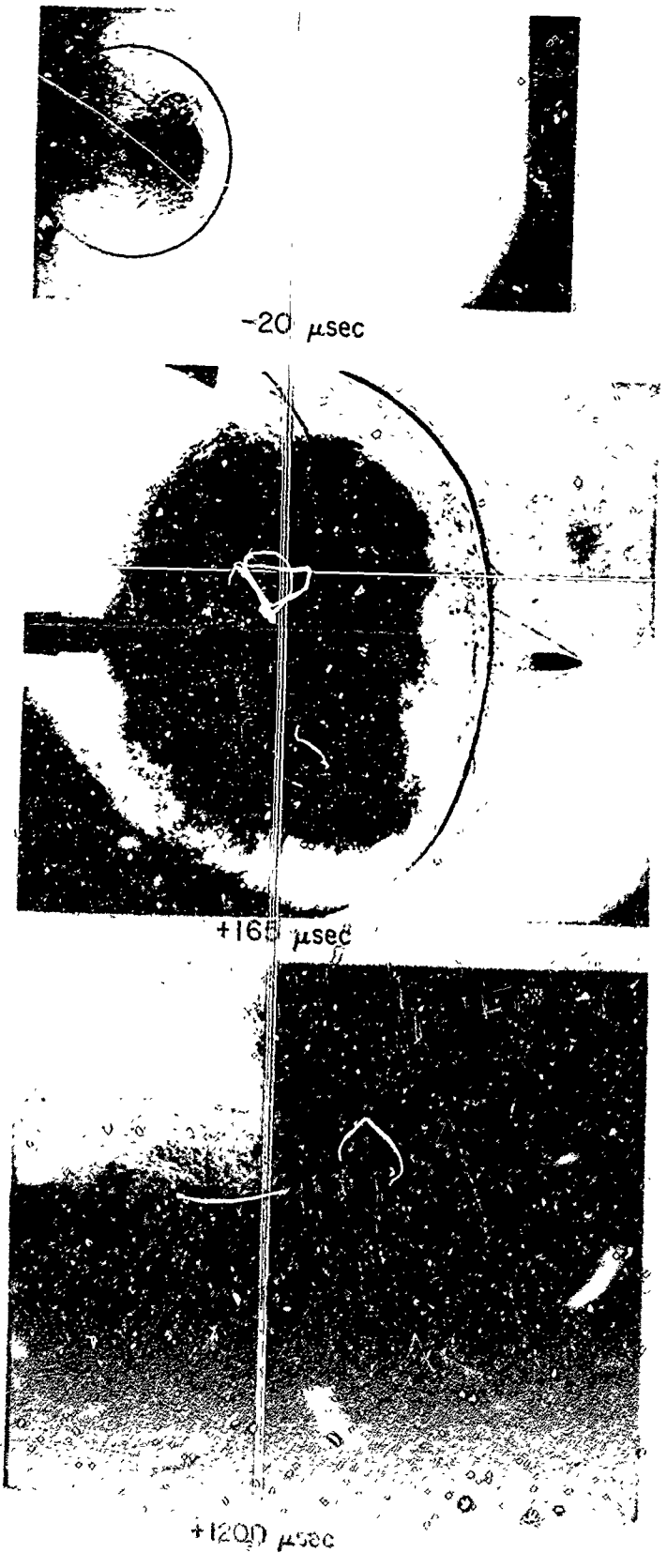

FIGURE 7 DATA SAMPLE FROM A SINGLE FIRING

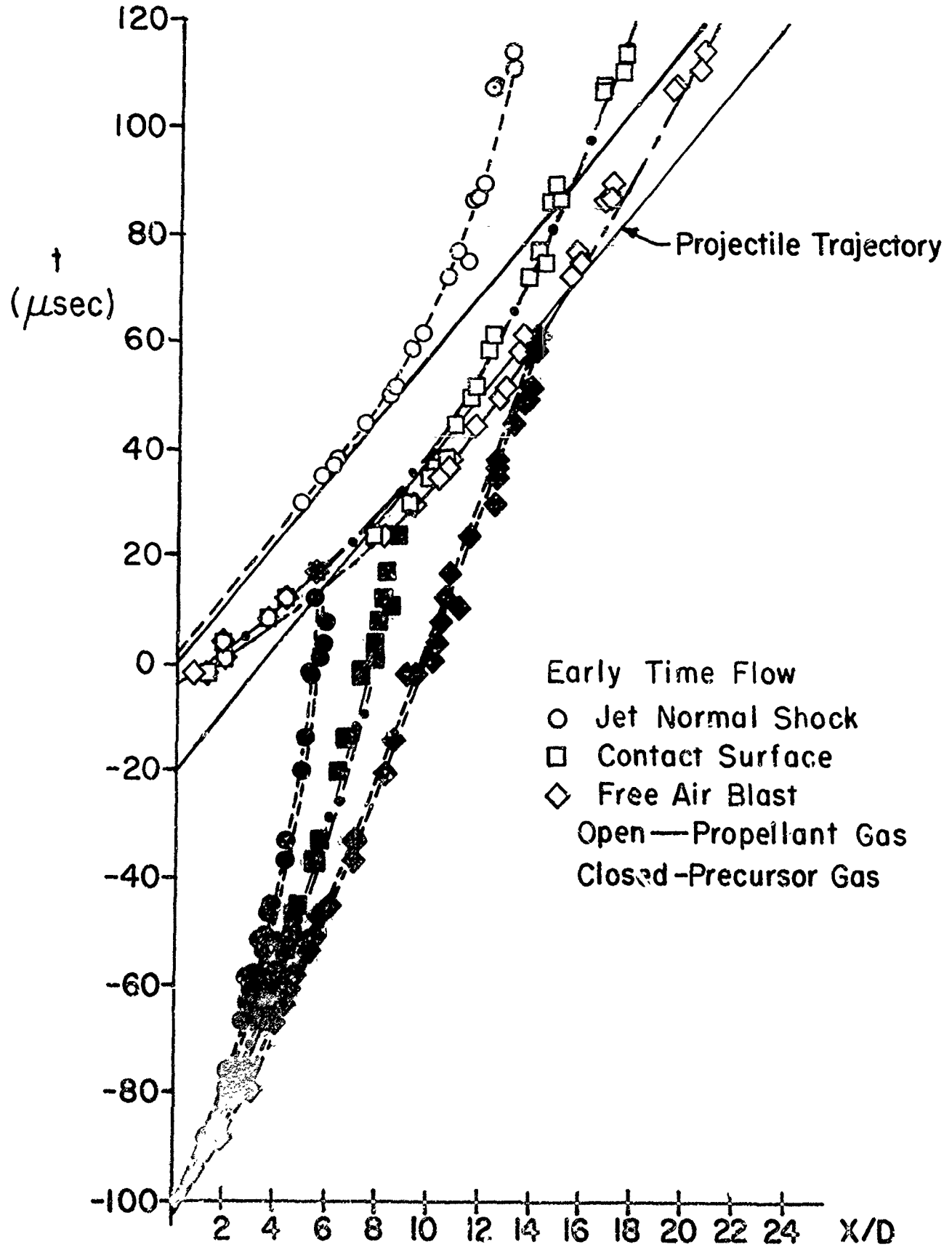

FIGURE 8 PRECURSOR FLOW DISCONTINUITY TRAJECTORIES

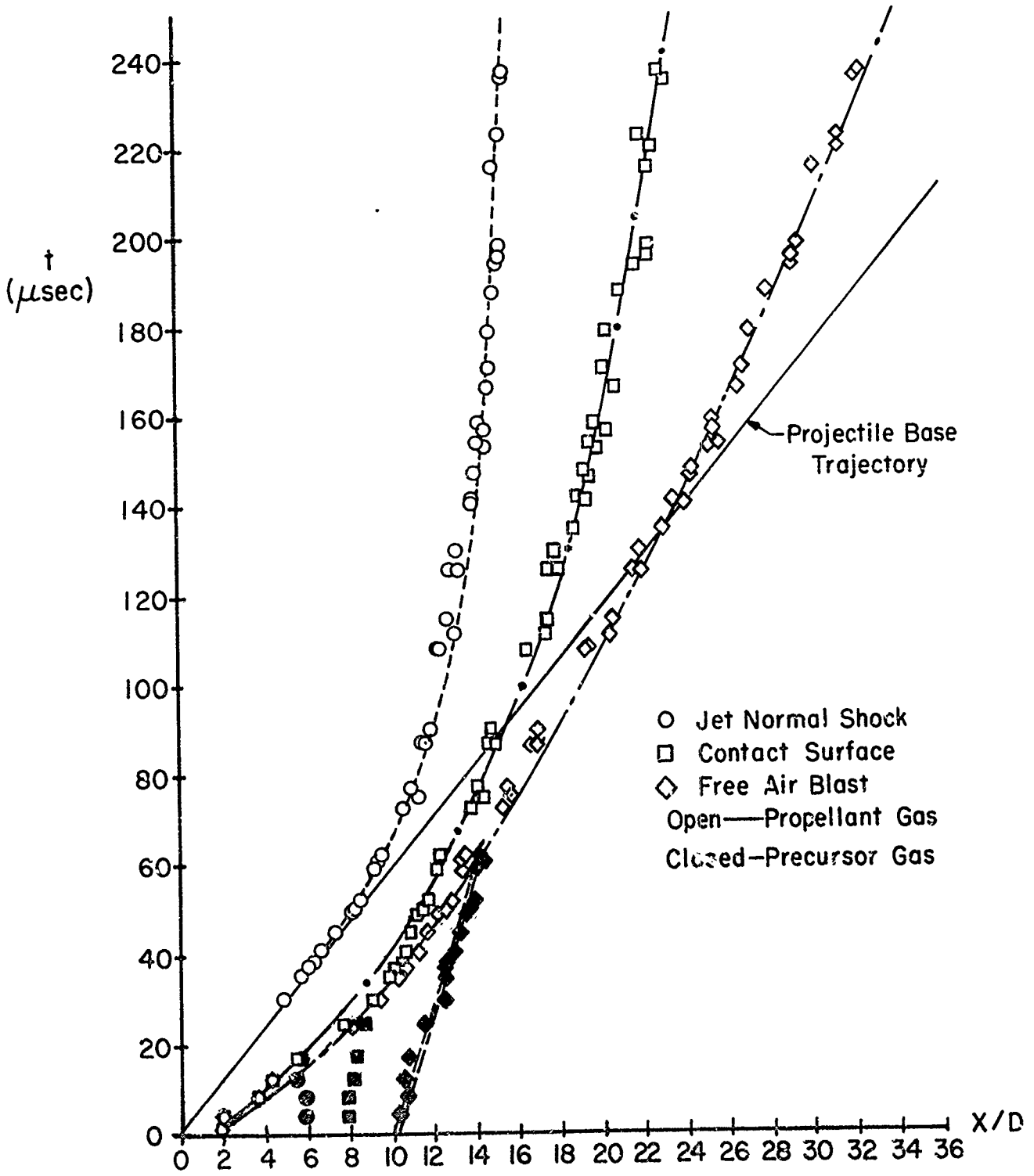

FIGURE 9 PROPELLANT GAS DISCONTINUITY TRAJECTORIES

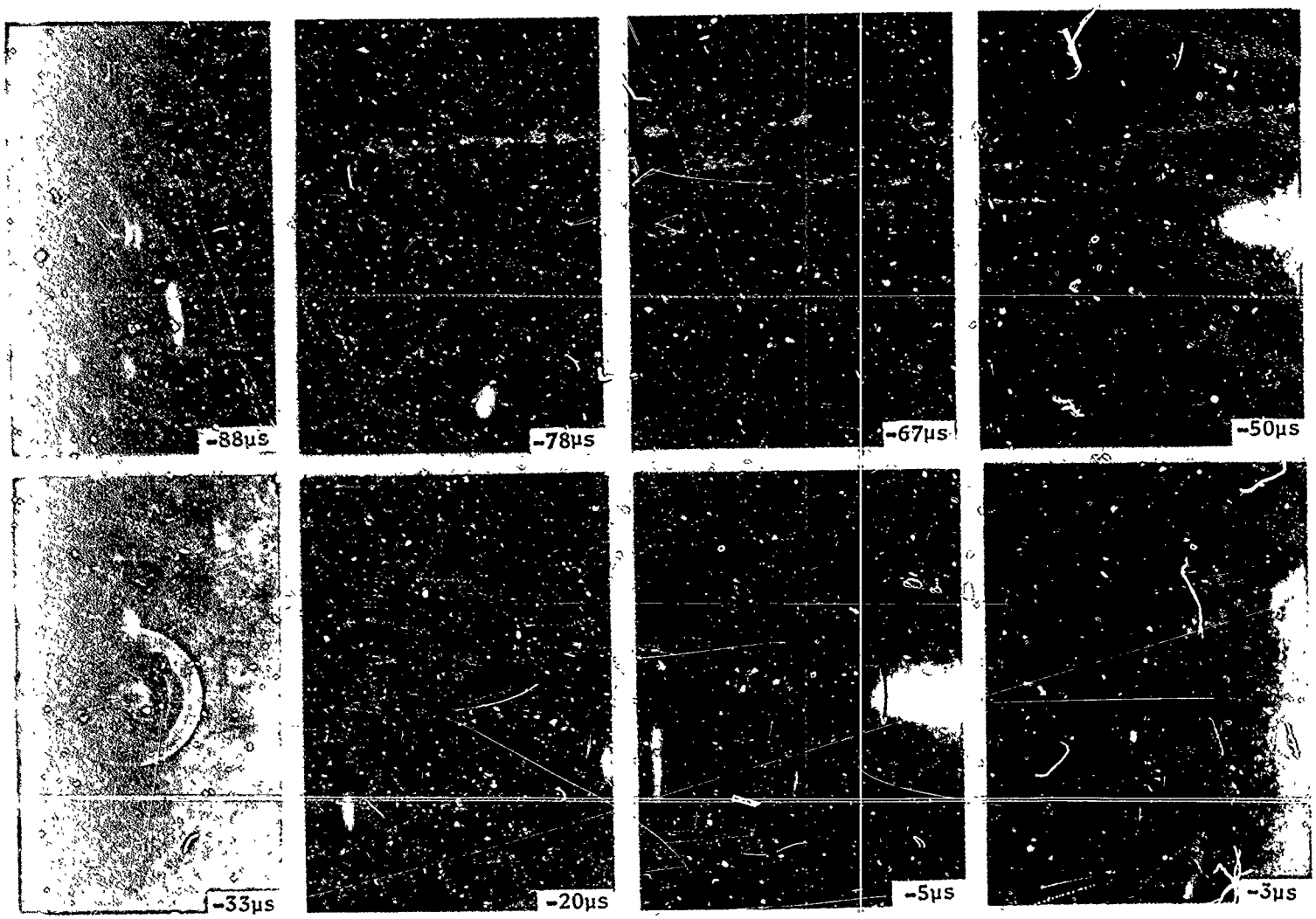

Figure 10. Representative Muzzle Flow Photographs (Scale: 10 Calibers)

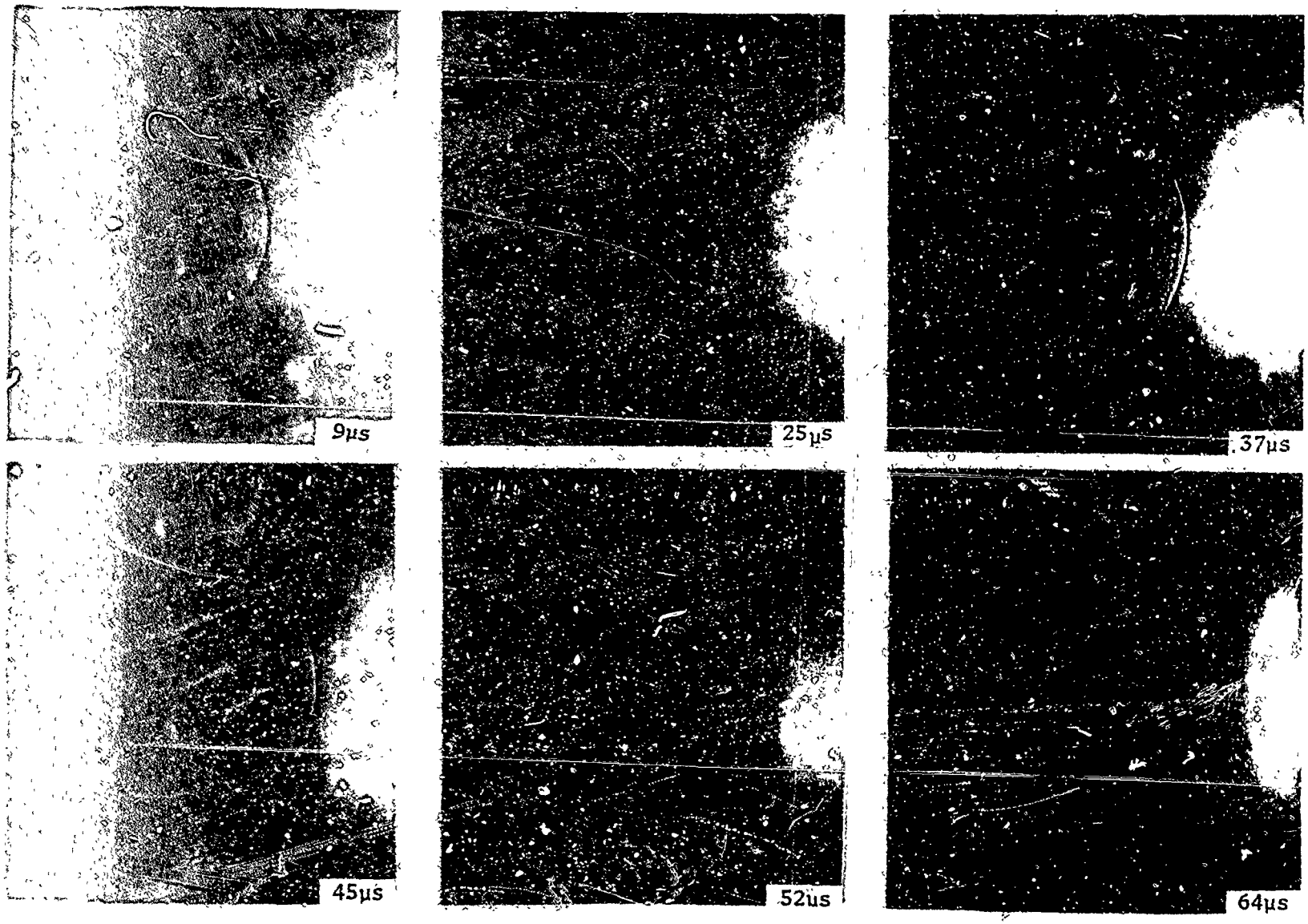

Figure 10. Representative Muzzle Flow Photographs (Scale: 10 Calibers)

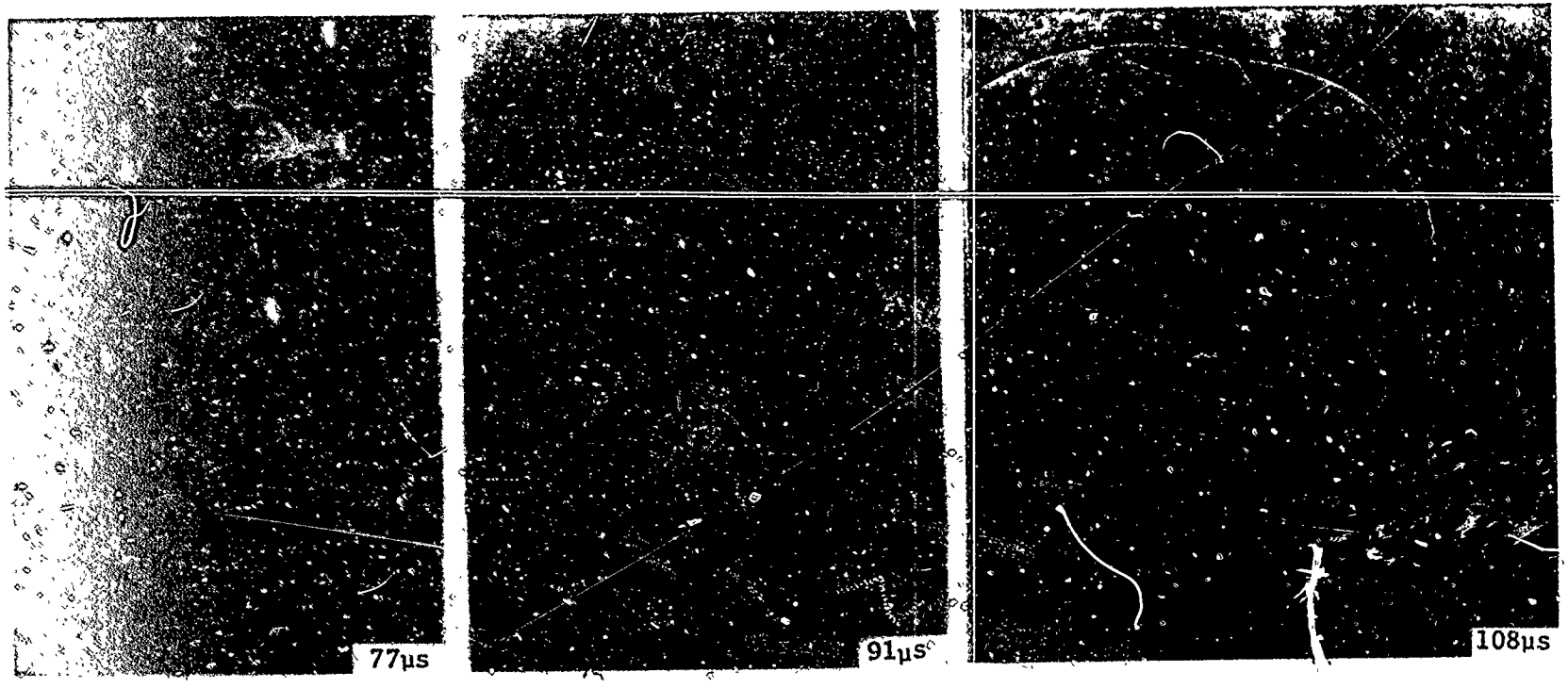

Figure 10. Representative Muzzle Flow Photographs (Scale: 10 Calibers)

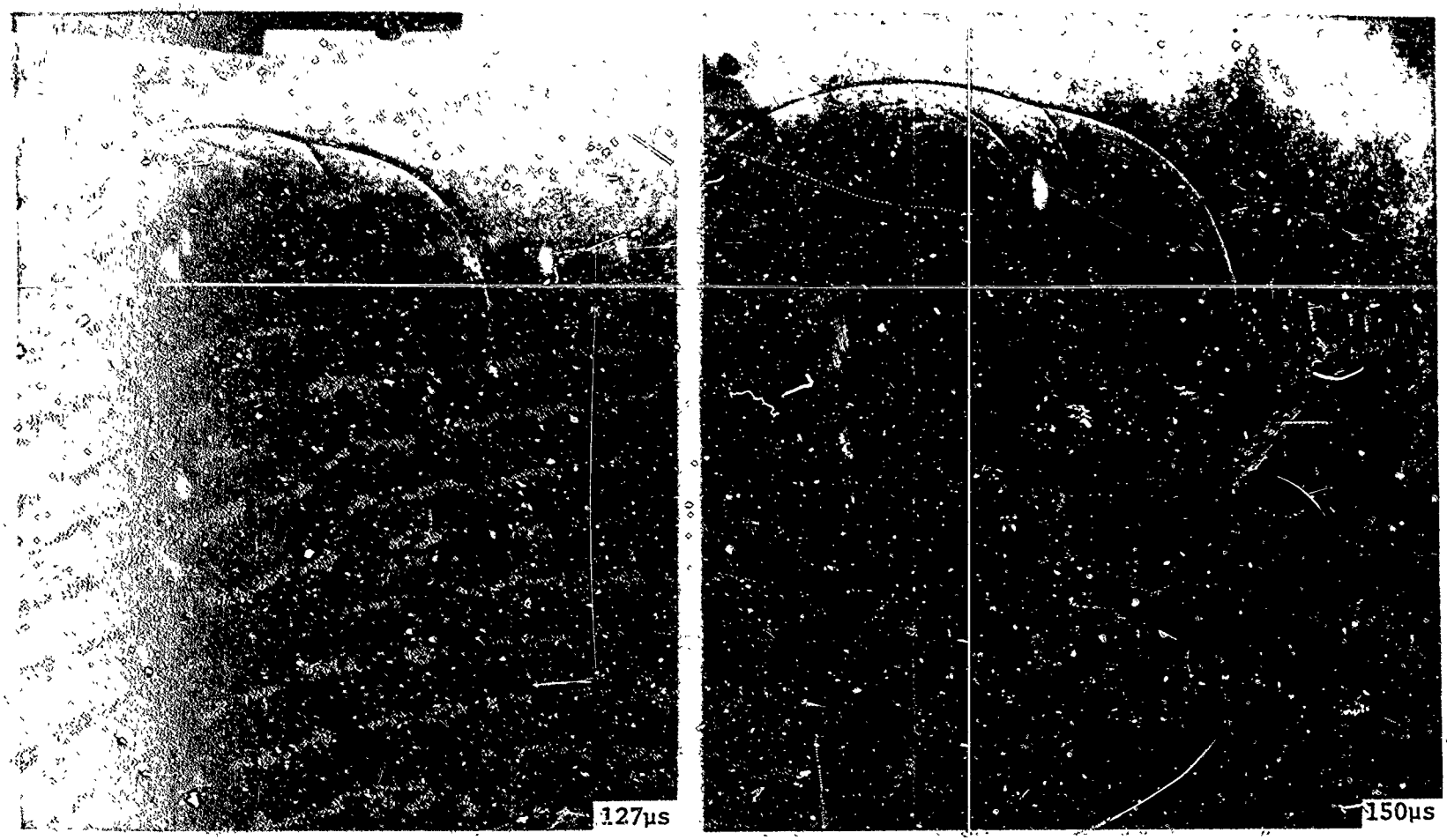

Figure 10. Representative Muzzle Flow Photographs (Scale: 10 Calibers)

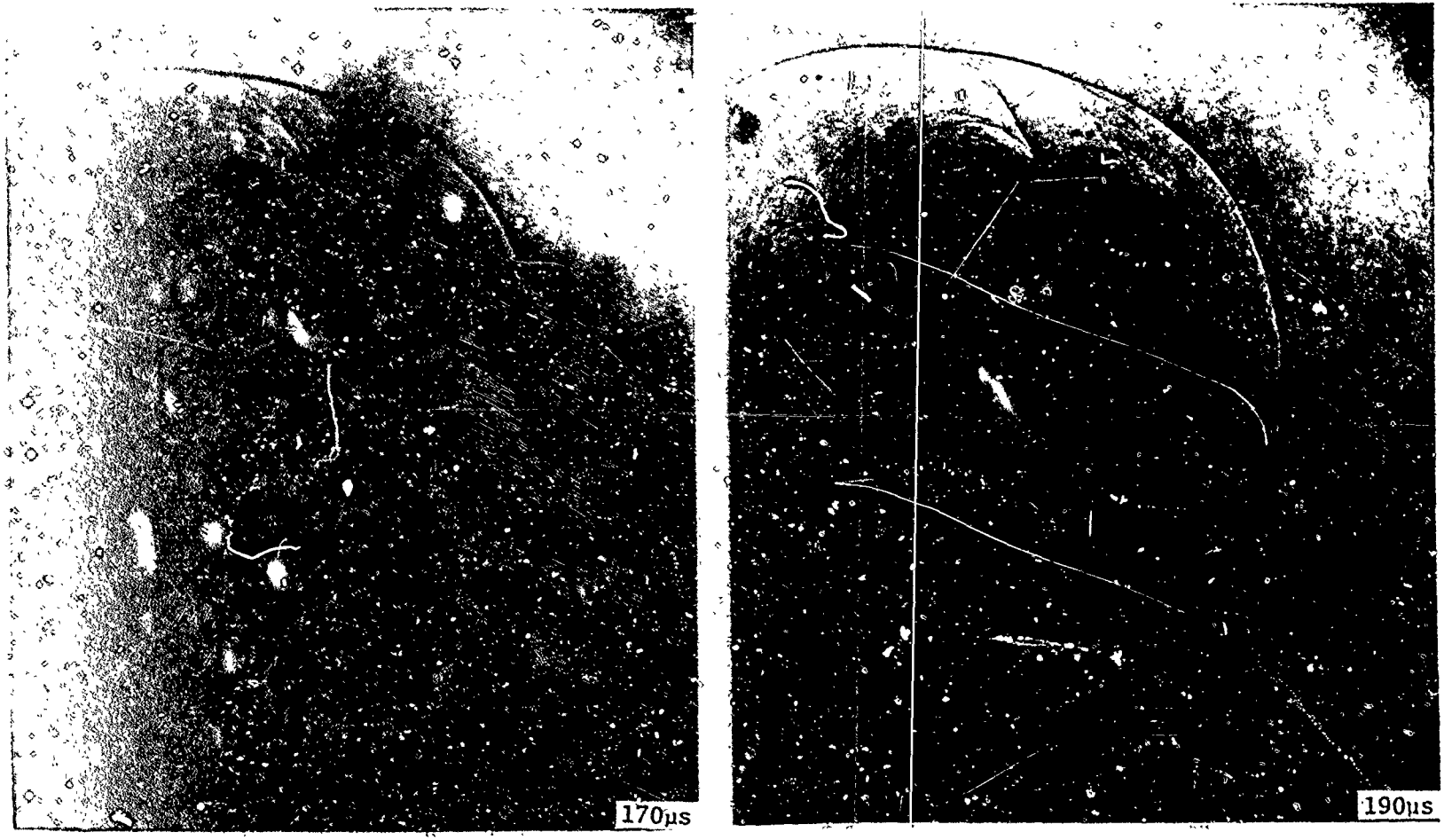

Figure 10. Representative Muzzle Flow Photographs (Scale: 10 Calibers)

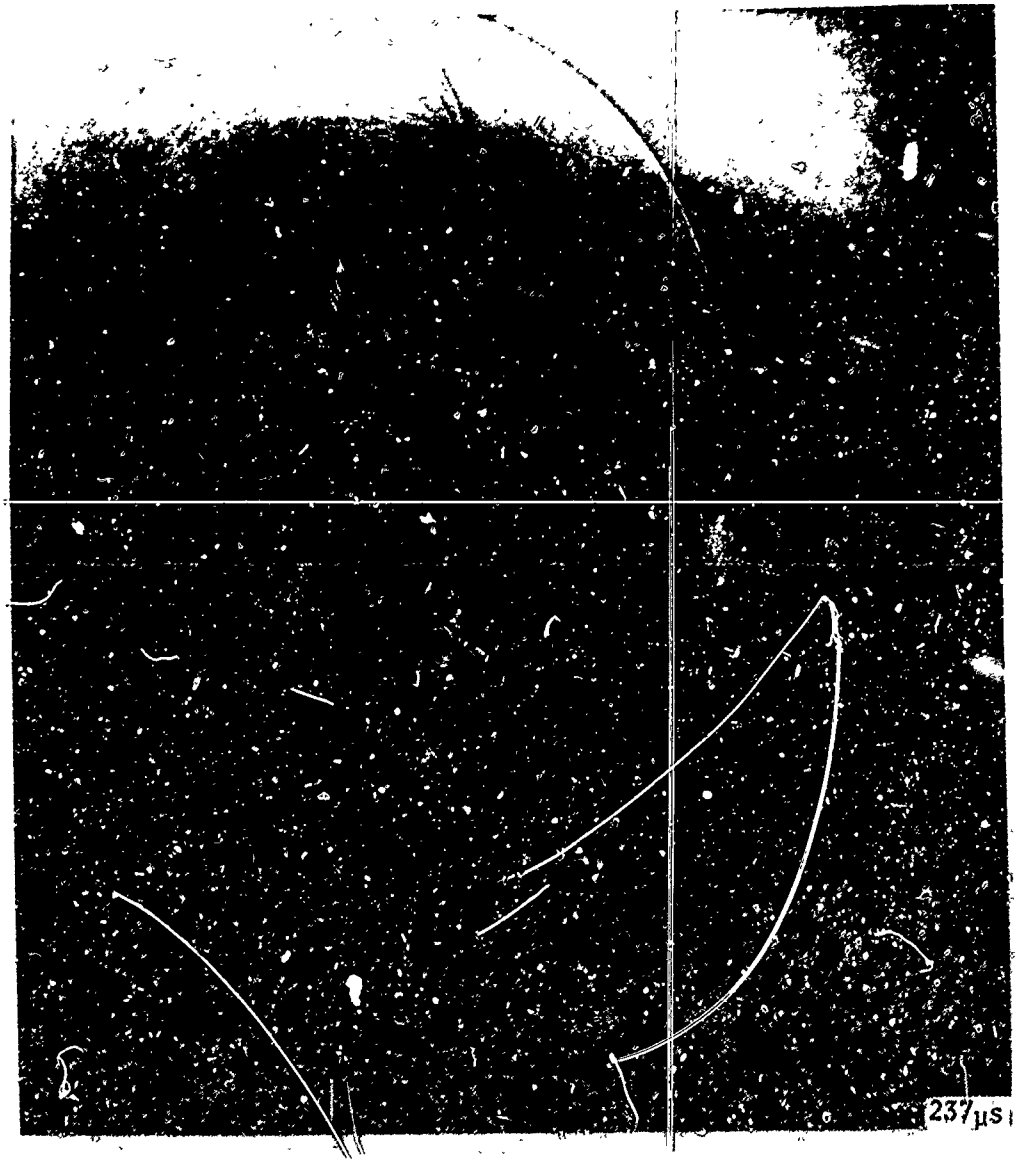

Figure 10. Representative Muzzle Flow Photographs (Scale: 10 Calibers)

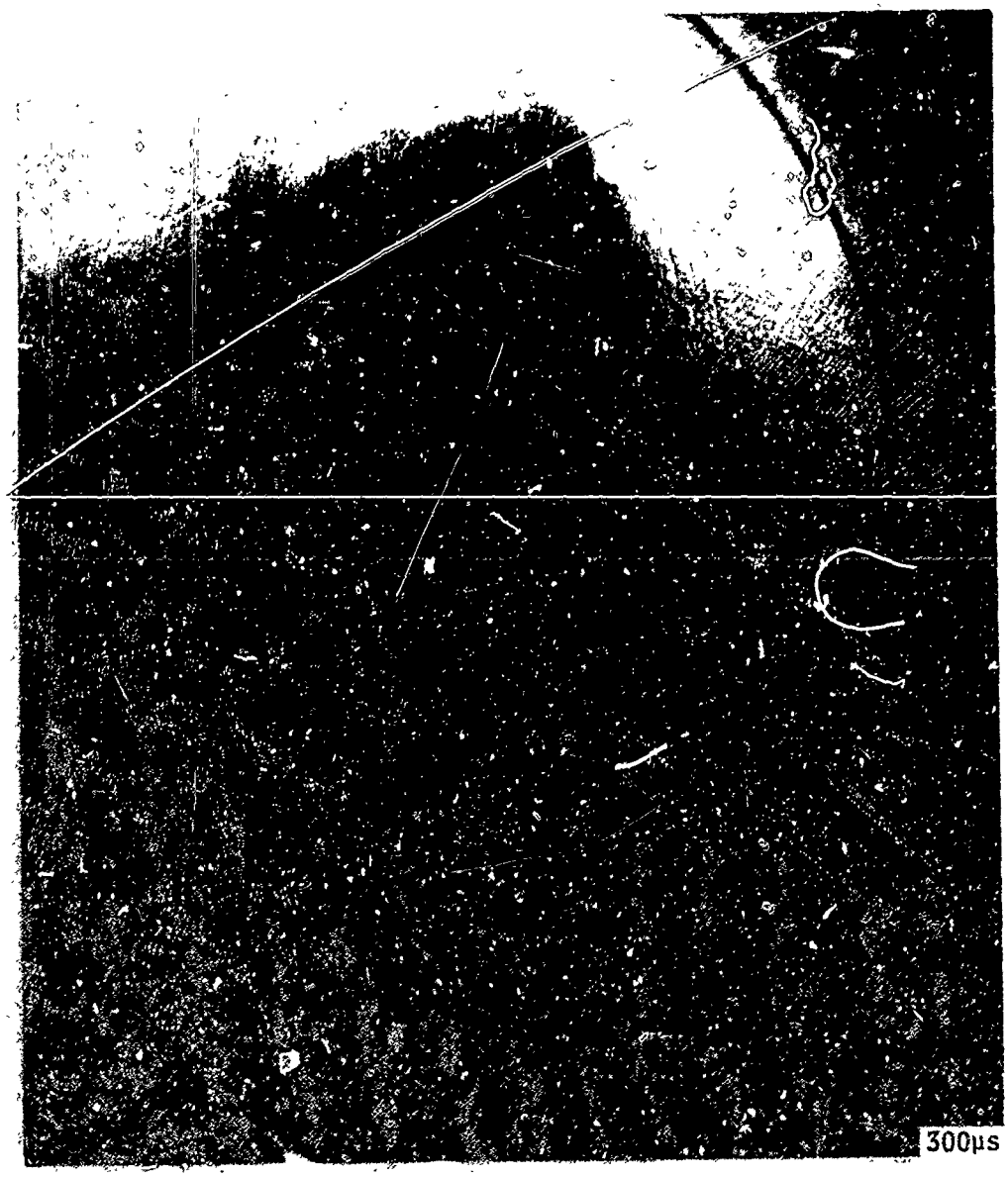

Figure 10. Representative Muzzle Flow Photographs (Scale: 10 Calibers)

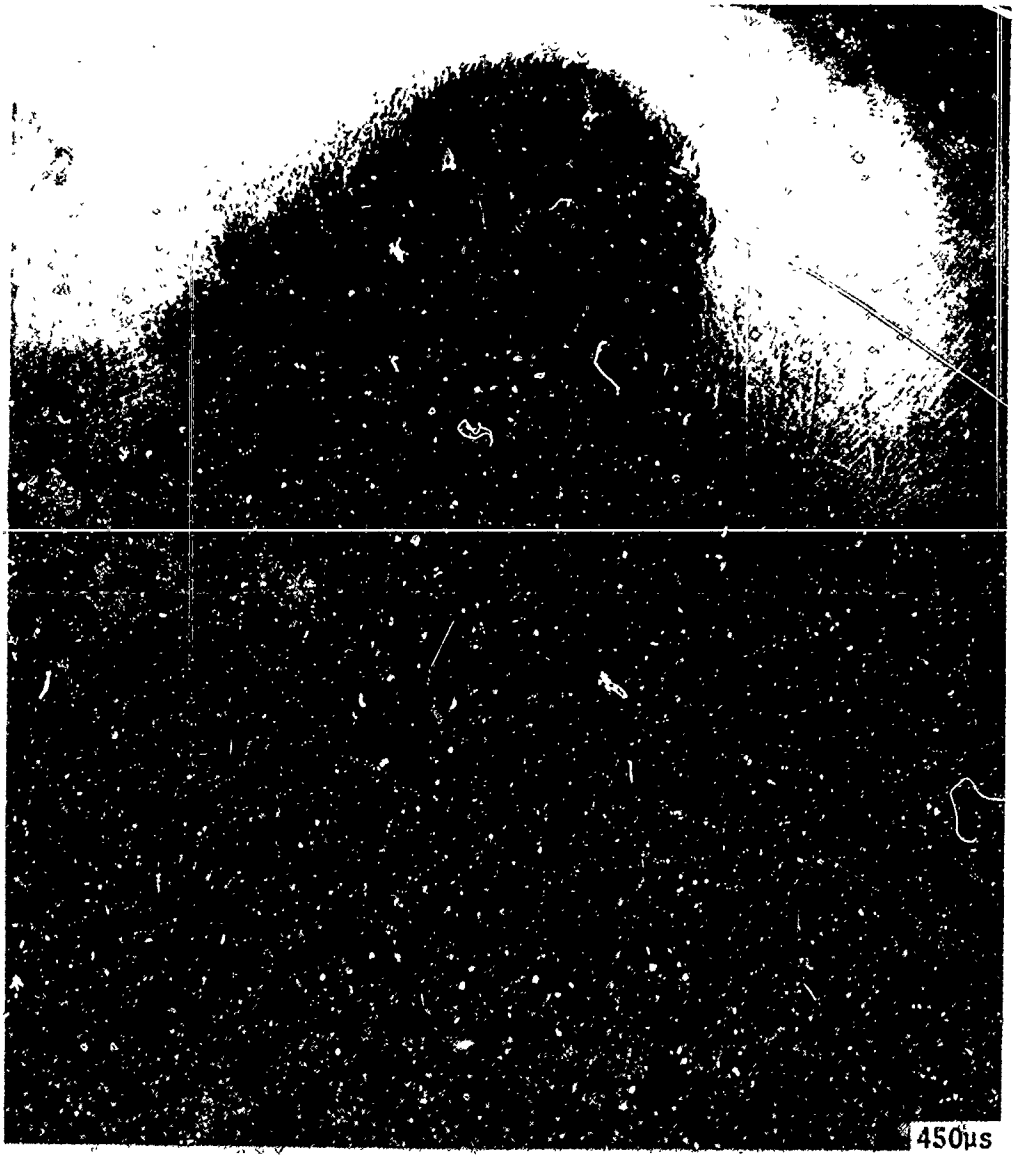

Figure 10. Representative Muzzle Flow Photographs (Scale: 10 Calibers)

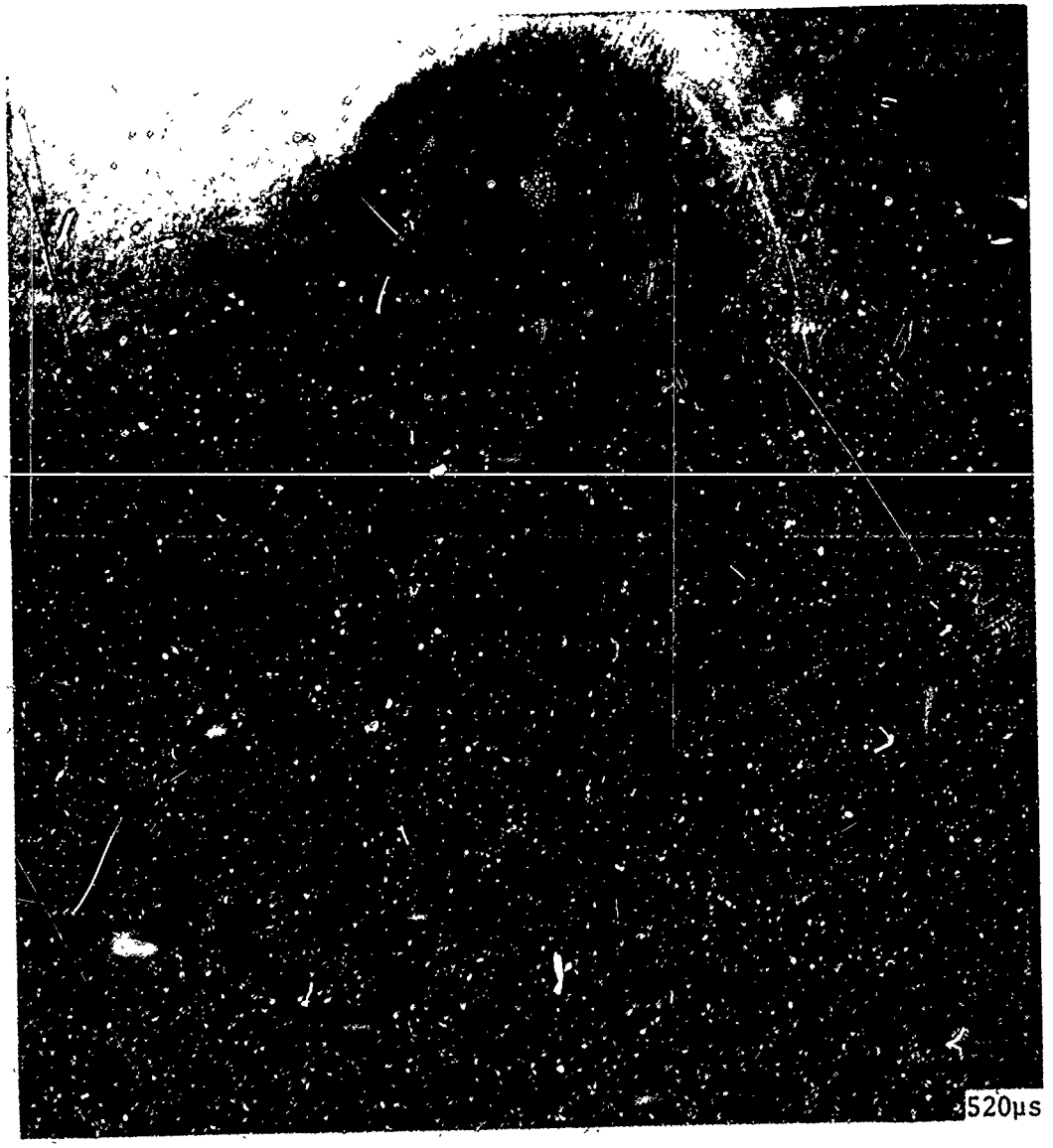

Figure 10. Representative Muzzle Flow Photographs (Scale: 10 Calibers)

Figure 10. Representative Muzzle Flow Photographs (Scale: 10 Calibers)

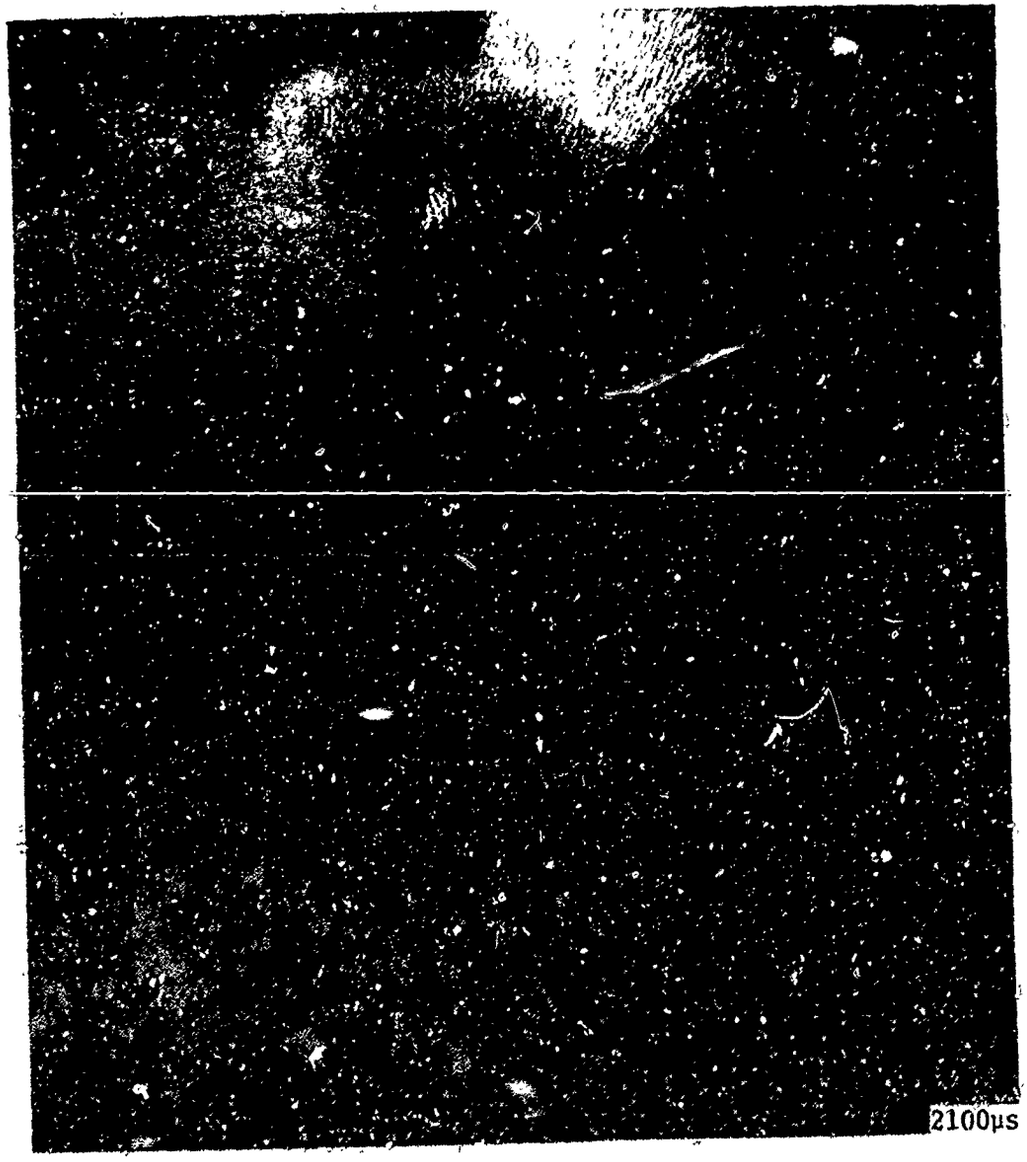

Figure 10. Representative Muzzle Flow Photographs (Scale: 10 Calibers)

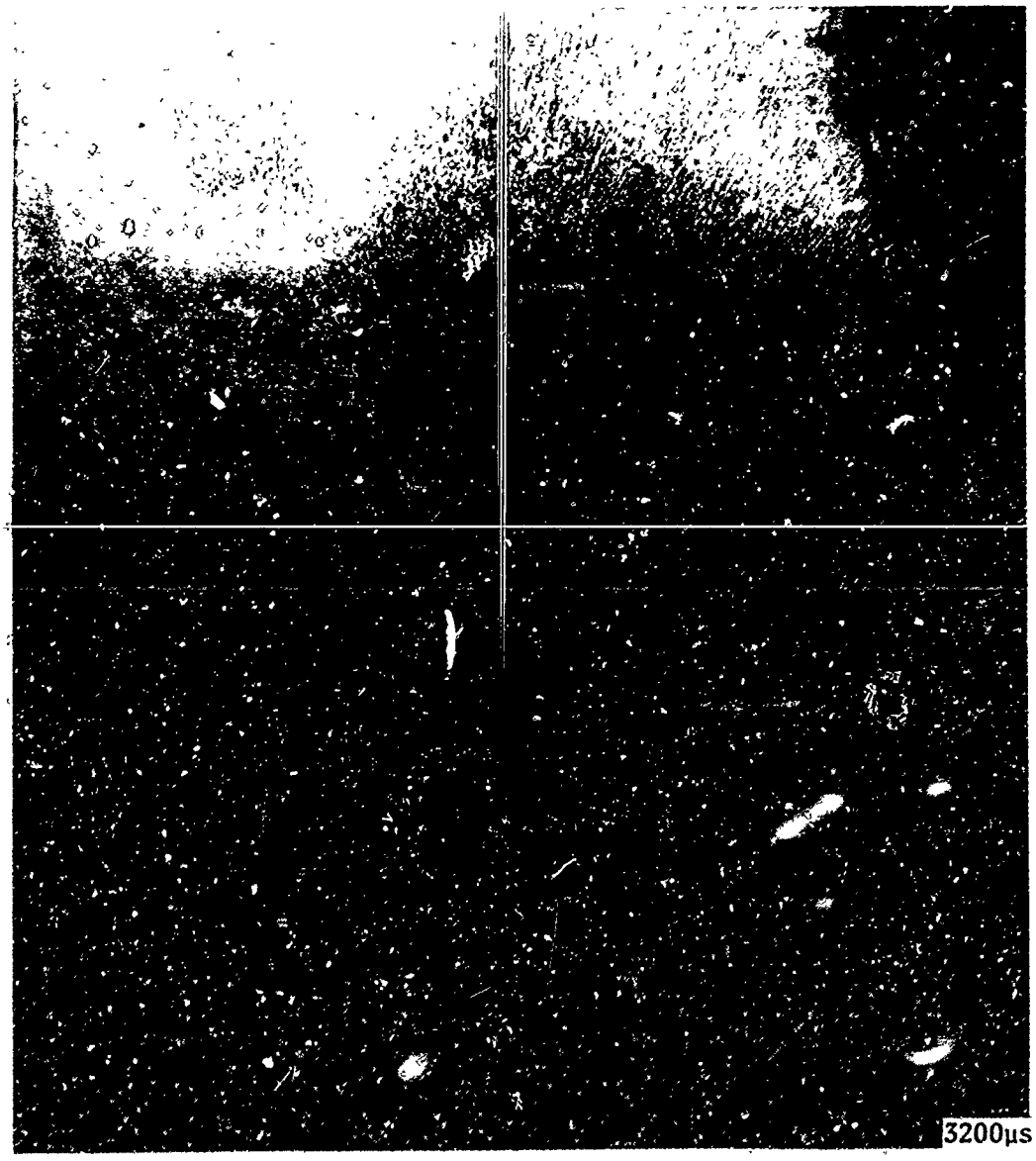

Figure 10. Representative Muzzle Flow Photographs (Scale: 10 Calibers)

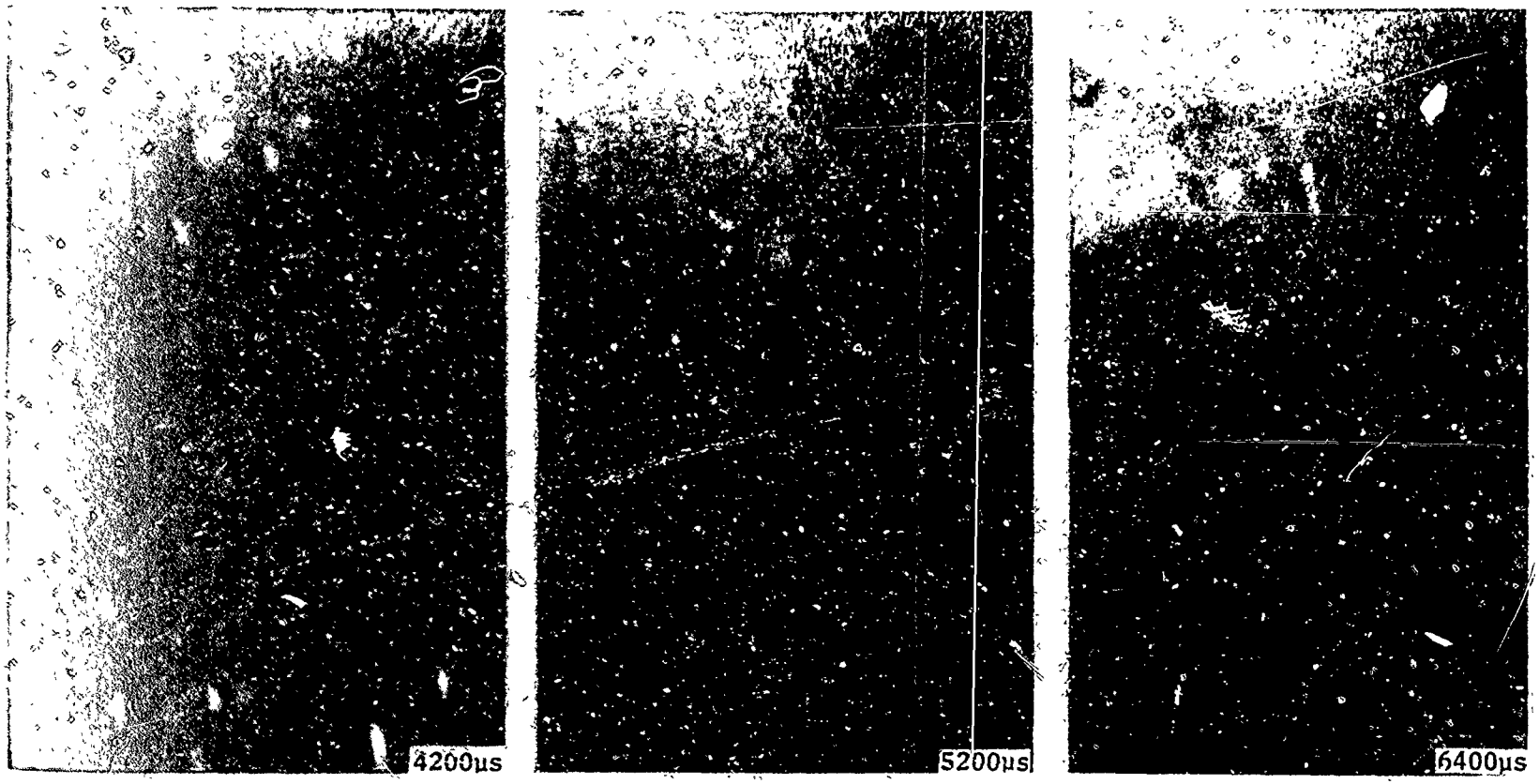

Figure 10. Representative Muzzle Flow Photographs (Scale: 10 Calibers)

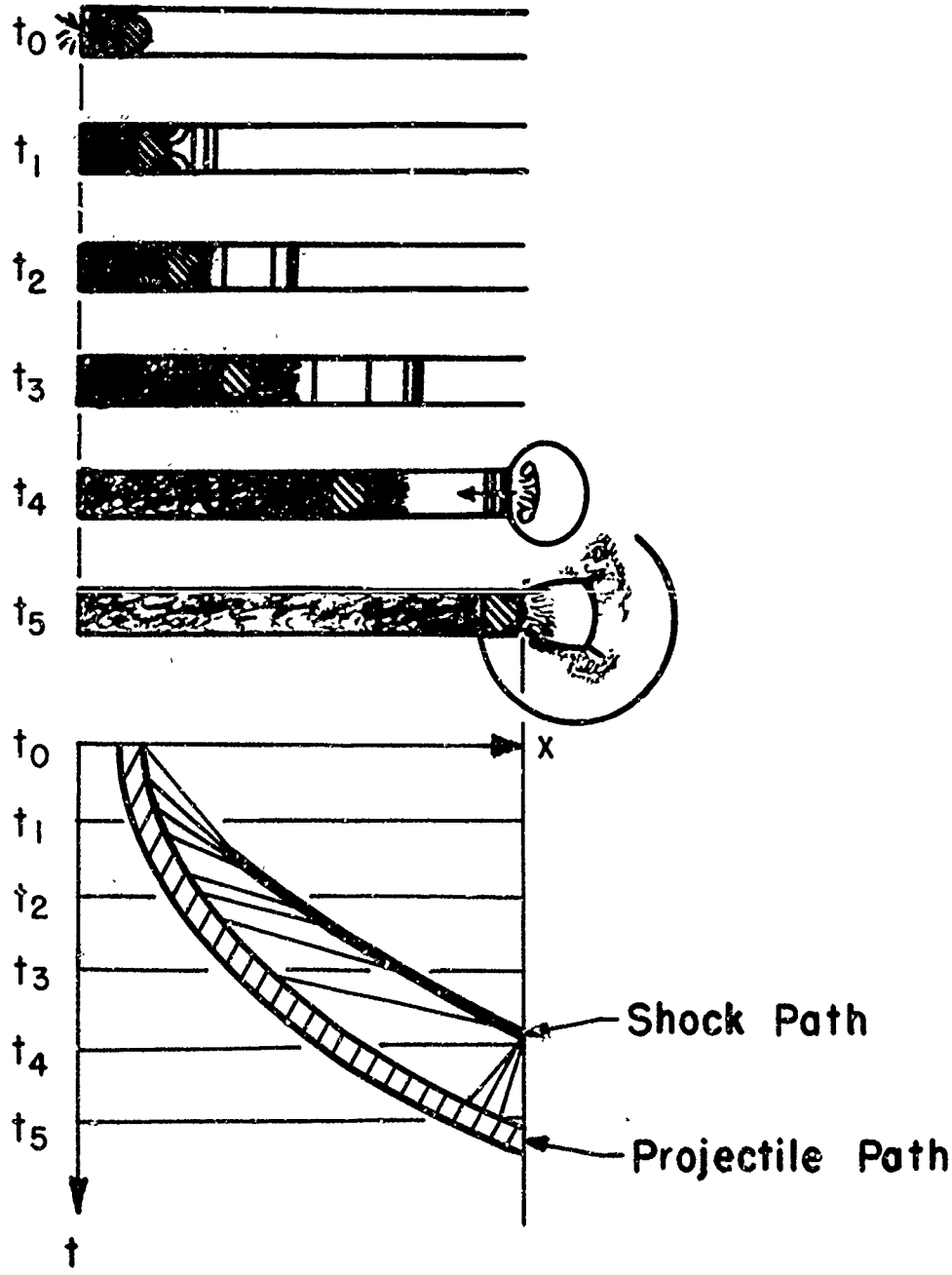

FIGURE 11 SCHEMATIC OF PRECURSOR FLOW DEVELOPMENT

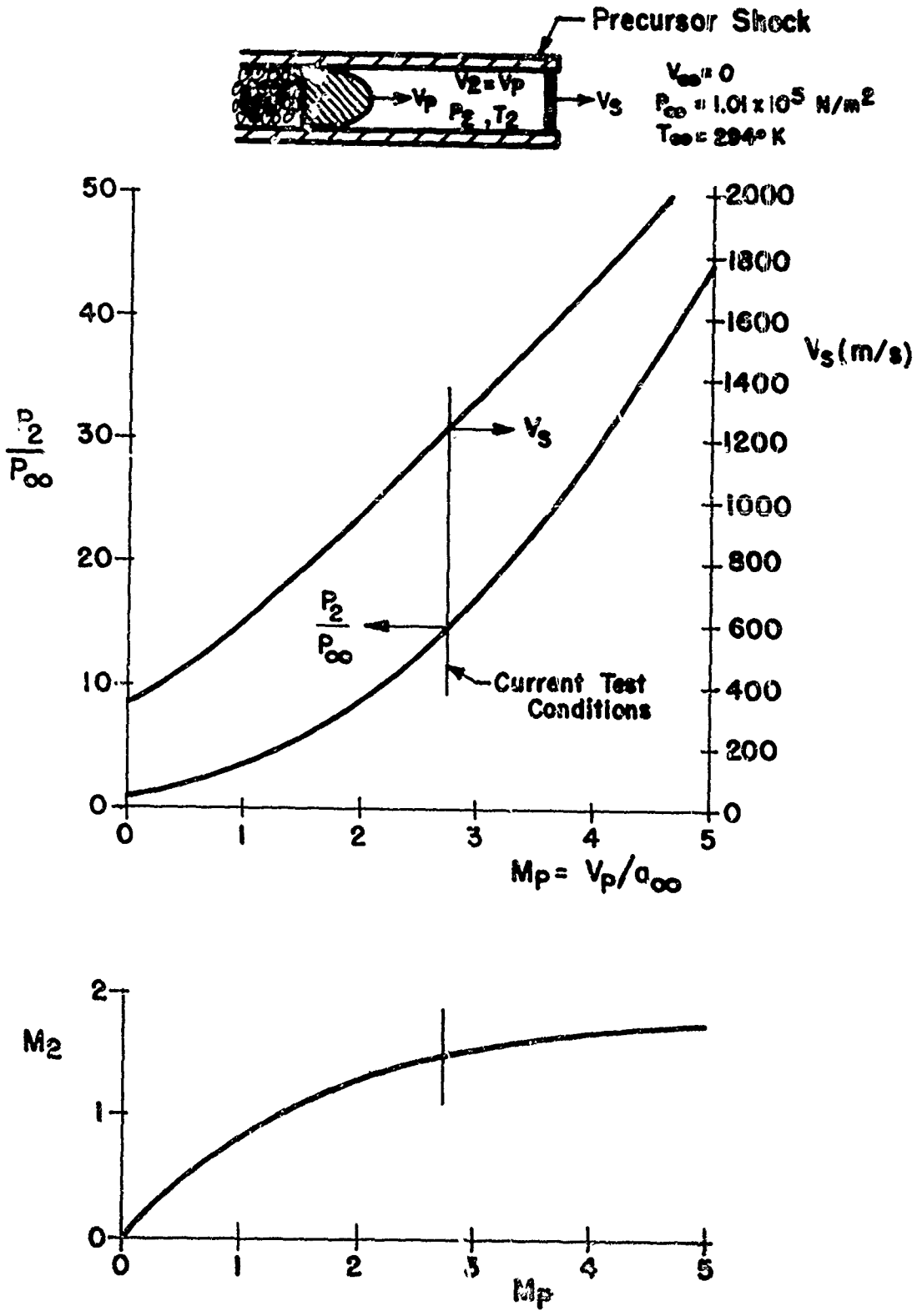

FIGURE 12 PRECURSOR MUZZLE FLOW PROPERTIES VERSUS PROJECTILE LAUNCH MACH NUMBER

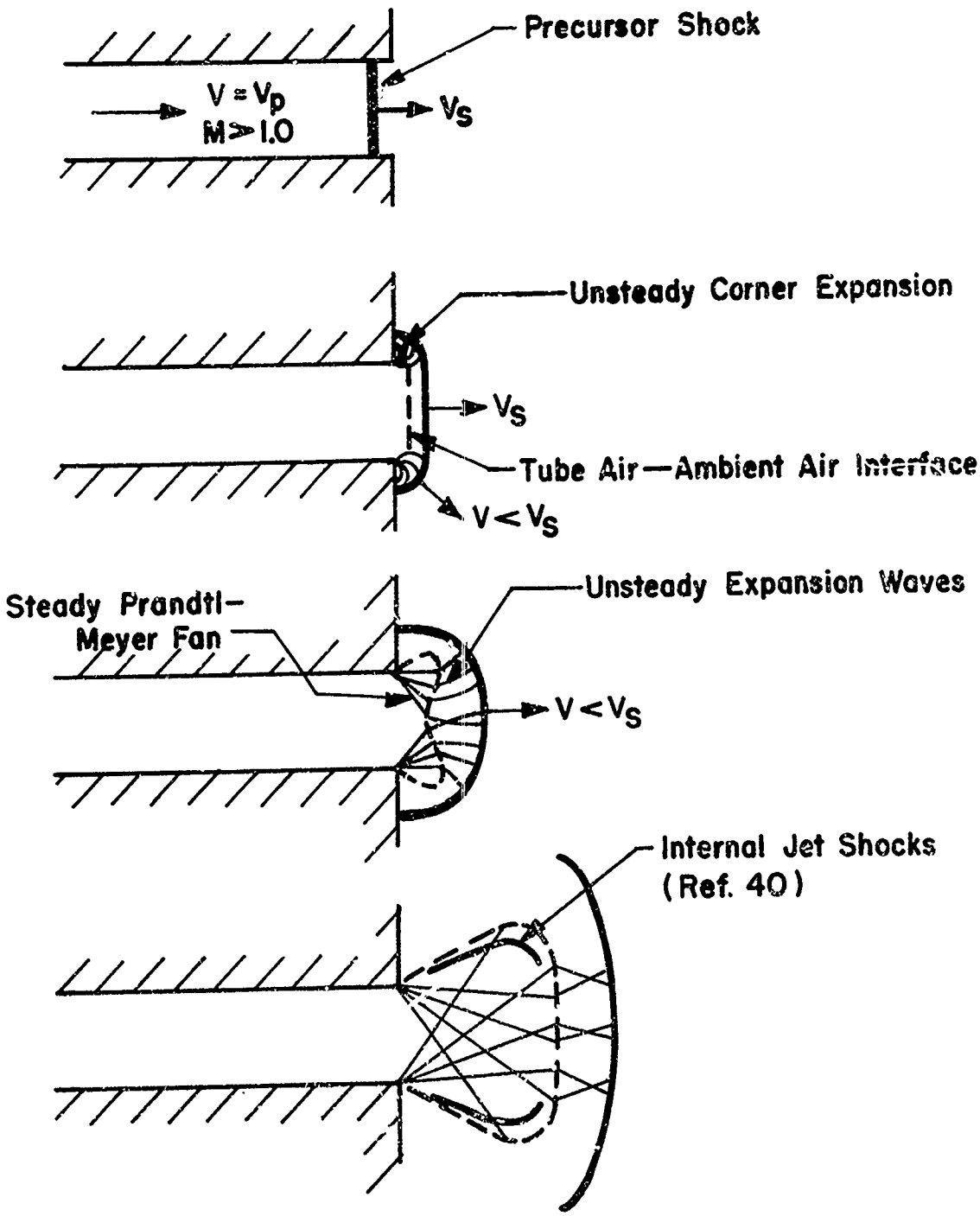

FIGURE 13 SCHEMATIC OF PRECURSOR FLOW EXPANSION

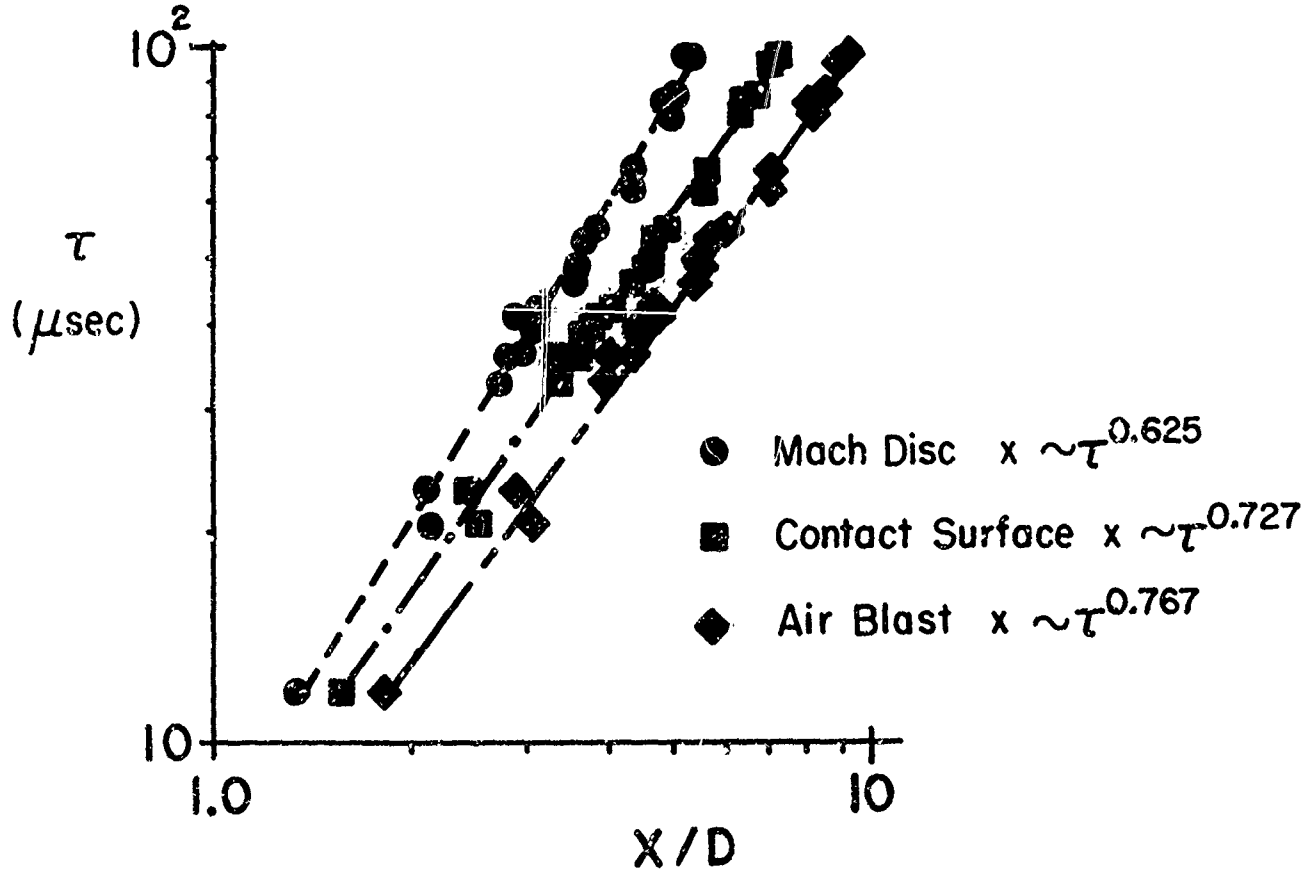

FIGURE 14 LOGARITHMIC PLOT OF PRECURSOR FLOW TRAJECTORIES FOR $0 < \tau \leq 100$ ($\tau = t + 100$)

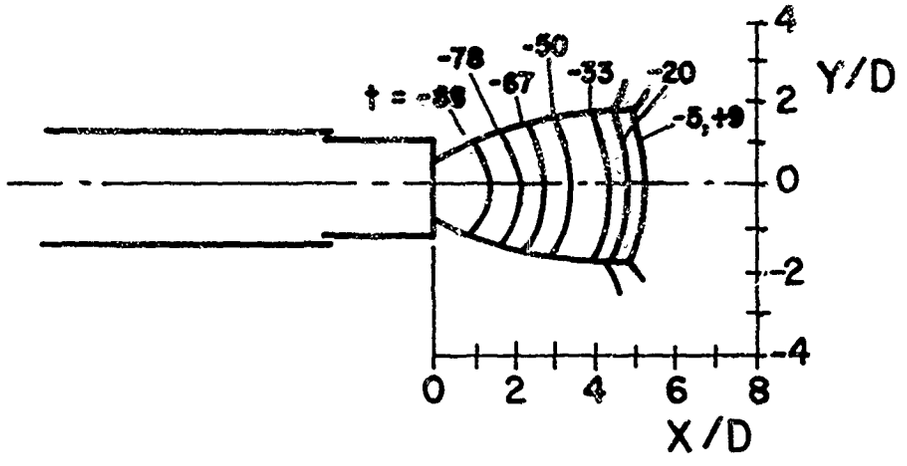

FIGURE 15A CONTOUR PLOT OF PRECURSOR JET SHOCK STRUCTURE (t in μsec)

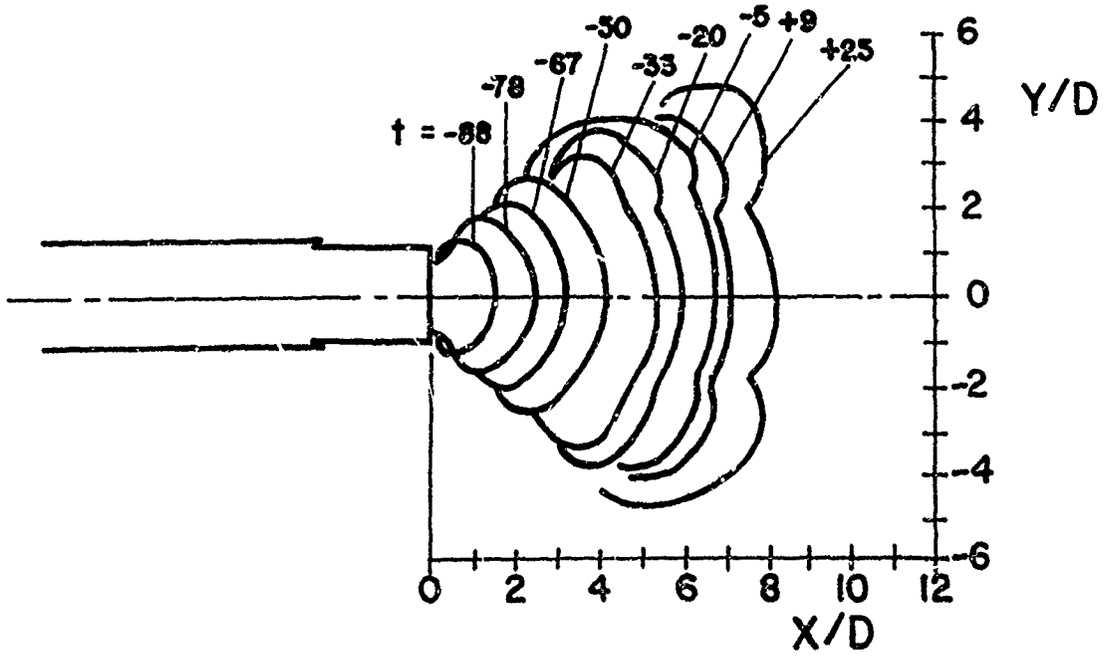

FIGURE 15B CONTOUR PLOT OF PRECURSOR JET CONTACT SURFACE (t in μsec)

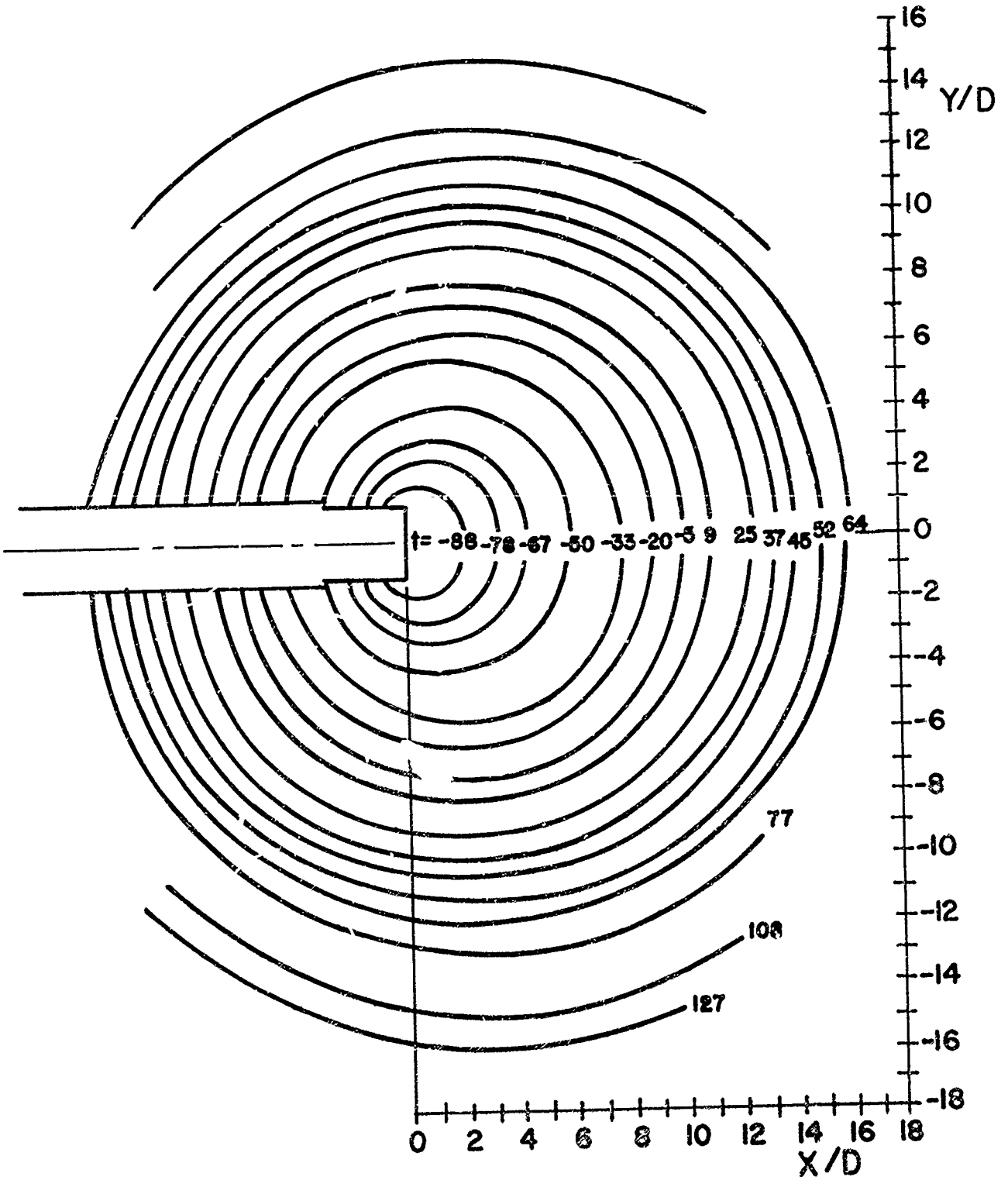

FIGURE 15C CONTOUR PLOT OF PRECURSOR AIR BLAST
(t in μsec)

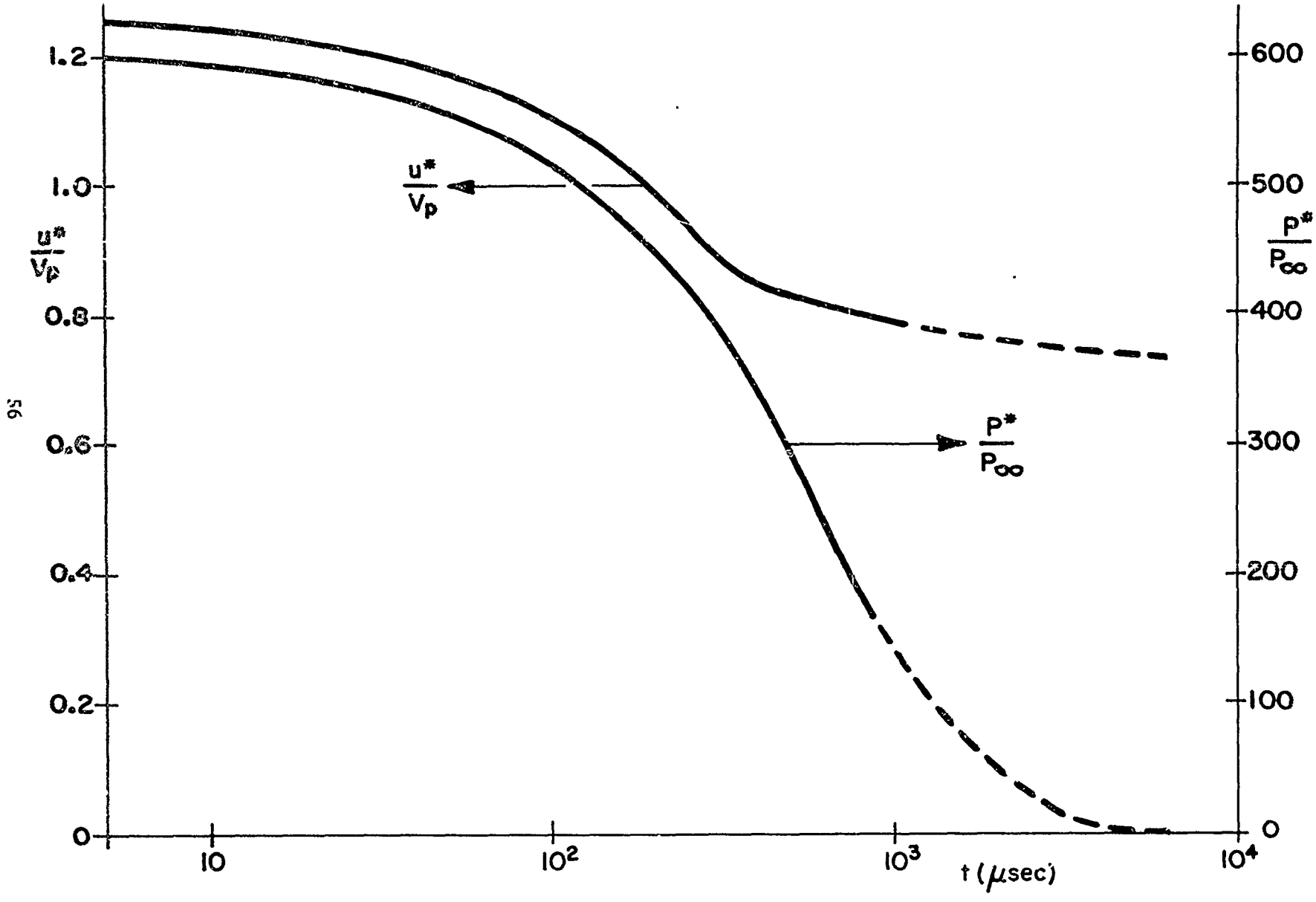

FIGURE 16 PROPELLANT GAS PROPERTIES AT MUZZLE DURING EMPTYING

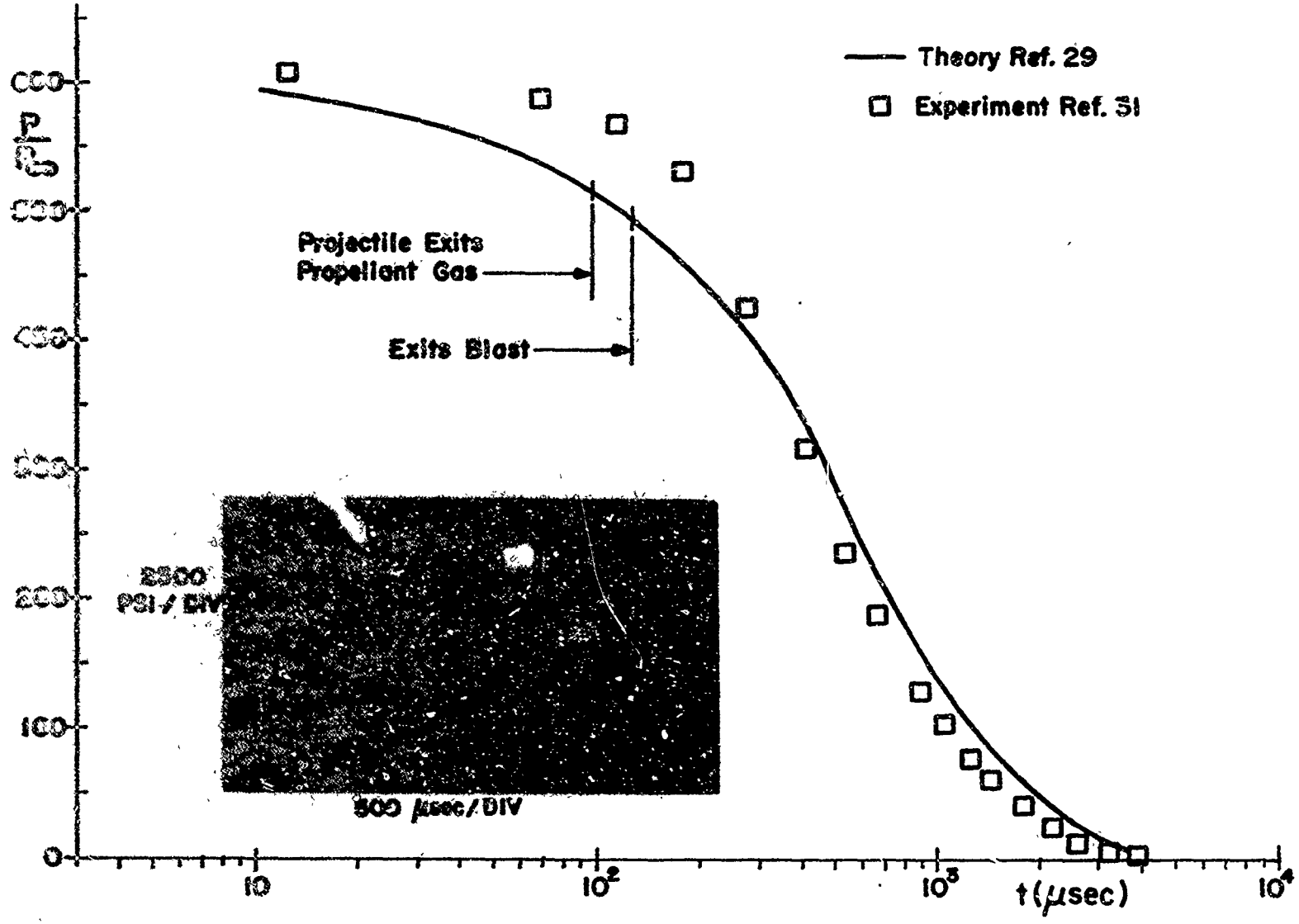

FIGURE 17 PROPELLANT GAS PRESSURE AT THE MUZZLE

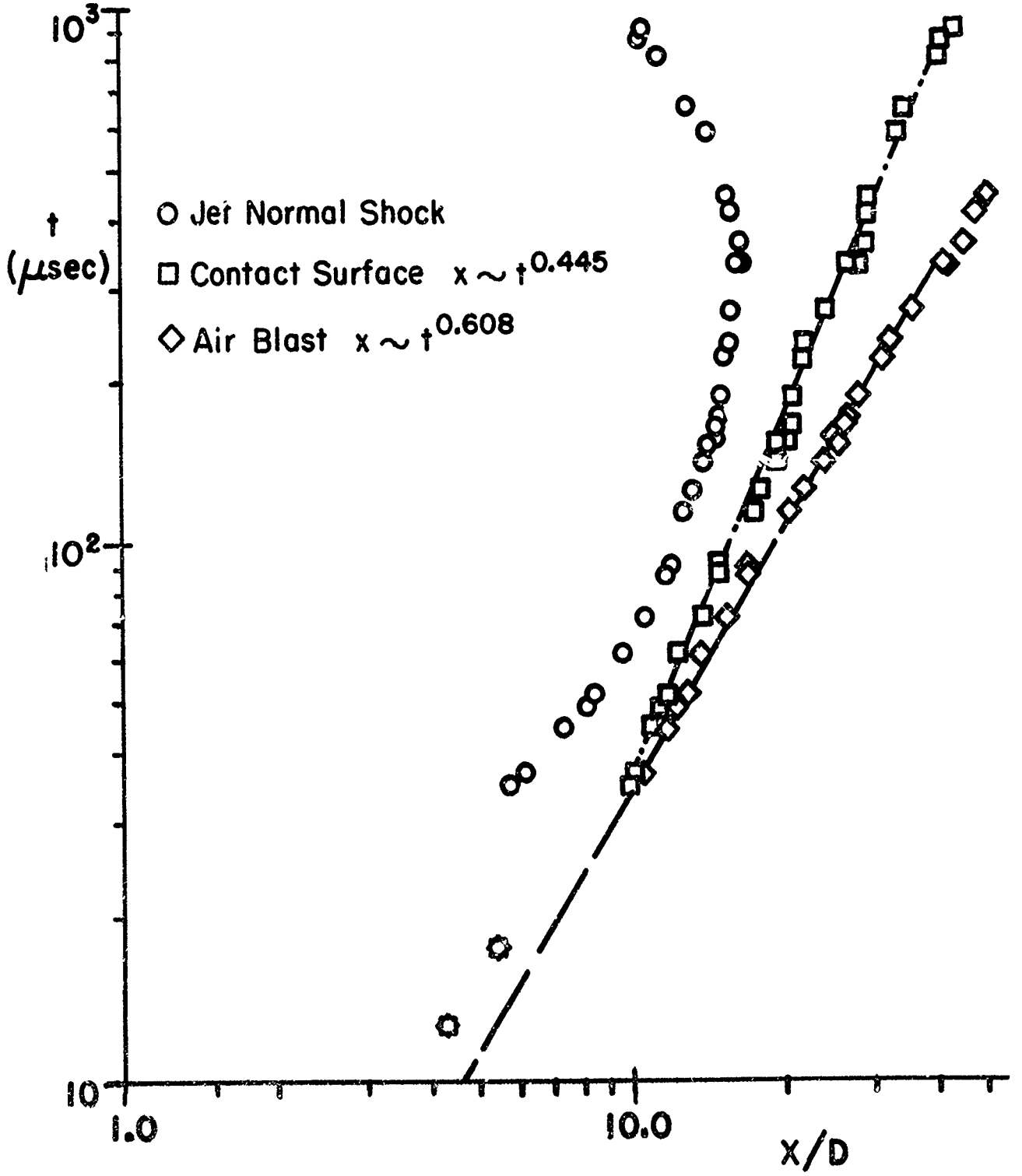

FIGURE 18 LOGARITHMIC PLOT OF PROPELLANT GAS DISCONTINUITY TRAJECTORIES

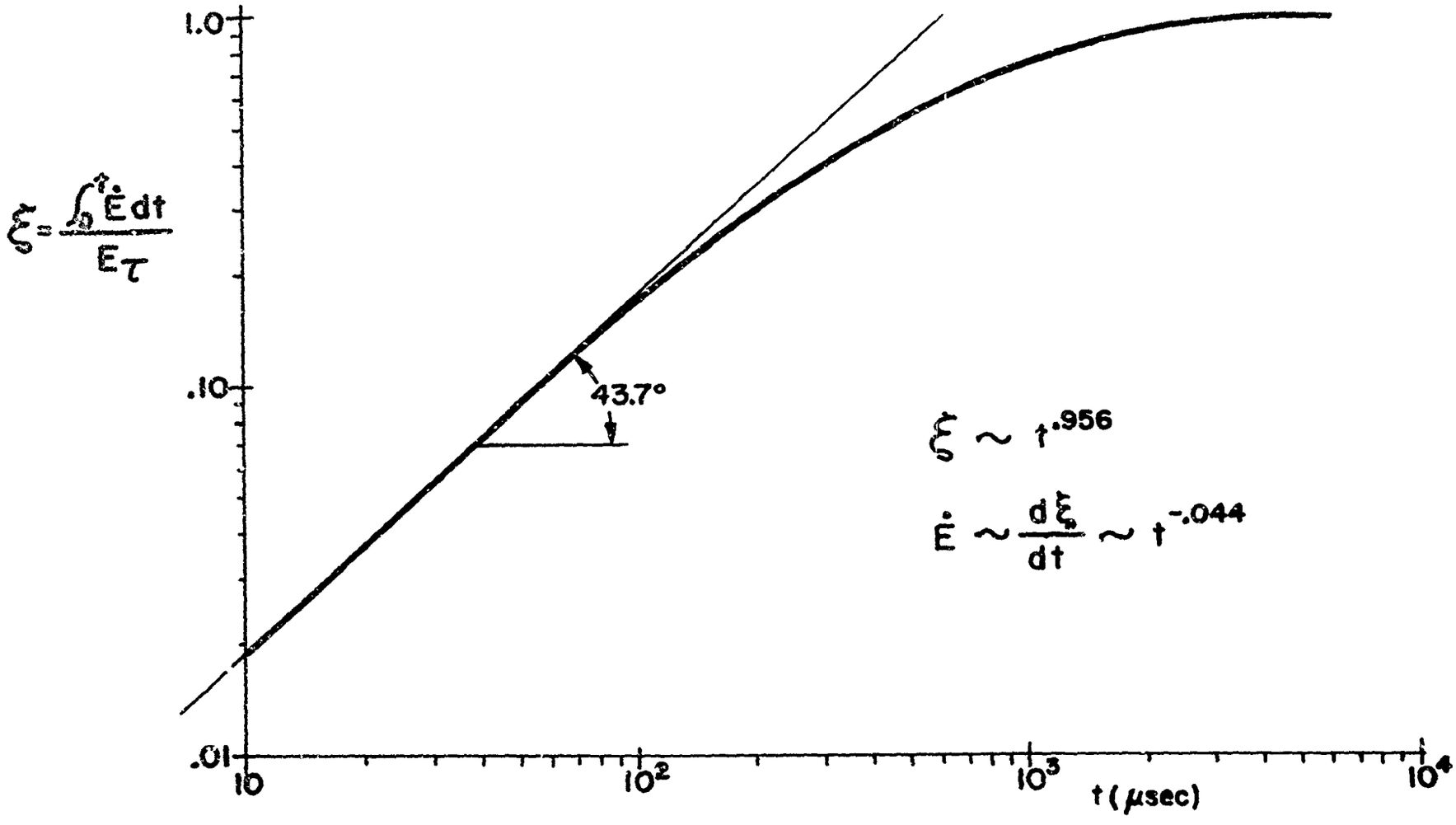

FIGURE 19 ENERGY EFFLUX WITH TIME

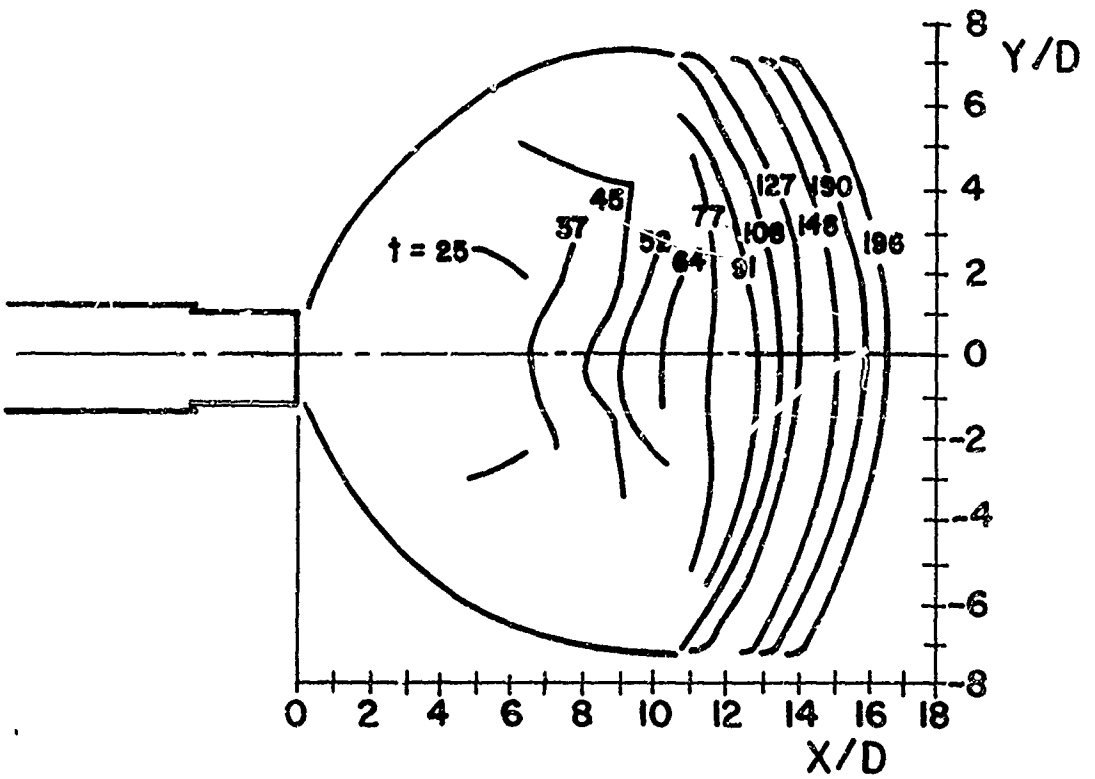

FIGURE 20A GROWTH OF PROPELLANT GAS JET SHOCK STRUCTURE (t in μsec)

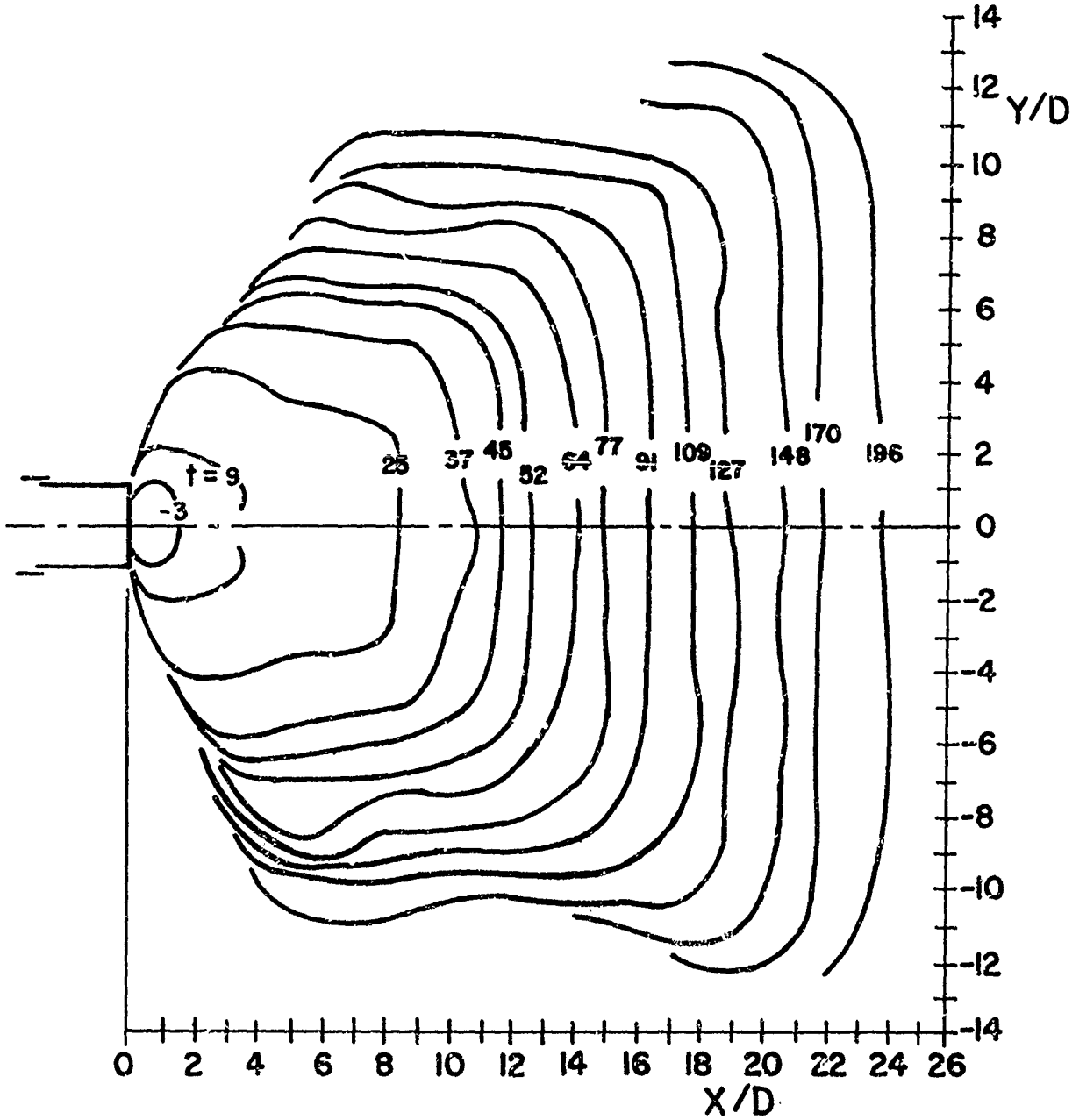

FIGURE 20B GROWTH OF PROPELLANT GAS JET CONTACT SURFACE (t in μsec)

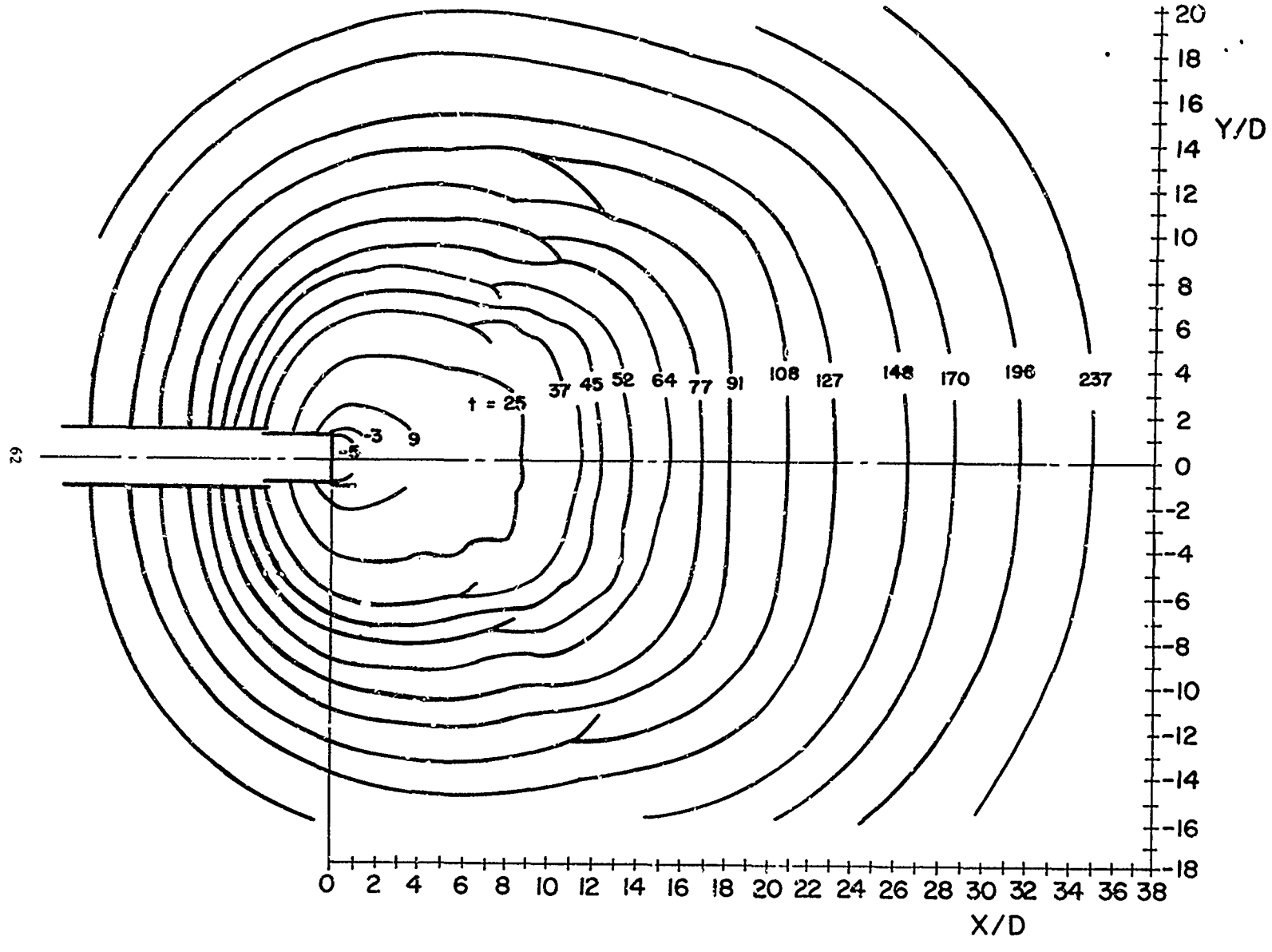

FIGURE 20C DEVELOPMENT OF PROPELLANT GAS BLAST (t in μsec)

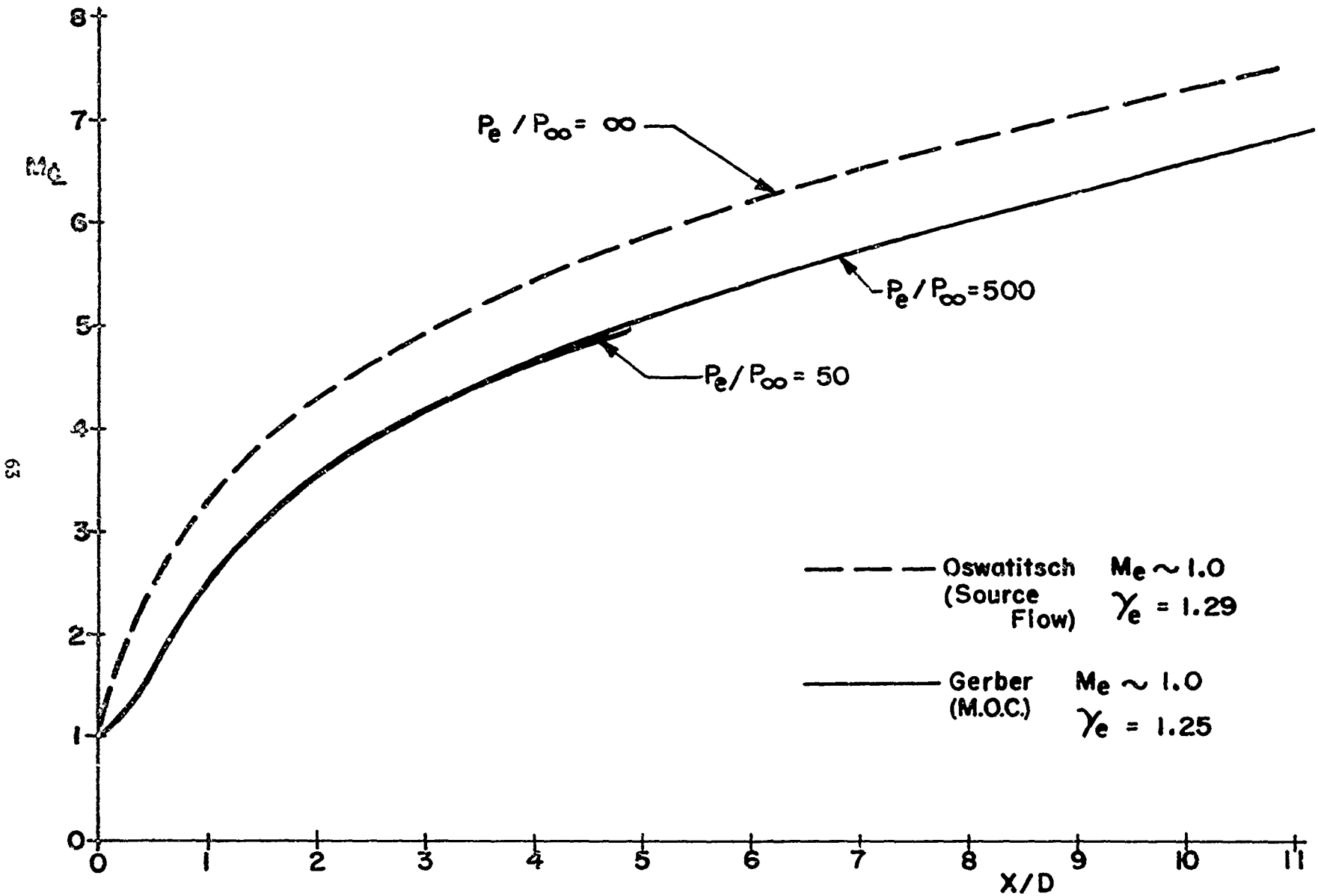

FIGURE 21 CENTERLINE MACH NUMBER DISTRIBUTION IN A STEADY JET

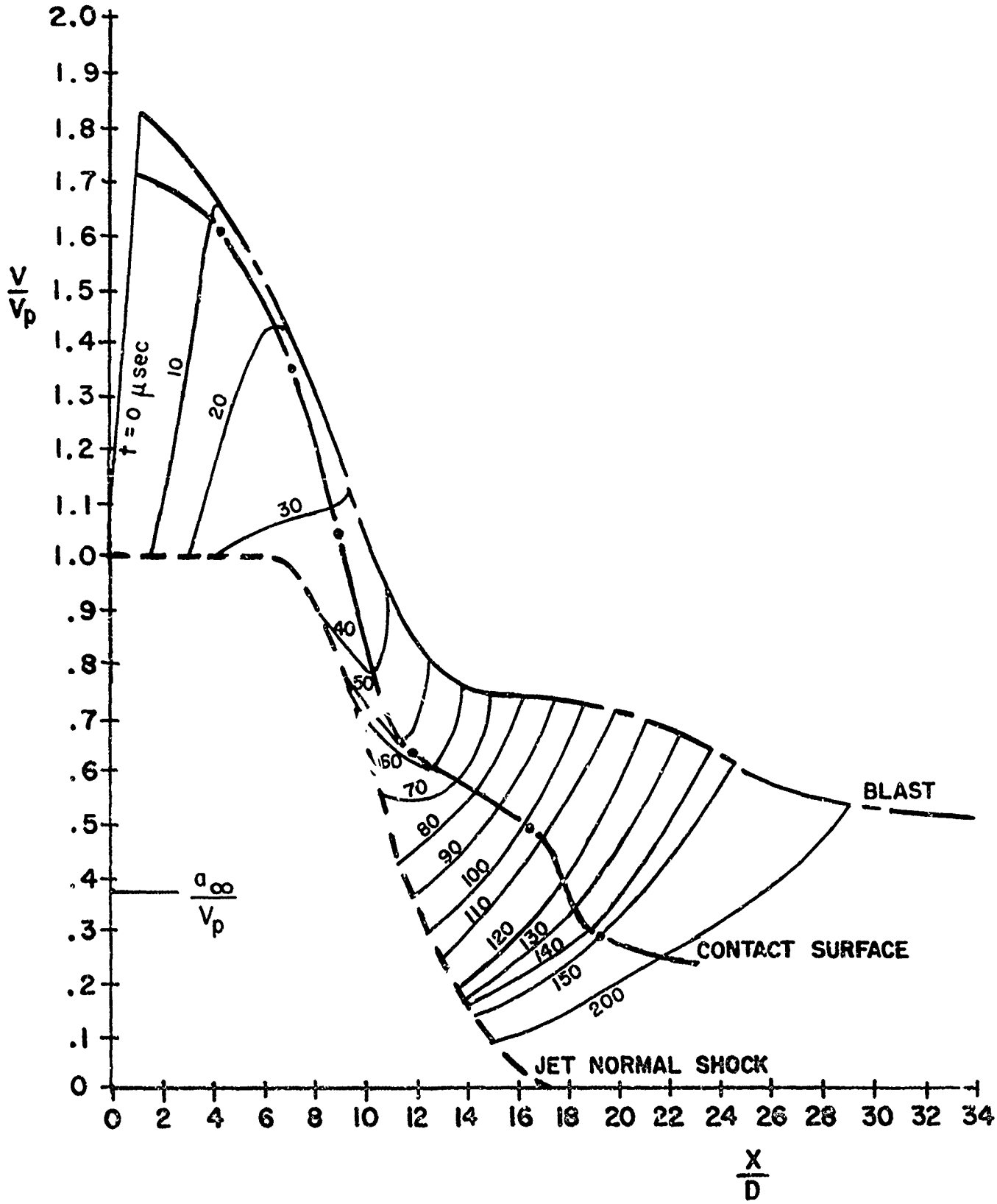

FIGURE 22 VELOCITY OF PROPELLANT GAS DISCONTINUITIES AT VARIOUS AXIAL LOCATIONS

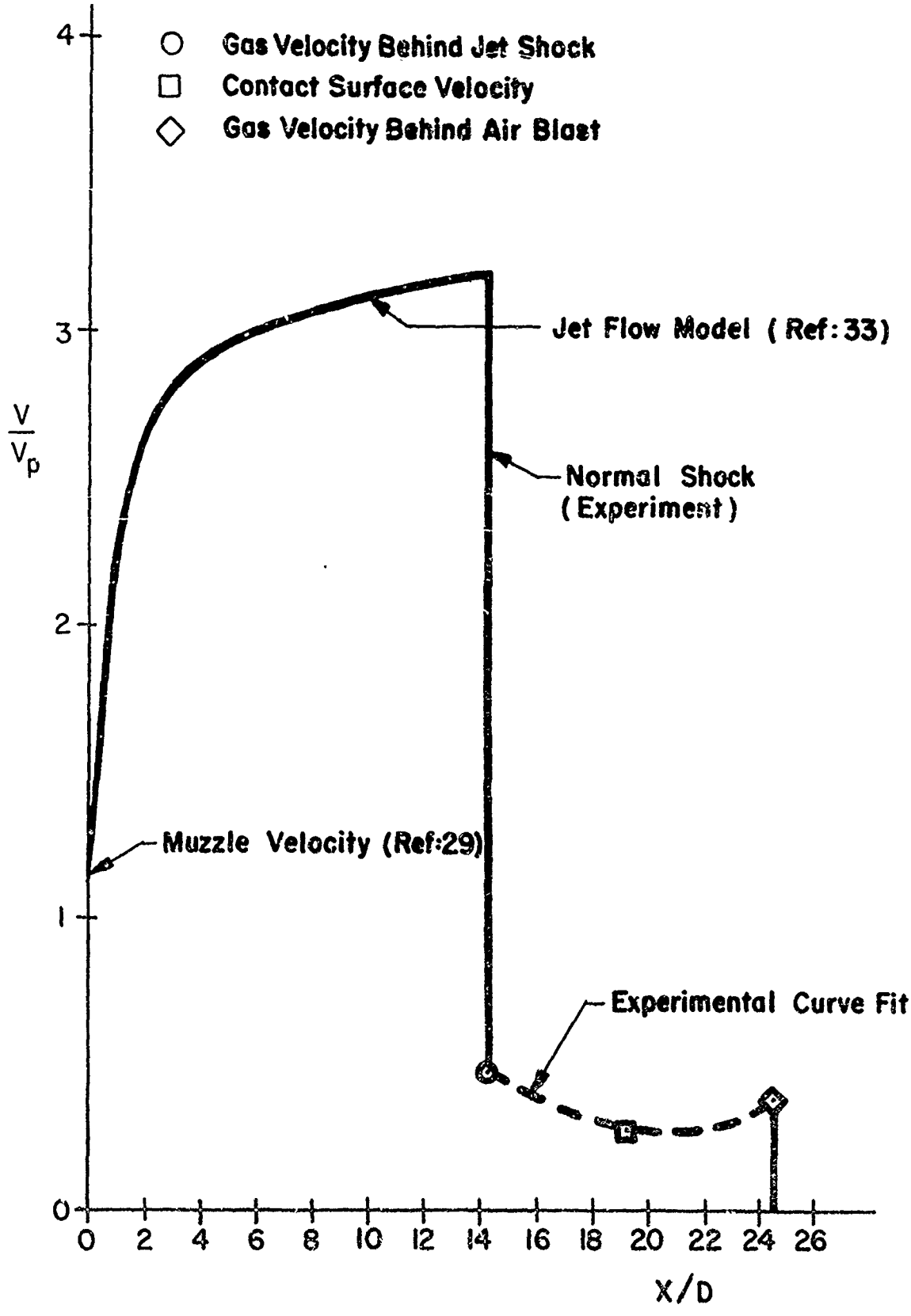

FIGURE 23 PLOT OF VELOCITY DISTRIBUTION ALONG THE AXIS OF SYMMETRY AT $t = 150\mu sec$

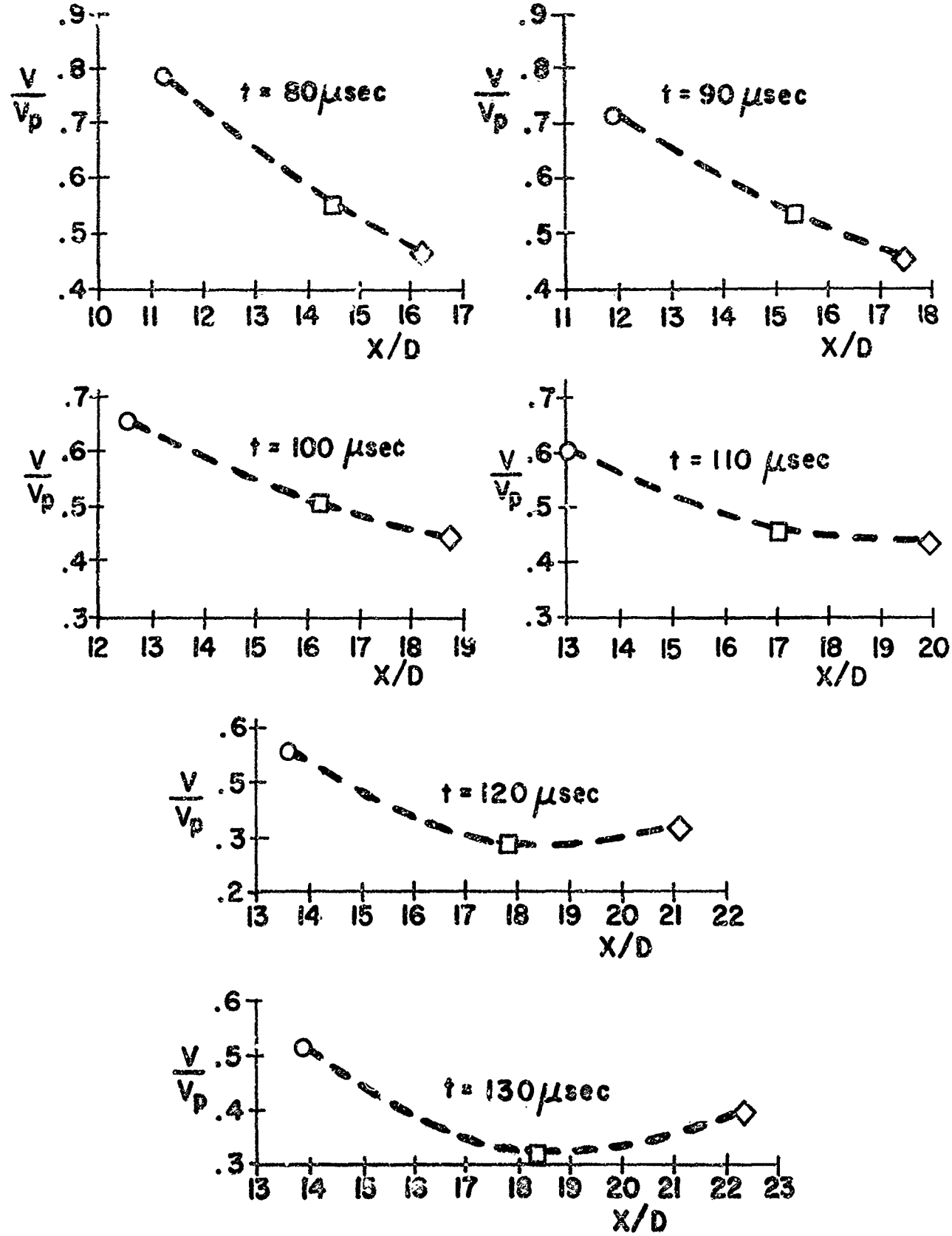

FIGURE 24 PLOT OF VELOCITY DISTRIBUTION ALONG THE AXIS OF SYMMETRY

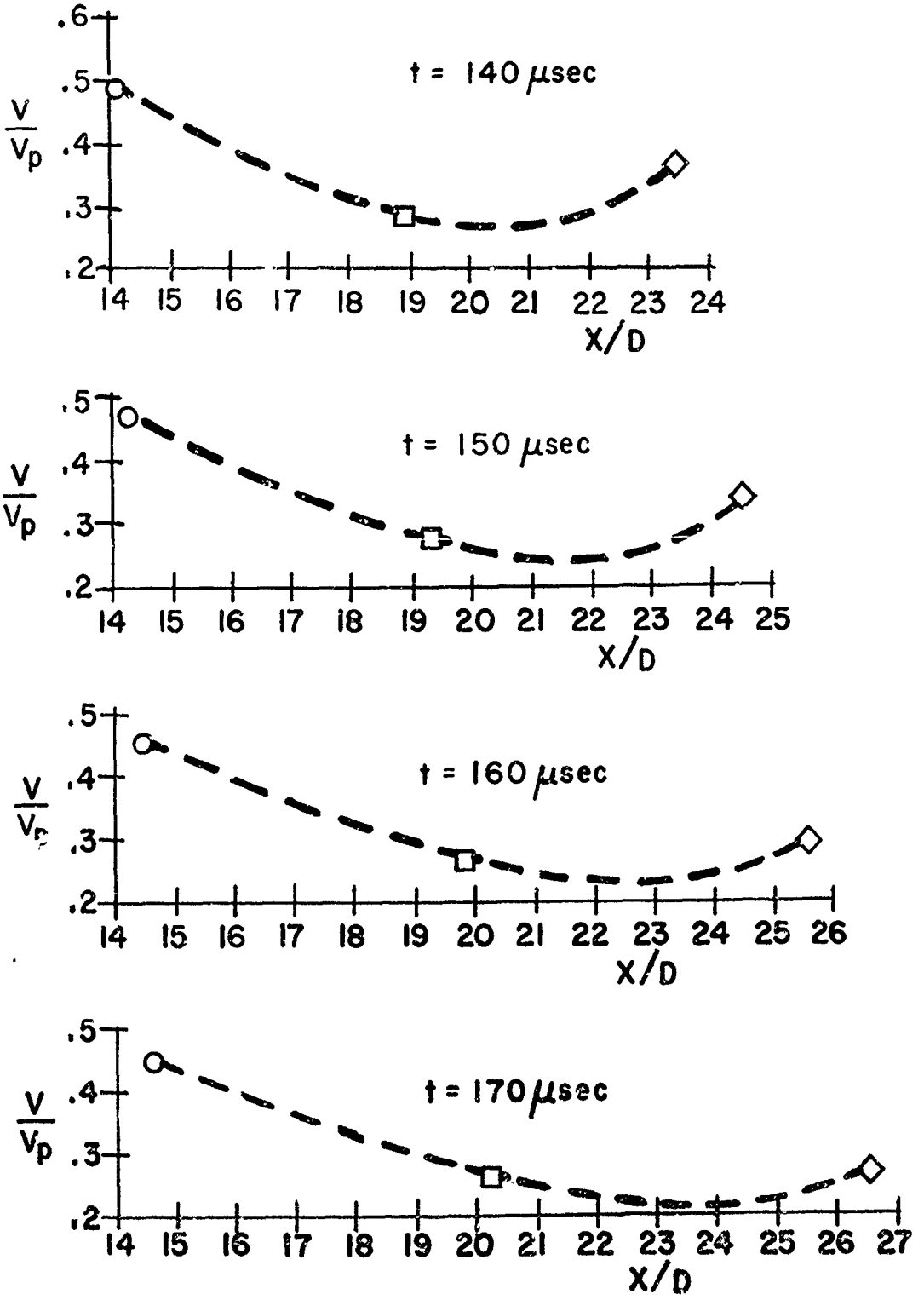

FIGURE 24 PLOT OF VELOCITY DISTRIBUTION ALONG THE AXIS OF SYMMETRY

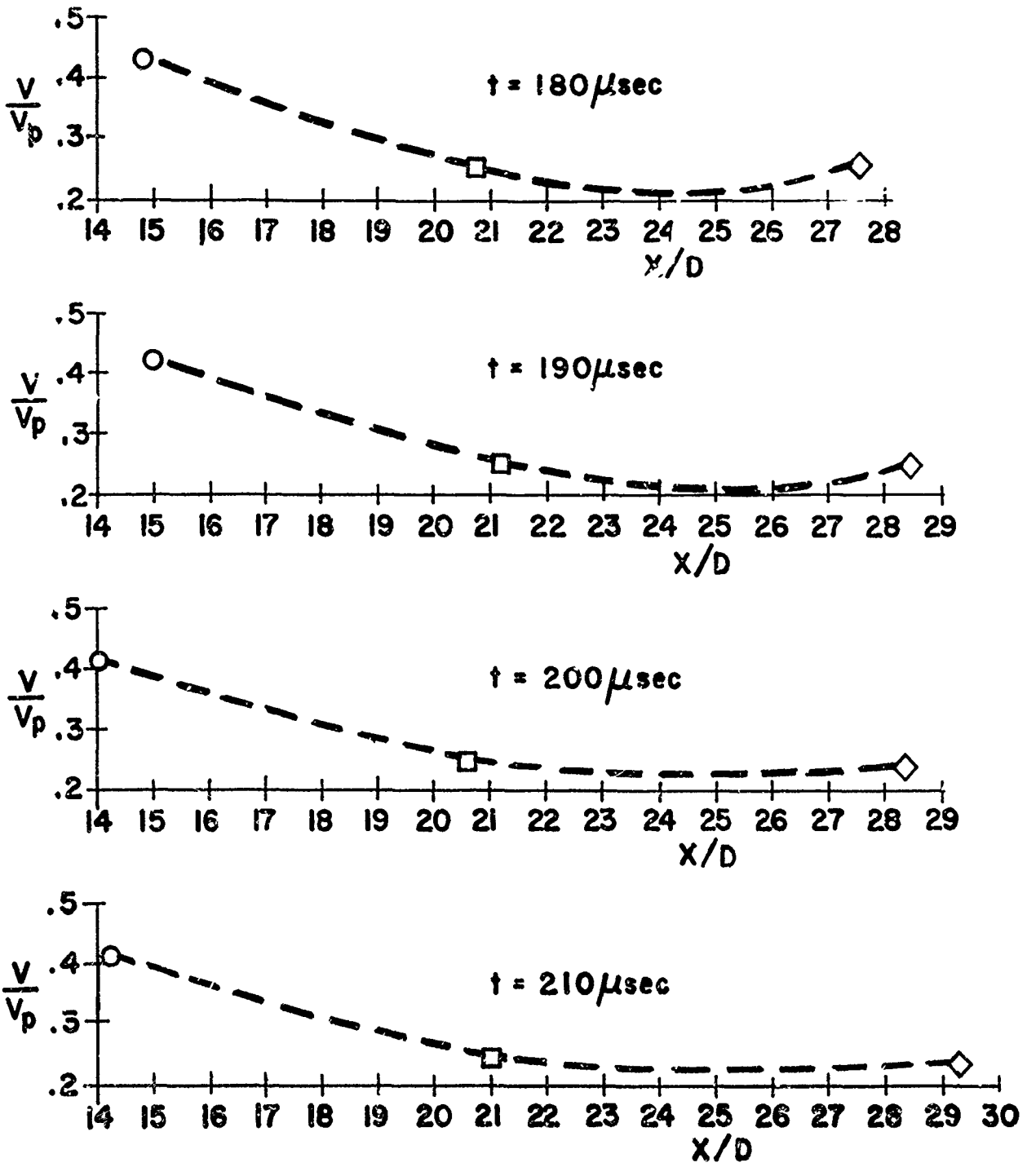

FIGURE 24 PLOT OF VELOCITY DISTRIBUTION ALONG THE AXIS OF SYMMETRY

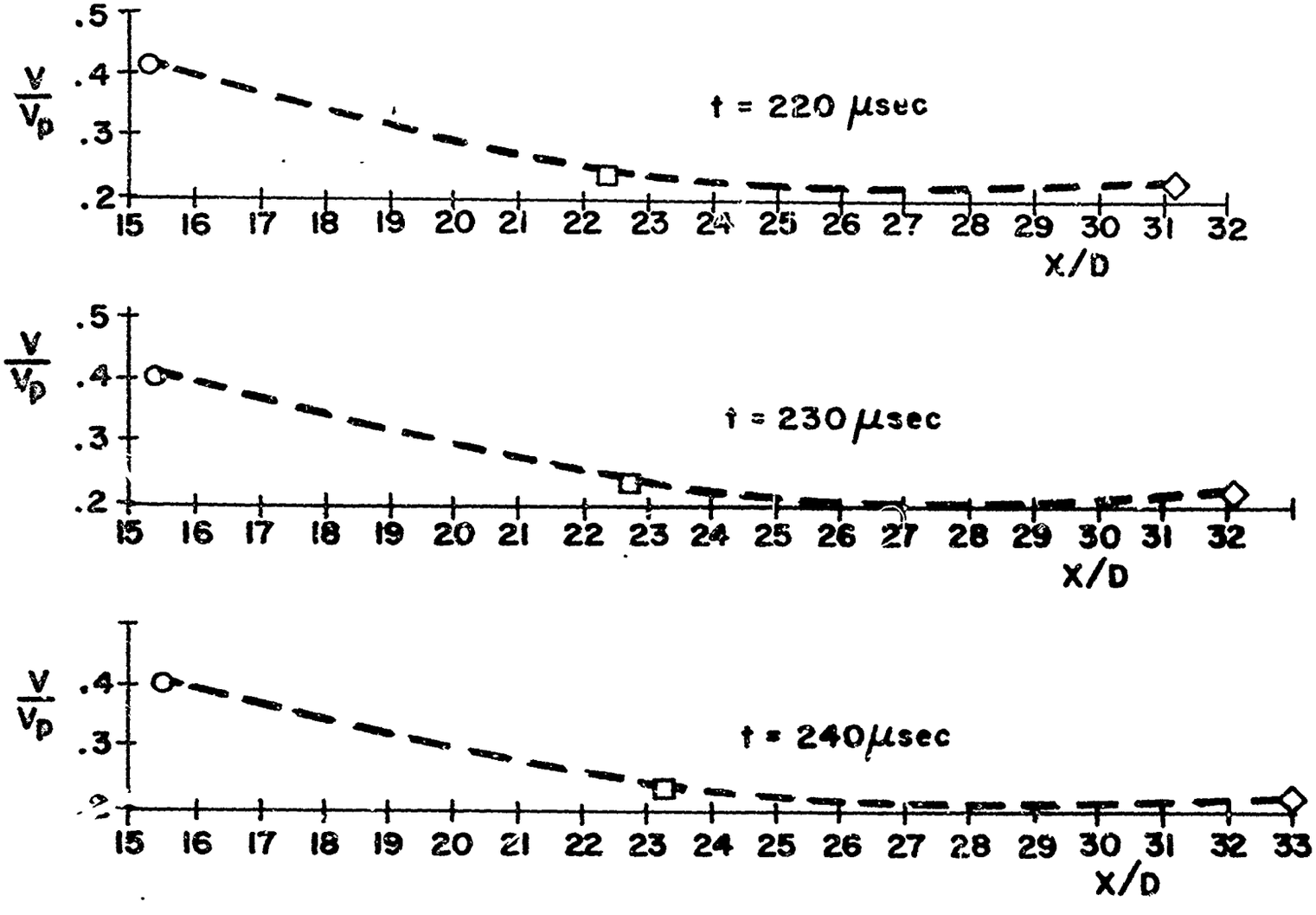

FIGURE 24 PLOT OF VELOCITY DISTRIBUTION ALONG THE AXIS OF SYMMETRY

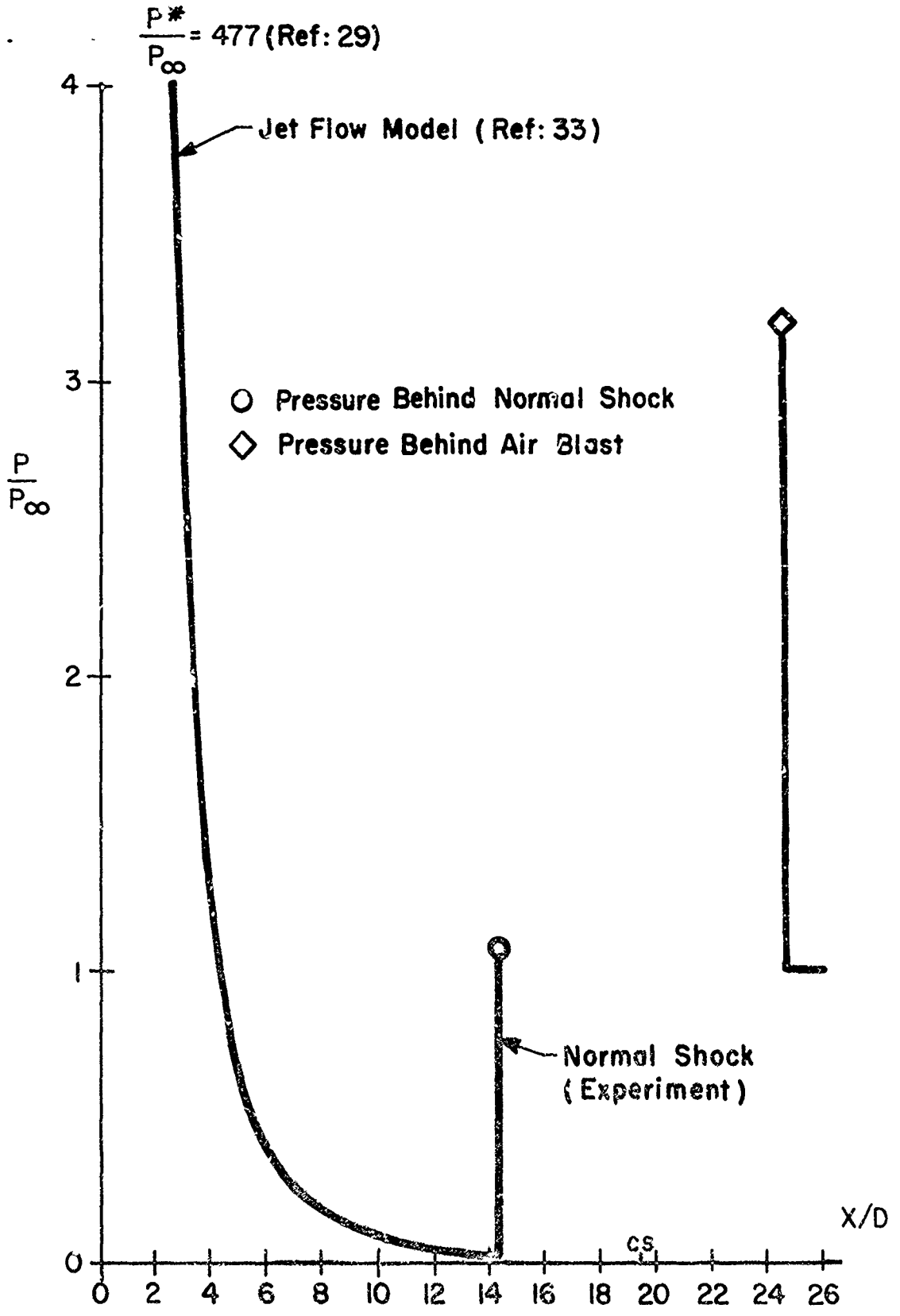

FIGURE 25 PLOT OF PRESSURE DISTRIBUTION ALONG THE AXIS OF SYMMETRY AT $t = 150 \mu sec$

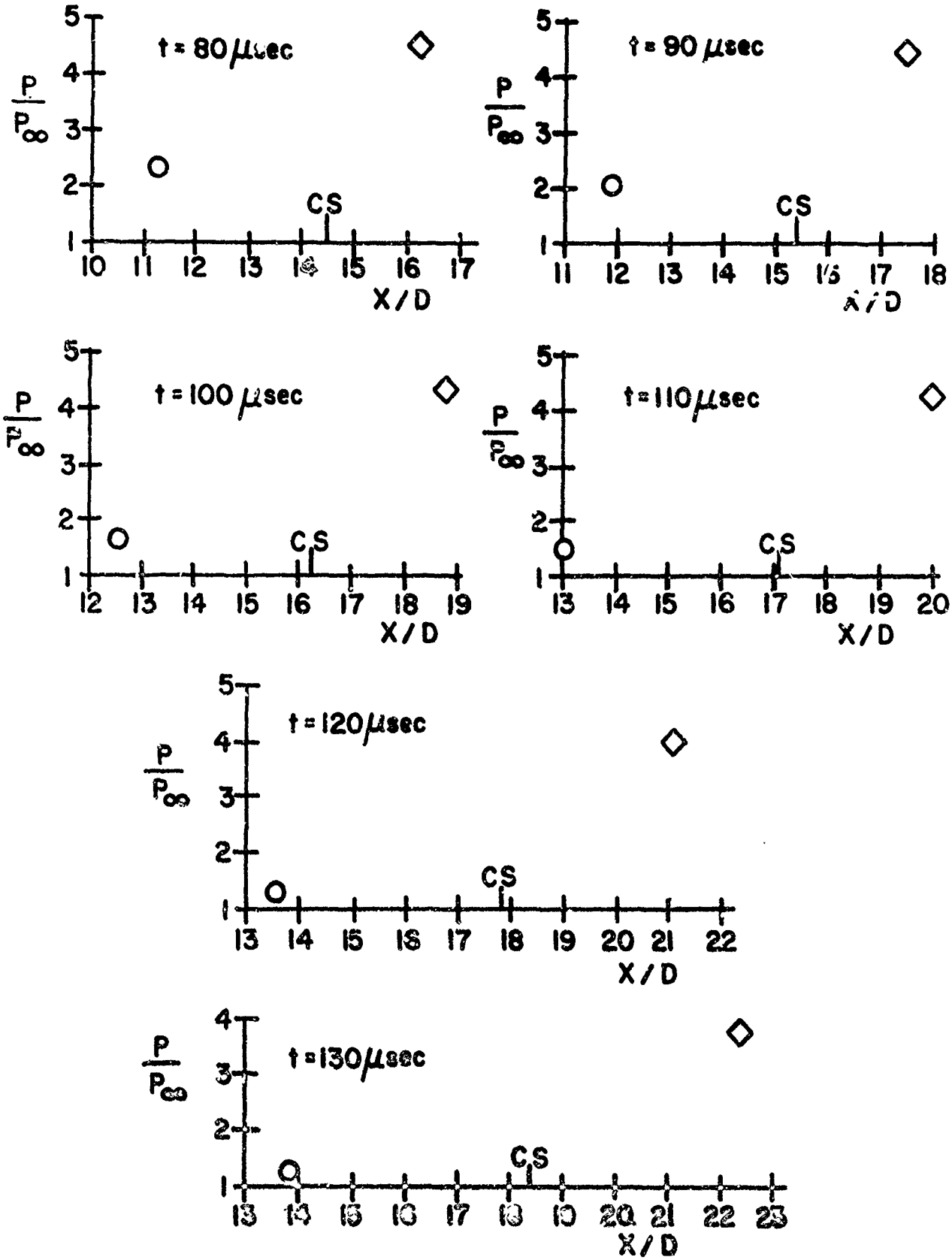

FIGURE 26 AXIAL PRESSURE DISTRIBUTION

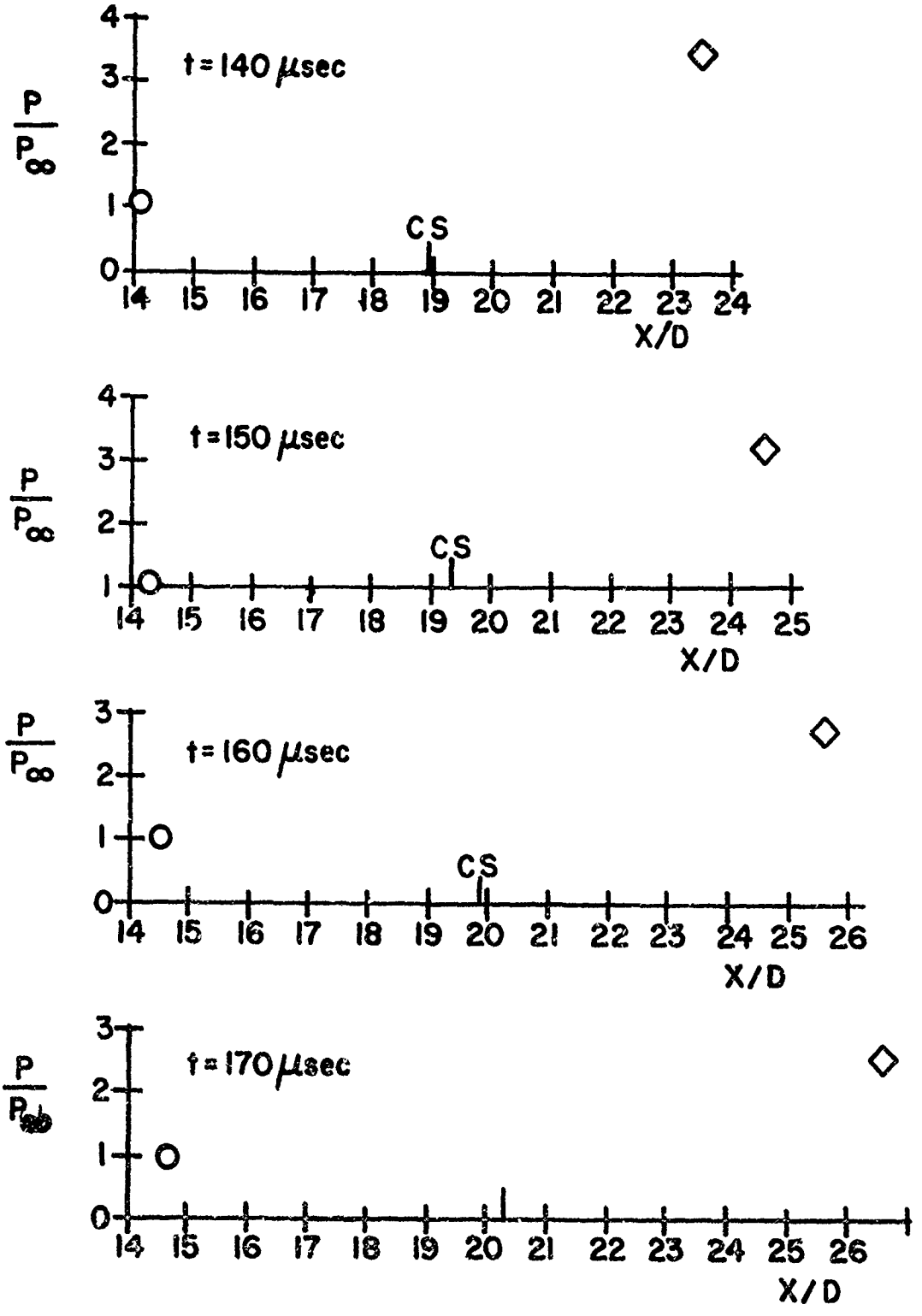

FIGURE 26 AXIAL PRESSURE DISTRIBUTION

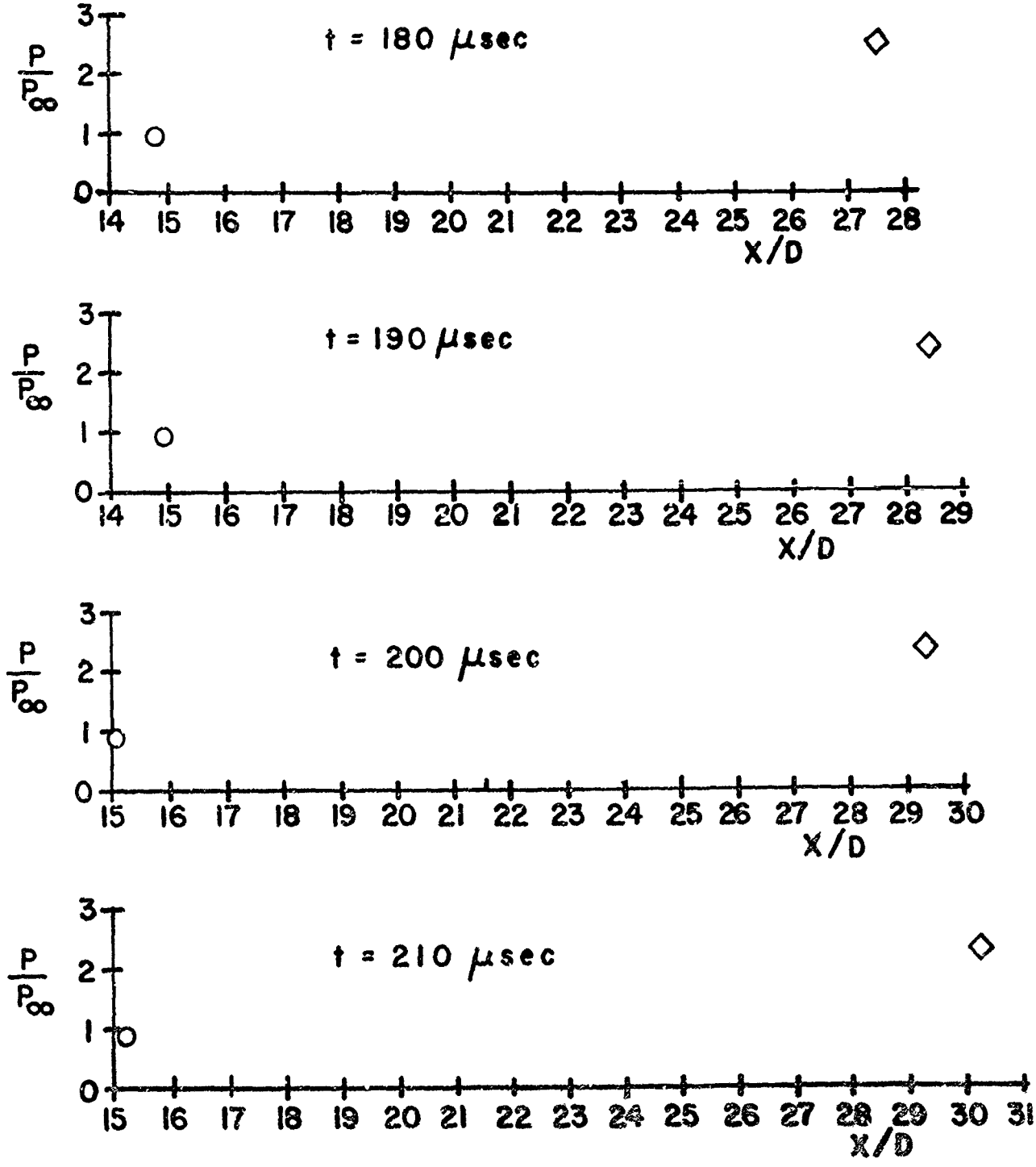

FIGURE 26 AXIAL PRESSURE DISTRIBUTION

REFERENCES

1. C. Cranz, Lehrbuch der Ballistik, J. Springer Verlag, Berlin, 1926.

2. C. Cranz and B. Glatzel, "Die Ausstromung Von Gasen Bei Hohen Anfangsdrucken", Ann. der Physik, Vol. 43, 1914.

3. R. Ladenburg, C. C. Van Voorhis, and J. Winckler, "Interferometric Studies of Supersonic Phenomena. Part I: A Supersonic Air Jet at 60 psi Tank Pressure", NAVORD Report 69-46, April 1946.

4. L. Prandtl, "Uber die Stationaren Wellen in Einem Gasstrahl", Physik Zeit., Vol. 5, 1904.

5. L. Mach, 'Optische Untersuchung der Luftstrahlen", Wiener Berichte, Vol. 106, 1897.

6. K. Oswatitsch, "Flow Research to Improve the Efficiency of Muzzle Brakes", Part I through III in Muzzle Brakes, E. W. Hammer, Ed., Franklin Institute, 1949.

7. J. J. Slade, "Muzzle Blast: Its Characteristics, Effects, and Control", National Defense Research Council, Report A-391, March 1946.

8. C. Millikan, E. Secher, and R. Buhler, "A study of Blast Deflectors, Final Report", National Defense Research Council, Report A-351, October 1945.

9. E. Robinson and E. Wilson, "Reduction of Smoke and Blast Obscuration Effect", National Defense Research Council, Report A-325, May 1945.

10. F. Smith, "Model Experiments on Muzzle Brakes", RARDE, Report 2/66, June 1966. (AD 487 121).

11. F. Smith, "Model Experiments on Muzzle Brakes, Part III: Measurement of Pressure Distribution", RARDE, Report 3/68, February 1968. (AD 845 519).

12. K. Oswatitsch, "Intermediate Ballistics", DVL, Report 358, December 1964. (AD 473 249).

13. T. D. Taylor, "Calculation of Muzzle Blast Flow Fields", Picatinny Arsenal, Report 4155, December 1970. (AD 881 523L)

14. C. M. Friedman, "Muzzle Blast Computations for Gun Fired Munitions", Picatinny Arsenal, to be published.

15. G. R. Moore, "Finite Difference Calculations of the Free-Air Gun Blast About the Muzzle of a 5"/54 Naval Gun", Naval Weapons Laboratory, Report TR-2794, September 1972. (AD 902 672)

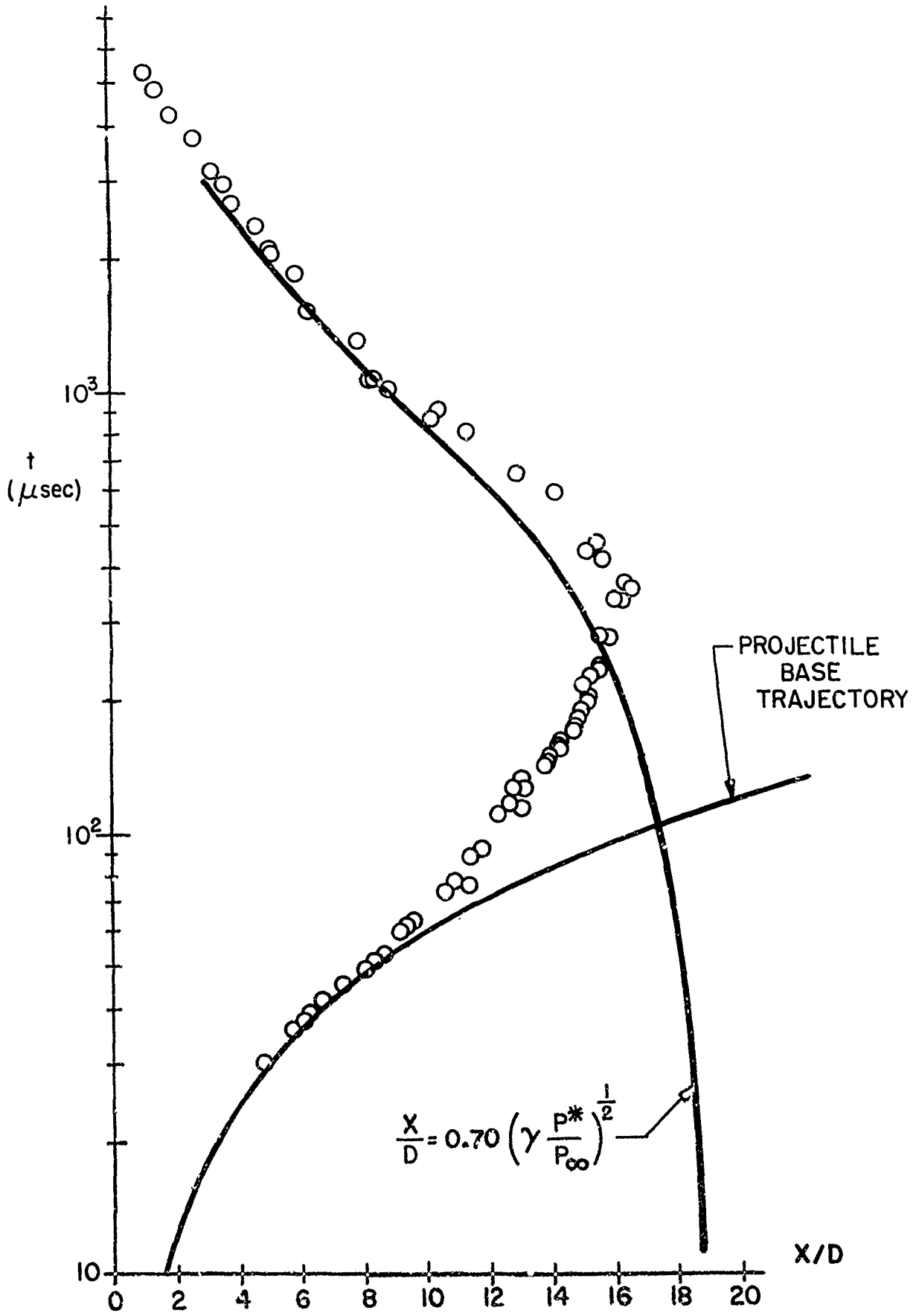

FIGURE 27 PROPELLANT GAS JET NORMAL SHOCK LOCATION

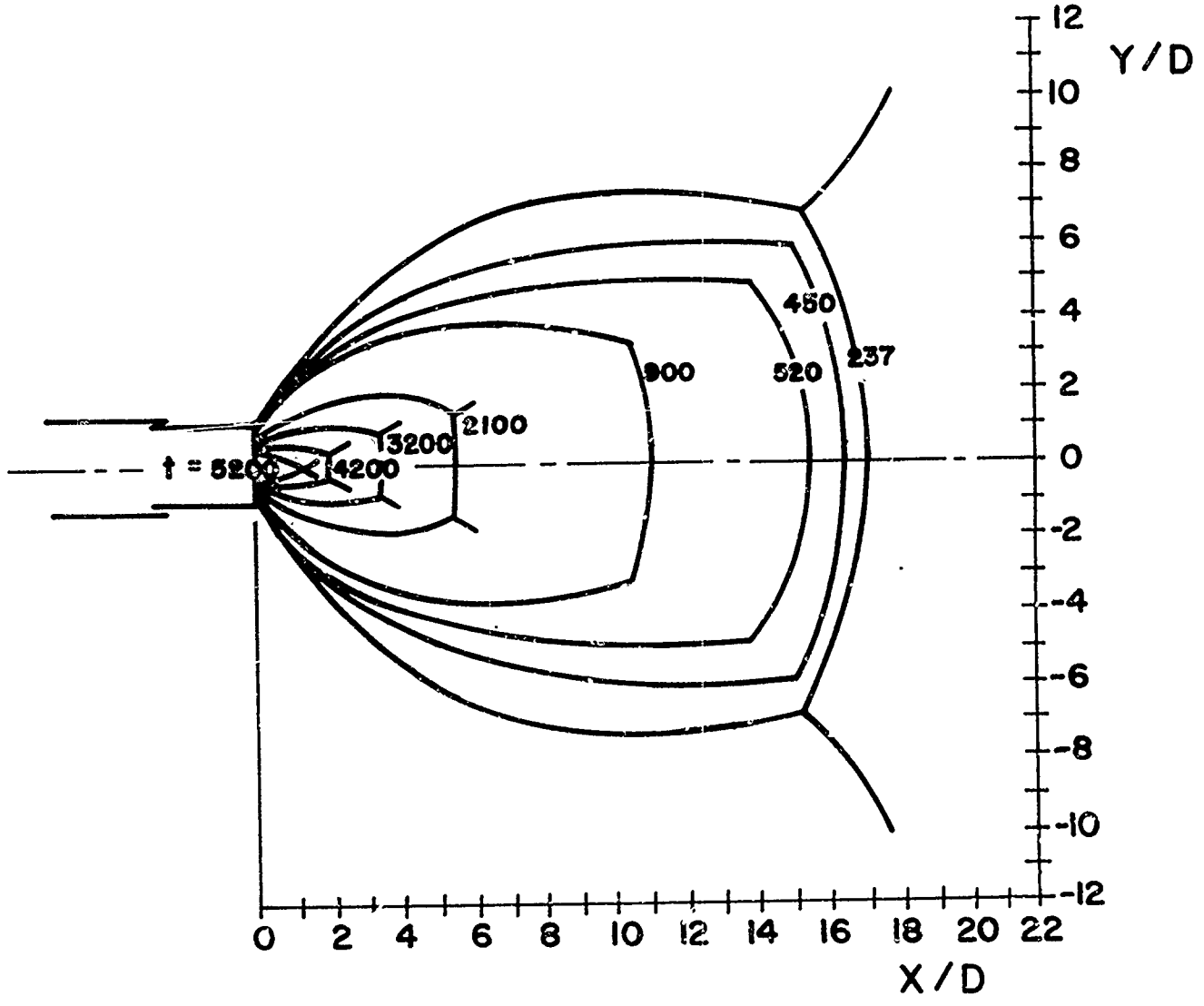

FIGURE 28A DECAY OF PROPELLANT GAS JET SHOCK STRUCTURE
(t in μsec)

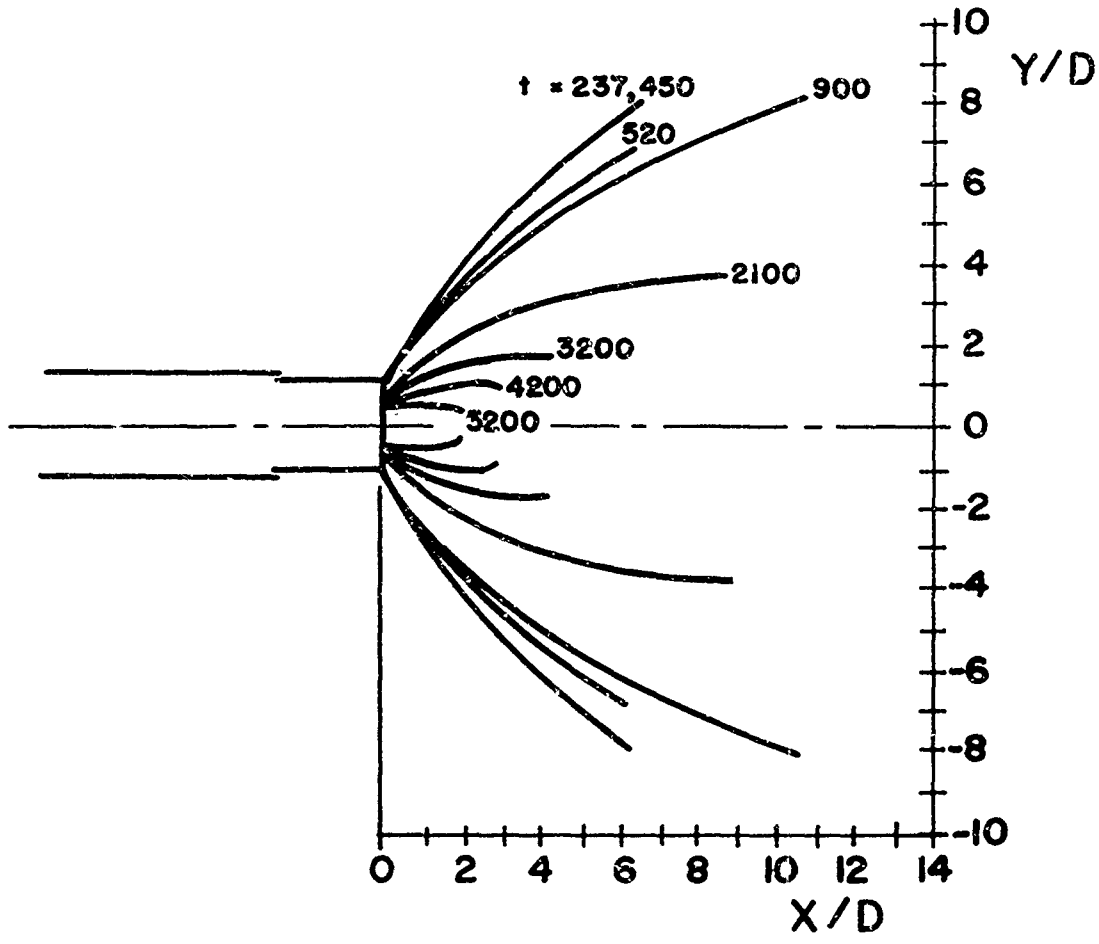

FIGURE 28B DECAY OF PROPELLANT GAS JET CONTACT SURFACE
(t in μsec)

REFERENCES

1. C. Cranz, Lehrbuch der Ballistik, J. Springer Verlag, Berlin, 1926.

2. C. Cranz and B. Glatzel, "Die Ausstromung Von Gasen Bei Hohen Anfangsdrucken", Ann. der Physik, Vol. 43, 1914.

3. R. Ladenburg, C. C. Van Voorhis, and J. Winckler, "Interferometric Studies of Supersonic Phenomena. Part I: A Supersonic Air Jet at 60 psi Tank Pressure", NAVORD Report 69-46, April 1946.

4. L. Prandtl, "Uber die Stationaren Wellen in Einem Gasstrahl", Physik Zeit., Vol. 5, 1904.

5. L. Mach, 'Optische Untersuchung der Luftstrahlen", Wiener Berichte, Vol. 106, 1897.

6. K. Oswatitsch, "Flow Research to Improve the Efficiency of Muzzle Brakes", Part I through III in Muzzle Brakes, E. W. Hammer, Ed., Franklin Institute, 1949.

7. J. J. Slade, "Muzzle Blast: Its Characteristics, Effects, and Control", National Defense Research Council, Report A-391, March 1946.

8. C. Millikan, E. Secher, and R. Buhler, "A study of Blast Deflectors, Final Report", National Defense Research Council, Report A-351, October 1945.

9. E. Robinson and E. Wilson, "Reduction of Smoke and Blast Obscuration Effect", National Defense Research Council, Report A-325, May 1945.

10. F. Smith, "Model Experiments on Muzzle Brakes", RARDE, Report 2/66, June 1966. (AD 487 121).

11. F. Smith, "Model Experiments on Muzzle Brakes, Part III: Measurement of Pressure Distribution", RARDE, Report 3/68, February 1968. (AD 845 519).

12. K. Oswatitsch, "Intermediate Ballistics", DVL, Report 358, December 1964. (AD 473 249).

13. T. D. Taylor, "Calculation of Muzzle Blast Flow Fields", Picatinny Arsenal, Report 4155, December 1970. (AD 881 523L)

14. C. M. Friedman, "Muzzle Blast Computations for Gun Fired Munitions", Picatinny Arsenal, to be published.

15. G. R. Moore, "Finite Difference Calculations of the Free-Air Gun Blast About the Muzzle of a 5"/54 Naval Gun", Naval Weapons Laboratory, Report TR-2794, September 1972. (AD 902 672)

16. T. Ishiguru, "Finite-Difference Calculations for Two-Dimensional Unsteady Expanding Flows", AIAA J., Vol. 10, No. 2, February 1972.

17. F. H. Maillie, "Finite Difference Calculations of the Free-Air Blast Field About the Muzzle and A Simple Muzzle Brake of A 105mm Howitzer", Naval Weapons Laboratory, Report TR-2938, May 1973.

18. G. Hyzer, Photographic Instrumentation Science and Engineering, Naval Air Systems Command, October 1965.

19. F. Bennett, H. Burden, and D. Shear, "Correlated Electrical and Optical Measurements of Exploding Wires", Ballistic Research Laboratories, Report 1133, June 1961. (AD 262 640)

20. H. P. Hitchcock, "Effect of Muzzle Blast on Maximum Yaw", Ballistic Research Laboratories, Memorandum Report 649, January 1953. (AD 7626)

21. W. F. Braun, Private Communication, Ballistic Research Laboratories, August 1973.

22. M. J. Piddington, "Comparison of the Exterior Ballistics of the M-193 Projectile When Launched from 1:12 in. and 1:14 in. Twist M16A1 Rifles", Ballistic Research Laboratories, Memorandum Report 1943, October 1968. (AD 844 934)

23. M. Mawbey, "A Scale Model Investigation of the Flow From the Open End of a Shock Tube of Rectangular Cross Section", Atomic Weapons Research Establishment, Report 0-61/65.

24. F. K. Elder and N. de Haas, "Experimental Study of the Formation of a Vortex Ring at the Open End of a Cylindrical Shock Tube", J. Applied Physics, Vol. 23, No. 10, October 1952.

25. I. M. Naboko, Et Al., "Formation of a Jet of Shock-Heated Gas Outflowing into Evacuated Space", Astronautica Acta, Vol. 17, No. 4 & 5, 1972.

26. J. D. Buckmaster, "An Investigation of Cylindrical Starting Flows", AIAA J., Vol. 2, No. 8, September 1964.

27. C. H. Lewis and D. J. Carlson, "Normal Shock Locations in Under-expanded Gas and Gas-Particle Jets", AIAA J., Vol. 2, No. 4, April 1964.

28. M. J. Werle, D. G. Shaffer, and R. T. Driftmeyer, "Free Jet Terminal Shocks", AIAA J., Vol. 8, No. 9, September 1970.

29. A. Celmins, Private Communication (Procedure to be Published as a BRL Report), Ballistic Research Laboratories, May 1973.

30. T. Brosseau, "Interior Ballistics Study of the M16A1 Rifle", Ballistic Research Laboratories, Memorandum Report 2190, May 1972. (AD 902 166L)

31. A. Baran and T. Brosseau, Private Communication, Ballistic Research Laboratories, June 1973.

32. E. S. Love, et al, "Experimental and Theoretical Studies of Axi-symmetric Free Jets", NASA, Technical Report R-6, 1959.

33. A. R. Vick, et al, "Comparison of Experimental Free-Jet Boundaries with Theoretical Results Obtained with the Method of Characteristics", NASA, Technical Note D-2327, June 1964.

34. J. Erdos and P. DelGuidice, "Muzzle Jet Aerodynamics of Sabot Discard", Advanced Technology Laboratories, to be published.

35. A. Sakuri, "Blast Wave Theory", in Basic Developments in Fluid Dynamics, Vol. 1, Academic Press, 1965.

36. R. Friedman, "Variable Energy Blast Waves", British J. Applied Physics, Ser. 2, Vol. 1, 1968.

37. P. Owen and C. Thornhill, "The Flow in an Axially Symmetric Supersonic Jet from a Nearly Sonic Orifice into a Vacuum", RARDE, Report 30/48, 1948. (AD 27 261)

38. R. Ladenburg, C. Van Voorhis, and J. Winckler, "Interferometric Studies of Faster Than Sound Phenomena, Part II: Analysis of Supersonic Air Jets", Physics Review, Vol. 76, No. 5, September 1949.

39. H. Brode, "A Calculation of the Blast Wave from a Spherical Charge of TNT", Rand Corporation, RM-1965, August 1957.

40. F. Oertel, "Laser Interferometry of Unsteady, Underexpanded Jets", BRL Report (to be published).

DISTRIBUTION LIST

No. of Copies	Organization
2	Commander Defense Documentation Center ATTN: DDC-TCA Cameron Station Alexandria, Virginia 22314
1	Director Defense Nuclear Agency Washington, DC 20305
1	Commander U.S. Army Materiel Command ATTN: AMCDL 5001 Eisenhower Avenue Alexandria, Virginia 22304
1	Commander U.S. Army Materiel Command ATTN: AMCRD, MG S. C. Meyer 5001 Eisenhower Avenue Alexandria, Virginia 22304
1	Commander U.S. Army Materiel Command ATTN: AMCRD, Dr.J.V.R.Kaufman 5001 Eisenhower Avenue Alexandria, Virginia 22304
1	Commander U.S. Army Materiel Command ATTN: AMCRD-T 5001 Eisenhower Avenue Alexandria, Virginia 22304
1	Commander U.S. Army Materiel Command ATTN: AMCRD-MT 5001 Eisenhower Avenue Alexandria, Virginia 22304
1	Commander U.S. Army Materiel Command ATTN: AMCRD-W 5001 Eisenhower Avenue Alexandria, Virginia 22304
1	Commander U.S. Army Aviation Systems Command ATTN: AMSAV-E 12th and Spruce Streets St. Louis, Missouri 63166
1	Director U.S. Army Air Mobility Research and Development Laboratory Ames Research Center Moffett Field, California 94035
2	Commander U.S. Army Electronics Command ATTN: AMSEL-RD AMSEL-CE Fort Monmouth, New Jersey 07703
2	Commander U.S. Army Missile Command ATTN: AMSMI-R AMSMI-RBL Redstone Arsenal, Alabama 35809
5	Commander U.S. Army Missile Command ATTN: AMSMI-RDK Mr. R. Becht (4 cys) Mr. R. Deep Redstone Arsenal, Alabama 35809
1	Commander U.S. Army Tank Automotive Command ATTN: AMSTA-RHFL Warren, Michigan 48090

DISTRIBUTION LIST

No. of Copies	Organization
2	Commander U.S. Army Mobility Equipment Research & Development Center ATTN: Tech Docu Cen, Bldg. 315 AMSME-RZT Fort Belvoir, Virginia 22060
1	Commander U.S. Army Armament Command Rock Island, Illinois 61202
6	Commander U.S. Army Frankford Arsenal ATTN: Mr. T. Boldt SARFA-U2100 Mr. J. Mitchell SARFA-U3100, S. Fulton SARFA-U3300 Mr. S. Hirshman Mr. A. Cianciosi L4100-150-2 Mr. C. Sleischer, Jr. Philadelphia, Pennsylvania 19137
8	Commander U.S. Army Picatinny Arsenal ATTN: SARPA-DR-D, S. Wasserman SARPA-DR-V, Mr. A. Loeb Mr. D. Mertz SARPA-D, Mr. Lindner SARPA-V, E. Walbrecht Mr. S. Verner SARPA-VE, Dr. Kaufman Mr. E. Friedman Dover, New Jersey 07801
1	Commander U.S. Army Watervliet Arsenal Watervliet, New York 12189
1	Commander U.S. Army Safeguard Systems Command Huntsville, Alabama 35804
1	Director U.S. Army Advanced Materiel Concepts Agency 5001 Eisenhower Avenue Alexandria, Virginia 22314
1	Commander U.S. Army Harry Diamond Laboratories ATTN: AMXDO-TI Washington, DC 20438
1	Commander U.S. Army Materials and Mechanics Research Center ATTN: AMXMR-ATL Watertown, Massachusetts 02172
1	Commander U.S. Army Natick Laboratories ATTN: AMXRE, Dr. D. Sieling Natick, Massachusetts 01762
1	Deputy Assistant Secretary of the Army (R&D) ATTN: Mr. C. L. Poor Washington, DC 20310
1	Commander U.S. Army Research Office (Durham) ATTN: CRD-AA-EH Box CM, Duke Station Durham, North Carolina 27706
1	Director U.S. Army Advanced Ballistics Missile Defense Agency P. O. Box 1500 Huntsville, Alabama 35809

DISTRIBUTION LIST

No. of Copies	Organization
3	Commander U.S. Naval Air Systems Command ATTN: AIR-604 Washington, DC 20360
3	Commander U.S. Naval Ordnance Systems Command ATTN: ORD-9132 Washington, DC 20360
2	Commander and Director U.S. Naval Ship Research and Development Center ATTN: Tech Lib Aerodynamic Lab Washington, DC 20007
3	Commander U.S. Naval Weapons Center ATTN: Code 753, Tech Lib Code 50704, Dr. W. Haseltine Code 3007, Mr. A. Rice China Lake, California 93555
4	Commander U.S. Naval Ordnance Laboratory ATTN: Code 031, Dr. K. Lobb Code 312, Mr. R. Regan Mr. S. Hastings Code 730, Tech Lib Silver Spring, Maryland 20910
3	Director U.S. Naval Research Laboratory ATTN: Tech Info Div Code 7700, D. A. Kolb Code 7720, Dr. E. McClean Washington, DC 20390
3	Commander U.S. Naval Weapons Laboratory ATTN: Code GX, Dr. W. Kemper Mr. F. H. Maille Dr. G. Moore Dahlgren, Virginia 22448
2	Commander U.S. Naval Ordnance Station Indian Head, Maryland 20640
1	Commander U.S. Naval Ordnance Station ATTN: Code FS13A, P. Sewell Indian Head, Maryland 20640
2	ADTC (ADBPS-12) Eglin AFB Florida 32542
1	AFATL (DLR) Eglin AFB Florida 32542
1	AFATL (DLRD) Eglin AFB Florida 32542
1	AFATL (DLRV) Eglin AFB Florida 32542
2	AFATL (DLRA, F. Burgess; Tech Lib) Eglin AFB Florida 32542
1	AFWL (DEV) Kirtland AFB New Mexico 87117

DISTRIBUTION LIST

No. of Copies	Organization
1	ARD (ARIL) Wright-Patterson AFB Ohio 45433
1	ARL Wright-Patterson AFB Ohio 45433
1	ASD (ASBEE) Wright-Patterson AFB Ohio 45433
1	Director National Bureau of Standards ATTN: Tech Lib U.S. Department of Commerce Washington, DC 20234
1	Headquarters National Aeronautics and Space Administration ATTN: Code EP, M. Adams Washington, DC 20546
1	Director NASA Scientific and Technical Information Facility ATTN: SAK/DL P. O. Box 33 College Park, Maryland 20740
1	Director Jet Propulsion Laboratory ATTN: Tech Lib 4800 Oak Grove Drive Pasadena, California 91103
2	Director National Aeronautics and Space Administration George C. Marshall Space Flight Center ATTN: MS-I, Lib R-AERO-AE, Mr. A. Felix Huntsville, Alabama 35812
1	Director National Aeronautics and Space Administration Langley Research Center ATTN: MS 185, Tech Lib Langley Station Hampton, Virginia 23365
1	Director National Aeronautics and Space Administration Lewis Research Center ATTN: MS 60-3, Tech Lib 21000 Brookpark Road Cleveland, Ohio 44135
1	Advanced Technology Laboratories ATTN: Dr. J. Erdos Merrick & Stewart Avenues Westbury, New York 11590
2	ARO, Inc. ATTN: Tech Lib Arnold AFS Tennessee 37389
1	Technical Director Colt Firearms Corporation 150 Huyshore Avenue Hartford, Connecticut 14061
1	General Electric Corporation Armaments Division ATTN: Mr. R. Whyte Lakeside Avenue Burlington, Vermont 05401
1	Winchester-Western Division Olin Corporation ATTN: Mr. D. Mettill New Haven, Connecticut 06504

DISTRIBUTION LIST

No. of Copies	Organization
1	Sandia Laboratories ATTN: Aerodynamics Dept Org 9320, R. Maydew P. O. Box 5800 Albuquerque, New Mexico 87115
1	California Institute of Technology Aeronautics Department ATTN: Prof. H. Liepmann Pasadena, California 91102
1	Guggenheim Aeronautical Laboratory California Institute of Technology ATTN: Tech Lib Pasadena, California 91104
3	Calspan Corporation ATTN: Mr. J. Martin Dr W. Wurster Dr. C. Skinner P. O. Box 23[illegible] Buffalo, New York 14221
2	Franklin Institute ATTN: Dr. Carfagno Dr. Wachtell Race & 20th Streets Philadelphia, Pennsylvania 19103
1	Director Applied Physics Laboratory The Johns Hopkins University 8621 Georgia Avenue Silver Spring, Maryland 20910
1	Massachusetts Institute of Technology Department of Aeronautics and Astronautics ATTN: Tech Lib 77 M[illegible]chusetts Avenue Cambridge, Massachusetts 02139
1	Director Guggenheim Aerospace Labs New York University New York Heights New York, New York 10053
1	Ohio State University Department of Aeronautics and Astronautical Engineering ATTN: Tech Lib Columbus, Ohio 43210
2	Polytechnic Institute of Brooklyn Graduate Center ATTN: Dr. G. Morretti Dr. R. Cresci Farmingdale, New York 11735
1	Director Forrestal Research Center Princeton University Princeton, New Jersey 08540
9	Princeton University Forrestal Laboratories ATTN: Dr. S. I. Cheng Princeton, New Jersey 08540
1	Southwest Research Institute ATTN: Mr. Peter S. Westine P. O. Drawer 28510 8500 Culebra Road San Antonio, Texas 78228
2	University of Michigan Department of Aeronautical Engineering ATTN: Dr. A. Kuethe Dr. M. Sichel East Engineering Building Ann Arbor, Michigan 48104

DISTRIBUTION LIST

Aberdeen Proving Ground

Ch, Tech Lib
Marine Corps Ln Ofc
Cdr, USATECOM
ATTN: AMSTE-BE
Mr. Morrow
AMSTE-TA-R
Mr. Wise
Dir, USAMSAA

UNCLASSIFIED

Security Classification

DOCUMENT CONTROL DATA - R & D

(Security classification of title, body of abstract and indexing annotation must be entered when the overall report is classified)

1. ORIGINATING ACTIVITY (Corporate author) U. S. Army Ballistic Research Laboratories Aberdeen Proving Ground, Maryland 21005	2a. REPORT SECURITY CLASSIFICATION 2b. GROUP

3. REPORT TITLE

THE FLOW FIELD ABOUT THE MUZZLE OF AN M-16 RIFLE

4. DESCRIPTIVE NOTES (Type of report and inclusive dates)

5. AUTHOR(S) (First name, middle initial, last name)

Edward M. Schmidt
Donald D. Shear

6. REPORT DATE	7a. TOTAL NO. OF PAGES	7b. NO. OF REFS
JANUARY 1974	86	40

8a. CONTRACT OR GRANT NO.	9a. ORIGINATOR'S REPORT NUMBER(S)
b. PROJECT NO. RDT&E 1T061102A33D	BRL REPORT NO. 1692
c.	9b. OTHER REPORT NO(S) (Any other numbers that may be assigned this report)
d.	8 FEB 1974

10. DISTRIBUTION STATEMENT

Distribution limited to US Government agencies only. Other requests for this document must be referred to Director, USA Ballistic Research Laboratories, ATTN: AMXBR-SS, Aberdeen Proving Ground, Maryland 21005. TOE

11. SUPPLEMENTARY NOTES	12. SPONSORING MILITARY ACTIVITY
	U. S. Army Materiel Command 5001 Eisenhower Avenue Alexandria, Virginia 22304

13. ABSTRACT

An experimental technique is developed which permits the obtaining of detailed time-displacement histories of observable discontinuities in the muzzle gas flow fields that form about weapons during firing. The technique is applied to the flow from the muzzle of an M-16 rifle firing standard ball ammunition. Data is presented both as full discontinuity contours and as discontinuity trajectories along the axis of symmetry. The former indicate the details of muzzle jet-free air blast coupling; while the latter demonstrate the applicability of analytical techniques to the flow field. Additionally, a data reduction scheme is proposed which permits the inference of property values in the flow based on a combination of empirical and analytical techniques.

14. KEY WORDS	LINK A		LINK B		LINK C	
	ROLE	WT	ROLE	WT	ROLE	WT
Transitional Ballistics						
Muzzle Gases						
M-16 Rifle						